universität wien

MASTERARBEIT/MASTER'S THESIS

Titel der Masterarbeit / Title of the Master's Thesis

„Effects of climate change on chemical composition and carbon content of physical soil fractions"

verfasst von / submitted by

Moritz Adrian Mohrlok

angestrebter akademischer Grad / in partial fulfilment of the requirements for the degree of

Master of Science (MSc)

Wien, 2021 / Vienna 2021

Studienkennzahl lt. Studienblatt / degree programme code as it appears on the student record sheet:	A 066 833
Studienrichtung lt. Studienblatt / degree programme as it appears on the student record sheet:	Masterstudium Ecology and Ecosystems
Betreut von / Supervisor:	Univ.-Prof. Dr. Andreas Richter

Acknowledgements

First, I would like to thank my family, my girlfriend and all my friends for your continuous support. Without your help this would have been a lot harder or not possible at all.

A special thank you of course goes out to my supervisor Andreas Richter, who was always ready to help, answered any questions and provided me with constructive feedback as well as the opportunity to present and discuss my results at multiple occasions, which added greatly to the development of this thesis. Also, without his leadership and flexibility in this global pandemic this work would have likely taken a lot longer.

A big thank you to the lab technicians: Margarete Watzka for measuring what must have been thousands of samples for me, Sabrina Pober who always knew where to find things and for ordering all the stuff I needed and of course Ludwig Seidl, who patiently repaired and troubleshot the Pyr-GC/MS system for me on multiple occasions.

Last, but not least, I would like to thank everyone at TER, who always provided an enjoyable work atmosphere and were always helpful. Special thanks to Hannes Schmidt for his spontaneous help with the microscopy, Victoria Martin who helped me a lot in the lab and developed the Pyr-GC/MS approach with me and of course Alberto Canarini, who supported me all the way through this thesis, in the end even from Japan via various late-night Zoom calls.

List of Abbreviations

CaOM	Clay-associated Organic Matter
ClimGrass	Grassland Carbon and Nutrient Dynamics in a Changing Climate
cPOM	Course Particulate Organic Matter
CUE	Carbon Use Efficiency
EA-IRMS	Elemental Analyzer-Isotope Ratio Mass Spectrometry
eCO_2	Elevated CO_2
ESM	Earth System Model
eT	Elevated Temperature
FACE	Free Air Carbon Enrichment
fPOM	Free Particulate Organic Matter
FW	Fresh Weight
GC/MS	Gas Chromatography/Mass Spectrometry
GC-TOF-MS	Gas Chromatography-Time-of-Flight-Mass Spectrometry
GHG	Greenhouse Gas
iPOM	Intra-aggregate Particulate Organic Matter
LSM	Land Surface Model
maA	Macro-aggregates
MaOM	Mineral-associated Organic Matter
miA	Micro-aggregates
NIST	National Institute of Standards and Technology
NMDS	Non-Metric Multidimensional Scaling
NMR	Nuclear Magnetic Resonance
OM	Organic Matter
OTU	Operational Taxonomic Unit
POM	Particulate Organic Matter
S:N-Ratio	Signal to Noise Ratio
SaOM	Sand-associated Organic Matter
scA	Silt & Clay-sized aggregates
SCM	Soil Continuum Model
SOC	Soil Organic Carbon
SOM	Soil Organic Matter
SPT	Sodium Polytungstate
Tukey-HSD	Tukey Honest Significant Difference

Table of Contents

→

PART 1

General Introduction

The anthropogenic emissions of greenhouse gases (GHG) into the atmosphere over the last decades and in the future will lead to increased average global surface temperatures (IPCC, 2014). This will alter biogeochemical cycling of all major elements and ecosystems, and impact species all around the globe. Consequences such as changes in precipitation, more frequent and more severe wildfires and torrential rains, or a rising sea-level threaten habitats and increase the risk of species extinction (IPCC, 2014). The potential loss of ecosystem services together with direct effects of a changing climate (e.g., desertification, extreme weather events, reduced food security and water availability), pose threats to our society in the future (IPCC, 2014). Adaptation to climate change and mitigation strategies to reduce GHG emissions are therefore some of the most important challenges to humanity in the 21st century.

The response of earth`s climate system to future changes is estimated today using Earth System Models (ESMs) or Land Surface Models (LSMs), which are coupled to global atmospheric circulation models, connecting atmosphere with land and ocean. Predicted CO_2 emissions are taken as an input and passed through the ESM or LSM. The result is an estimate of radiative forcing and corresponding temperature increase (IPCC Working Group I, 2013). Accurate predictions of climate change and policy decisions informed by these in part rely on the performance of ESMs. If certain model components are systematically under- or overestimated (or not even included at all), model predictions might be not reliable. This in turn will lead to misleading information on future GHG concentrations and global temperatures. It is therefore necessary to develop a solid and robust knowledge base on biogeochemical cycles, global carbon (C) pools and fluxes, which form the base of ESMs.

The Role of Soils in the Global Carbon Cycle

Soils are an important part of global biogeochemistry, especially regarding the C-cycle. In their seminal book Biogeochemistry, Schlesinger & Bernhardt (2013) estimated the global active C pool at about 40,800 petagrams (10^{15}) C, most of it stored in the oceans (38,000 Pg). In terrestrial ecosystems, the largest amount of C is stored in soils (about 3800 Pg C in the first three meters of soils including peatlands and permafrost, Lal & Stewart, 2019). This is a lot more than what is contained in the atmosphere and biosphere (about 800 and 600 Pg respectively, Lal & Stewart, 2019).

Through photosynthesis, plants fix atmospheric CO_2 and produce organic compounds that make up their biomass. Soil macro- and mesofauna, as well as changing environmental conditions (such as freezing-thawing, or drying-rewetting) break down dead plant material into smaller pieces (particulate organic matter, POM) that enter the soil system (Frouz, 2018; Swanston & Trumbore, 2009). Plants also actively and passively exude organic compounds through their roots to attract symbiotic microorganisms and increase nutrient and water acquisition (Bais et al., 2006). This carbon adds to the dissolved organic matter pool (DOM) in soils.

Most C in soils is contained in Soil Organic Matter (SOM), which can be defined as a "[…] mixture of recognizable plant and animal parts and material that has been altered to a degree that it no longer contains its original structural organization" (Oades, 1989, cited in Amundson, 2001). It is interesting to note that this definition does not account for microbial remains, i.e., microbially-derived 'solid' organic matter, thought to make up a significant part of SOM (Liang et al., 2019). Another more recent definition is given by Lehmann & Kleber (2015). They proposed "viewing soil organic matter as a continuum spanning the full range from intact plant material to highly oxidized carbon […]". This definition includes the previously mentioned plant and animal remains, as well as bacterial and fungal necromass. The soil microbiome uses SOM as an energy source (catabolism) to build up their own biomass (anabolism). CO_2 released during autotrophic respiration by plants and heterotrophic respiration by microbes completes the soil C cycle in the soil-atmosphere-plant-continuum (Norman & Anderson, 2005).

While primary production influences the C input into soil, the decomposition of Soil Organic Carbon (SOC) controls the C release from soils to the atmosphere. Consequently, microbial decomposition plays an important role in the global C-cycle (Liang et al., 2019). Due to the large amount of C stored in soils, an increase of this flux can increase global atmospheric CO_2 concentrations, accelerating climate change through the greenhouse effect (Von Lützow et al., 2006; Rustad et al., 2000).

Mechanisms of Carbon stabilization

The turnover time (τ) of soil carbon is defined as the time until the carbon stock is completely depleted when there are no more inputs. It can be calculated for soils in a steady state as:

$$\tau_0 = \frac{C}{S} \quad (1)$$

with C being the mass of SOC and S being the sum of all C fluxes out of the system (Swanston & Trumbore, 2009). Processes that protect SOM from decomposition and therefore decrease the turnover time and increase the residence time of SOM in soils, are generally referred to as C-stabilizing processes (Von Lützow et al., 2006). Three main mechanisms of C stabilization in soils are generally defined (see Lützow et al., 2006): Selective preservation, inaccessibility, and binding to mineral surfaces. Other authors describe physical disconnection and sorption-desorption processes as the main preservation mechanism, in addition to freezing in permafrost (Schmidt et al., 2011).

The concept of selective preservation is based on the theory of chemical recalcitrance, making molecules with certain structure or elemental composition less preferable for microorganisms (Von Lützow et al., 2006; Marschner et al., 2008). Over time, they accumulate in soils as long as substrates of higher quality are available. Traditionally, chemical recalcitrance of big organic molecules in soils was seen as the main mechanism of C sequestration. However, in the last two decades this view has been challenged, since for example experiments with stable isotopes revealed that complex polyaromatic molecules such as lignin are decomposed relatively quickly (Baveye & Wander, 2019;

Lehmann & Kleber, 2015; Von Lützow et al., 2006) and that the addition of labile substrates even enhanced the mineralization of recalcitrant molecules through the priming effect (Hamer & Marschner, 2005). Selective preservation can explain a "progressive change of residue composition during the initial stages of decomposition […]" but not "[…] the long-term stabilization of potentially labile compounds" (Von Lützow et al., 2006).

Organic matter (OM) cannot be decomposed if it is inaccessible to microbes or their extracellular enzymes. During aggregate formation (see below), residue in any stage of decomposition can be occluded within aggregates, protecting it from microbes (Von Lützow et al., 2006; Six et al., 2002). Another way of spatial inaccessibility can be a lack of water, since it is needed as transport medium for both substrates and extracellular enzymes (Schimel, 2018). If soil moisture is too low to form a water film that connects microbe and substrate, decomposition cannot happen. The probability for substrate to be decomposed also depends on its concentration in the soil: Lower concentrations lead to lower decomposition rates because of the decreased likelihood of a microbe encountering a substrate molecule (Don et al., 2013).

SOM can sorb to mineral surfaces, forming strong organo-mineral associations (Kleber, Sollins, & Sutton, 2007; Lehmann & Kleber, 2015; Von Lützow et al., 2006). This sorption can happen through ligand exchange forming organo-mineral complexes, cation bridges with polyvalent cations (Ca^{2+}, Mg^{2+}, Fe^{3+}, Al^{3+}) and weak electrostatic van der Waals-forces (Kleber et al., 2007; Von Lützow et al., 2006). All these associations are highly dependent on the chemical structure of OM and other abiotic factors, such as which minerals are involved, or surface area and soil pH. Nevertheless, 50-75% of SOM can be found in organo-mineral associations in temperate soils (Christensen, 2001).

Lehmann & Kleber (2015) combined both the concepts of inaccessibility of substrates and mineral protection in their "soil continuum model" (SCM). It consists of progressive degradation of plant and animal residues into large biopolymers and microbe-assimilable small biopolymers and monomers. Each size stage can be either protected from decomposition by occlusion within aggregates or by binding to mineral surfaces. The

smaller the compounds, the easier they are protected (by increased water-solubility and overall greater reactivity).

As a more recent concept, Lehmann et al. (2020) proposed that C persistence in soils is a result of the interactions of microbes and their substrate, which depends on the chemical diversity of the substrate and is subjected to variations in time and the heterogeneity of their habitat: Microbes favour molecules that have a higher concentration in soils, because investing in metabolizing rare compounds is energetically less rewarding. This leads to a higher general diversity of compounds and with that a higher cost and lower benefit associated with their decomposition, increasing the overall persistence of C. Fluctuations in time (e.g., soil water content or temperature) and spatial heterogeneity can further influence this interaction positively or negatively, and together this "functional complexity" (Lehmann et al., 2020) could be used to explain and predict carbon accumulation in soils.

Carbon Pools in Soils

Models generally divide SOC into three pools with different turnover times, often defined as the "active", "intermediate" and "passive" pool (e.g., Swanston & Trumbore, 2009). The active pool consists of undecomposed material or material in the early stages of decomposition such as plant litter, microbial necromass or root exudates that have a turnover time of "hours to months to years" (Swanston & Trumbore, 2009). As the probability of protection increases with decreasing particle size (see above), turnover time increases to "decades to centuries" (intermediate pool, Swanston & Trumbore, 2009) or even "thousands of years" (passive pool, Swanston & Trumbore, 2009). These pools have different sizes, with the "passive pool" is thought to contain most of the SOC (Schnecker et al., 2016).

Different C pools in soils can be isolated in laboratories by using physical and chemical fractionation techniques. Chemical separation methods were often used in soil science to isolate humic substances that were thought to constitute the largest part of SOM. However, in the last decades this view was challenged and today, physical separation

methods are seen as a better way to gain representative SOM fractions (Baveye & Wander, 2019; Lavallee et al., 2020; Lehmann & Kleber, 2015). Fractions derived from separation with a density solution, e.g., sodium polytungstate (SPT, $Na_6[H_2W_{12}O_{40}]$, ρ = 1.6 – 2.0 g cm^{-3}), are often associated with different SOM pools, and be used to infer active, intermediate and passive soil pools used in models. Their amount, C content, isotopic composition, as well as results from experiments with these fractions may be used to calibrate models (Crow et al., 2007; C. Poeplau et al., 2013; Von Lützow et al., 2007; Zimmermann et al., 2007). In a first step, a light fraction with a density lower than 1.6 to 2 g cm^{-3} is isolated. This fraction is mainly contains POM and is comparable to the active pool, consisting of relatively fresh plant inputs with a low turnover time (Zimmermann et al., 2007). The intermediate pool is represented by plant material (POM) in later stages of decomposition that has been protected from further decomposition by occlusion within soil aggregates. After the light fraction is removed, this occluded fraction is usually isolated by ultrasonication to disperse aggregates and a further SPT step. The remaining material (also called the heavy fraction) with a density greater than 1.6 to 2 g cm^{-3} consists of the mineral-associated OM (MaOM) and sand particles, which can be further separated by sieving to 63 µm. MaOM is regarded as slow-cycling (as discussed above) and comparable to the passive pool of models. There is also some OM contained in the sand-fraction (heavier than POM but larger than 63 µm). This fraction (together with dissolvable OM) is usually only a small proportion of total SOM and therefore usually not intensively investigated (Lavallee et al., 2020).

While this separation can be done on bulk soil, it is often done with previously isolated aggregate size classes to include the different roles of SOM stabilization that aggregates of different sizes have (Six et al., 2004). Tisdall & Oades (1982) proposed that there is a hierarchical order of aggregates in temperate soils: Macroaggregates (> 250 µm diameter) consisting of microaggregates (< 250 µm) plus organic molecules that bind these together. Microaggregates in turn consist of primary particles (silt and clay) mostly held together by electrostatic forces. They can also be formed inside of macroaggregates. POM can be included anywhere in this soil matrix, for example between microaggregates inside a macroaggregate or inside of a microaggregate (Wilpiszeski et al., 2019). Soil disturbance

can release stable microaggregates from macroaggregates which then can clump together to form new macroaggregates (Six et al., 2000a). A combination of slaking (immersing dry soil in a defined volume of water for a specific amount of time) and wet-sieving (sieving with mesh sizes corresponding to aggregate size classes under water) can be used to isolate stable aggregates of different sizes (Von Lützow et al., 2007).

Elevated Temperature

According to kinetic theory, chemical reactions occur faster when temperature is increased and the availability of substrates is not limited (Arrhenius, 1889). The change in the reaction rate for every 10 °C change in temperature is defined as the Q_{10}-value. This value is used to describe the temperature sensitivity of SOM as it depends on the activation energy needed for decomposition and the temperature (Feng & Simpson, 2008):

$$Q_{10} = \frac{k_{T+10}}{k_T} = \exp\left[\frac{10 \times E_a}{R \times T \times (T+10)}\right] \quad (2)$$

With k being the reaction rate at the absolute temperature T (in K), E_a the activation energy needed for the reaction and R being the gas constant (8.314 J mol^{-1} K^{-1}). SOM decomposition rates should increase with increasing surface temperatures caused by climate change. This might cause a positive feedback-loop, in which C stocks of soils are reduced and the concentration of CO_2 in the atmosphere is further increased, which in turn further accelerates warming (Conant et al., 2011). Experimental evidence on this is however inconclusive and the response of SOM stocks to warming seems to be depending on a lot of factors, e.g., the ecosystem studied and the amount and length of warming (Poeplau et al., 2017) as well as the intrinsic temperature sensitivity of different SOM compounds present at a specific site (Davidson & Janssens, 2006).

Conant et al. (2011) created a framework to conceptualize how elevated temperature can affect the interactions of decomposers and their substrate within the soil matrix and how that affects sorption and desorption of mineral-associated organic matter. Depolymerization rates generally increase due to increased enzyme activity, which leads

to more assimilable substrates for microbes. Enzyme activity ultimately depends on both the concentration of enzymes and of available substrate. Their concentration is influenced by microbes which produce extracellular enzymes based on their energy and nutrient demands. If the already produced enzymes become more active (as long as there is enough substrate and enough OM is depolymerized), microbes might downregulate their production.

The microbial demand is also influenced directly by temperature. Microbial Carbon Use Efficiency (CUE), defined as C that is used for growth over C that is taken up (the fraction of assimilated substrate that ends up in microbial biomass; Dijkstra et al., 2011; Spohn et al., 2016) is thought to change with temperature. Higher temperatures theoretically increase microbial energy costs for maintenance which therefore favour respiration over growth, decreasing CUE and increasing CO_2 fluxes from soil to atmosphere. Over time however, lower CUEs might reduce microbial biomass and decrease OM decomposition on a bigger scale again (Allison et al., 2010). It has also been shown however, that CUE is irresponsive to warming in the short- and in the long-term (Walker et al., 2018). The effects of increased microbial activity on the CO_2 efflux in warmed soils are diminished by a smaller microbial biomass after the ecosystem reaches a new steady state (Walker et al., 2018).

The time that is needed for an ecosystem to reach a new steady state is often much longer than the usual time frame of soil warming experiments. In fact, most experiments track changes on a very limited time scale (years rather than decades). Results from years of artificial warming might not translate to similar ecosystem responses after decades of warming, which is much more relevant in the sense of anthropogenic climate change (Walker et al., 2020). While increased reaction rates might affect microbial growth and respiration in the short term, warming-induced shifts of microbial communities might only show after multiple years (Radujković et al., 2018). Evidence obtained from comparing soils that have been warmed since decades to soils warmed for only some years (Sigurdsson et al., 2016), shows that the often observed sharp increase in respiration following warming returns to values characteristic of ambient soil after some time (Pendall, 2018). Walker et al. (2018) has shown that, while microbial traits such as growth

or respiration remained elevated in communities subjected to decades of warming compared to ambient controls, normalizing these values to the microbial biomass resulted in no differences. This indicates that there was no adaptation of the microbial metabolism to warming, supported by the result that CUE remained stable with increased temperature in this experiment (Pendall, 2018) and that there was no shift in microbial community profiles obtained from amplicon sequencing of the same sites (Radujković et al., 2018). Modelling results based on this data shows that reduced substrate availability might reduce microbial biomass in the long-term (Walker et al., 2018).

Warming likely increases microbial respiration (per unit of biomass) in the short term, this leads to reduced amounts of easily available substrates which in the longer run reduces microbial biomass. Assuming plant inputs remain stable over this time, a reduced active microbial biomass reduces the probability of microbes encountering and decomposing SOM. Changing soil moisture regimes with climate change can add to the disconnection of microbes and substrate. While the remaining microbes are more active than before, the initially increased CO_2 efflux from the ecosystem returns to previous levels. However, the soil net C balance is negative since the initially respired C does not re-enter the soil (Pendall, 2018). Although microbes are the main players regulating the soil-atmosphere feedback, these results show the importance of investigating substrate quantity and quality. When microbes cannot access or use OM in soils, they cannot respire it, regardless of temperature.

How increasing temperature affects the SOC-climate change feedback highly depends on the temperature sensitivity of the different pools. From an energetic point of view, the amount of energy needed for decomposition increases with increasing protection. The slow-cycling pool can therefore be characterized as having a higher activation energy than the fast-cycling pool. According to kinetic theory (see equation 2), the decomposition rate increases proportionally more with increasing temperature in the pool with higher activation energy compared to one with lower activation energy. Global warming therefore should affect the passive SOC pool that contains the highest amount of C more than the other SOC pools (Conant et al., 2011). This difference in temperature sensitivity is not considered in SOC models, since evidence is often missing or inconclusive (Knorr et

al., 2005; Christopher Poeplau et al., 2017). Model-based predictions of future SOC stocks and CO_2-fluxes to the atmosphere may therefore be too conservative and not accurately include SOC dynamics.

SOM Quality

The different origins of SOM (plant residues and exudates, animal products, microbial necromass and decomposition products) and constant biotic and abiotic transformations result in a chemically diverse mixture of molecules. Since each of these molecules has its own temperature sensitivity in theory (Davidson & Janssens, 2006), it is important to study the chemical composition of SOM to assess vulnerability of a specific site to climate change. While methods using (spatially resolved) spectroscopy can show elemental or molecular distributions directly embedded in soil architecture (Lehmann et al., 2008; Schlüter et al., 2019), their cost, effort and destructive nature make application on a large scale rather unfeasible (Wilpiszeski et al., 2019). Beside solid-state NMR, that has been widely used to assess the chemical composition of SOM (Chukov et al., 2018; Kögel-Knabner, 1997), different chemical degradation techniques can be used to further isolate compounds with specific properties (Von Lützow et al., 2007). However, chemical methods are usually selective by nature (Derenne & Quéné, 2015) and obtaining a holistic view of SOM quality is therefore subject to interpretation and can be labour-intensive. A method that is similar in its application as solid-state NMR spectroscopy is analytical pyrolysis gas chromatography mass spectrometry (Pyr-GC/MS). Pyr-GC/MS is a tool that can provide information on SOM on a larger scale (Derenne & Quéné, 2015). A sample is brought to a high temperature (in an oxygen-free atmosphere) where the complex molecules of SOM break up into smaller compounds, which can then be separated via gas chromatography and identified in a mass spectrometer. Some of these resulting compounds are characteristic for a specific type of the original macromolecule (e.g., for polyaromatics, lipids, lignin…), so the chemical composition of the original sample can be inferred. In addition, the substances derived from the pyrolysis can be used as a chemical fingerprint of the sample, and changes in this fingerprint with changing environmental conditions can then be used to gain insights into changes of SOM quality caused by environmental processes (Klein et al., 2020).

Elevated CO_2

Elevated atmospheric CO_2 concentrations affect gross primary productivity and plant growth and pose a major indirect effect of soil carbon cycling. For example, plants subjected to elevated CO_2 can keep their stomata closed more often to fix the same amount of C, which reduces evapotranspiration and increases their water-use efficiency. This reduced need for water by plants can alleviate drought stress in soils and maintain soil connectivity (Dieleman et al., 2012; Drigo et al., 2008; Kuzyakov et al., 2019). However, there are also more direct effects on SOM. Primary production generally increases under increased atmospheric CO_2 concentrations. This in turn leads to an increase of litter inputs and rhizodeposition (Drigo et al., 2008; Kuzyakov et al., 2019). This increase of soil C could be substantial and offset further anthropogenic CO_2 emissions in theory. For example, Schimel et al. (2000) modelled an annual increase of 0.08 Pg C in US soils mostly explained by CO_2 fertilization (for the period of 1980-1993).

This additional C in soils, however, may also stimulate the microbial community. In general, more labile C available for microbes (e.g., through increased rhizodeposition) will result in an increase in their biomass and activity (Drigo et al., 2008; Kuzyakov et al., 2019). This in turn might increase the decomposition of SOM (through the priming effect, Fontaine et al., 2003) and offset the increased input caused by eCO_2. The net C balance however in the end depends on a lot of factors such as the nutrient status of the soil (Kuzyakov et al., 2019).

Elevated atmospheric CO_2 concentrations may also change the quality of plant litter and exudates and can potentially influence microbial decomposition in this way (Drigo et al., 2008; Pendall et al., 2004). For example, plant tissue is generally exhibiting higher C:N ratios when grown under elevated CO_2 conditions compared to ambient conditions (Cotrufo et al., 1998). A reduced residue quality can decrease microbial decomposition (Six et al., 2001). However, according to stoichiometric theory, a higher resource C:N ratio also leads to larger losses of carbon from soil (Mooshammer et al., 2014; Zechmeister-Boltenstern et al., 2015). Soil aggregation can also be influenced by CO_2-induced changes of plant input. Six et al. (2001) investigated the effect of elevated CO_2 on soil aggregation

under different plant species (*Trifolium repens* and *Lollium perenne*). The higher-quality substrate of *T. repens* (higher quality meaning a higher N concentration of this rhizobial-associated species compared to *L. perenne*) resulted in a higher macro-aggregate turnover, while the low-quality input of *L. perenne* increased aggregation and occlusion of POM. The increase in aggregate turnover from increased high-quality *T. repens*-inputs was explained by a stimulation of microbial activity which increased the production of microbially-derived binding agents (supporting aggregate formation) but at the same time also depleted labile C-pools more rapidly, resulting in earlier degradation of these newly formed aggregates. The low-quality *L. perenne* substrate did not induce this priming effect, which resulted in the stabilization of OM. This shows that the effect of elevated CO_2 on SOM can vary strongly with plant species composition and therefore have contrasting results.

Combination of Climate Change Factors

The increased plant input could in theory offset the increased C output by a more active microbiome because of elevated temperatures. However, most data concerning the effect of elevated temperature or elevated CO_2 is derived from experiments that only manipulate one of these factors and does not necessarily take into account that such combined effects are interactive rather than additive (Dieleman et al., 2012). Additionally, each climatic factor can induce a nonlinear rather than a linear response, which is difficult to catch without intermediate treatments in experiments and adds another layer of complexity (Piepho et al., 2017; Zhou et al., 2008). The resulting effect of the combination of increases in both temperature and CO_2-levels is therefore difficult albeit very important to predict. Overall, the combination of both factors can result in additive, synergistic or antagonistic effects on a measured parameter compared to the effect of a single factor (Dieleman et al., 2012). An example for an additive effect would be the mentioned balancing-out of temperature-induced increases in decomposition rates and soil respiration by increased belowground plant input from higher atmospheric CO_2 concentrations (Pendall et al., 2004). The effect of one factor goes in one direction, the effect of the other factor in the opposite direction, the net result in the end is no change. In a synergistic interaction, the combined effect of two factors on one variable would be

larger than the effect of the individual factors alone, in an antagonistic interaction it would be lower (Mantyka-Pringle et al., 2019). If for example soil C stocks are higher in the combined treatment compared to the elevated CO_2-treatment alone, temperature could have a synergistic effect, additionally increasing belowground C-allocation (e.g., by reducing plant nutrient limitation through temperature-induced increased reaction rates and microbial activity). In contrast, increases in leaf area by both elevated CO_2 and temperature might overall increase evapotranspiration, reducing soil water content stronger than elevated temperature alone (Dieleman et al., 2012).

A meta-analysis by Dielemann et al. (2012) revealed that, when combining both factors, the effect of elevated CO_2 was generally stronger than that of temperature. The authors argue that this could be because of the larger relative increase of the CO_2-concentration compared to the relative increase in temperature, resulting in larger effect sizes for CO_2. This would however be in line with projected climate change. Simple additive interactions were rare, so informing models based on results of single-factor experiments could over- or underestimate an ecosystem's response to environmental change. The authors also recognized that their study was impaired by a lack of data, further emphasizing the need for multifactorial experiments that combine treatments. Overall, there still is a lot of controversy on combined or interactive effects of climatic factors on SOM dynamics (Dieleman et al., 2012; Ma et al., 2020; Song et al., 2019; Yue et al., 2017), and understanding them better is necessary for improved predictions.

Understanding how soil C processes will change in a future climate is important for predicting future atmospheric CO_2 concentrations and thus global temperature. Future climate change effects are governed by the complex interplay of increased plant species compositions and productivity and microbial decomposition within the three-dimensional soil matrix, which is controlled by a variety of SOM protection mechanisms. Although the overall results will likely differ from ecosystem to ecosystem, studies that elucidate the response of different SOC fractions to combined warming and elevated CO_2 treatments are key to fine-tune the feedback mechanisms between SOC and climate warming. This shall lead to improved models that allow more accurate predictions and in turn inform policy decisions that help prevent further acceleration of anthropogenic climate change.

The goal of the study presented here, was to elucidate the effect of a combined warming and elevated CO_2 treatment on SOM storage, and SOM quality in different physical fractions of a temperate grassland soil. A combination of aggregate size class-separation, density fractionation and analytical pyrolysis-GC/MS was used on samples from a multifactorial climate-manipulation experiment to achieve this goal.

PART 2

Manuscript

Effects of climate change on chemical composition and carbon content of physical soil fractions

Introduction

Soil Organic Matter (SOM) stores about four times more C than the atmosphere and six times more than the global vegetation (Lal & Stewart, 2019). The biotic and abiotic processes that regulate SOM formation, transformation and decomposition link atmospheric C and Soil Organic C (SOC) (Liang et al., 2019). As continuously rising anthropogenic CO_2 emissions will increase global surface temperatures in the next decades (IPCC et al., 2014), the fate of SOM will play a crucial role, acting either as a source or sink for atmospheric C (Song et al., 2019). This will either amplify or alleviate consequences of climate change (IPCC Working Group I, 2013; Lavallee et al., 2020).

The soil-atmosphere feedback is regulated by the interaction of plant inputs and soil microbes. The microbial activity and with that SOM decomposition depends on environmental parameters such as pore connectivity (enabling gas exchange) or water and nutrient availability (Christensen, 2001). The physical, three-dimensional structure of soil is the habitat of microbes, enabling their interaction with substrate and ultimately the processes of SOM formation and decomposition (Bronick & Lal, 2005).

A soil structure model based on a hierarchical order of aggregates of different sizes was proposed by Tisdall & Oades in 1982: Primary particles of soil, such as silt (63-2 µm in diameter) and clay (<2 µm) clump together through electrostatic forces and form micro-aggregates (miA, 63 µm – 250 µm) or silt and clay-sized aggregates (scA, < 63 µm). Polysaccharides produced by soil biota, such as root mucilage or microbial extracellular substances, act as organic binding agents, forming stable macro-aggregates (maA, > 250 µm) out of miA (Six et al., 2000a). Through decomposition of binding agents or through (physical) stress events (e.g., drying-rewetting cycles (Navarro-García et al., 2012) or tillage (Six et al., 2000a)), maA are constantly turned over (Six et al., 2000a). miA in turn are thought to be a more stable sink for SOM and can stabilize it for longer times (Lehmann et al., 2007).

Models that predict the response of soil carbon stocks to climate change often partition SOM into three pools: An active pool with a fast turnover, an intermediate pool and a

passive pool with a slow turnover (Swanston & Trumbore, 2009). These modelled pools do not directly correspond to any measurable soil carbon pool (Poeplau et al., 2018), but physical methods are used to isolate soil fractions that act as proxies for these pools (Crow et al., 2007; C. Poeplau et al., 2013; Von Lützow et al., 2007; Zimmermann et al., 2007). An established method to isolate physical fractions is the use of a density agent (e.g., sodium polytungstate, SPT) in combination with a dispersion step (e.g., ultrasonication) to destroy aggregates (Zimmermann et al., 2007).

Physical fractions contain organic matter in different stages of decomposition and levels of protection: Free Particulate Organic Matter (fPOM) or plant-derived organic matter between aggregates, occluded or intra-aggregate POM (iPOM), and mineral-associated OM (MaOM), that mainly stems from processed (microbially-derived) material. The stability of OM, or the resistance towards microbial decomposition, is thought to differ between these fractions (Lützow et al., 2007): fPOM, consisting mostly of relatively fresh plant inputs is easily available for microbes and represents the most active pool. iPOM is similarly plant-derived, however it is occluded within larger soil structures (aggregates) and therefore physically disconnected from and unavailable to decomposers (Don et al., 2013; Zimmermann et al., 2007). Aggregate turnover releases the occluded POM and make it available for decomposition (Six et al., 2000a; Zimmermann et al., 2007). Physical protection increases the residence time of iPOM in soil compared to fPOM, making it comparable to an intermediate SOM pool. MaOM represents the passive pool, because of the high activation energy that is thought to be needed to decompose OM that is adsorbed to minerals, making it unfavourable as an energy source for microbes (Zimmermann et al., 2007).

Density fractionation can be performed on bulk soil or on previously isolated aggregate size classes. The latter has the advantage of combining information on soil structure and the properties of aggregates of different sized with that of different SOM pools, possibly improving model predictions.

The multiple pathways of SOM formation as well as constant biotic and abiotic transformations result in a highly complex and diverse mixture of molecules (Derenne &

Quéné, 2015). If these formation processes are accelerated or slowed down by climate change, the chemical composition can change as well. Characterizing the chemical composition of OM might therefore give indirect insights into changes to the underlying SOM processes.

Older, more decomposed SOM (e.g., MaOM) generally consists of more microbially-derived N-containing compounds such as peptidoglycans or chitin and microbial polysaccharides than younger POM, which typically contains more lignin, phenols and alkanes (Geng et al., 2019; Schnecker et al., 2016). Thus, the chemical composition of SOM shifts from being having a more plant-derived chemical signature to a more microbial-derived signature over time.

The methodology used to describe the chemical composition of OM changed from chemical degradation to spectroscopical methods in the past decades (Kögel-Knabner, 2017). One of the spectroscopic methods is analytical pyrolysis, where a soil sample is heated in the absence of oxygen. This breaks up the chemical bonds of high molecular weight compounds, resulting in smaller, volatile substances that can then be separated and analysed in a GC/MS system (Derenne & Quéné, 2015; Kögel-Knabner, 2000). A fingerprint of the original chemical composition of a sample can be constructed from the relative abundances of the pyrolysates afterwards. Some substances can be further assigned to certain origin classes (such as lipids, carbohydrates or aromatics), which adds more ecological information (Derenne & Quéné, 2015). Pyrolysis-GC/MS was used to analyse the chemical composition of SOM in previous studies. This was for example done to characterize SOM in NaOH-extracts from different ecosystems (Vancampenhout et al., 2009), to elucidate the difference of SOM pools in density fractions (Poirier et al., 2005) and to investigate the effect of warming on the SOM chemical composition in different soil fractions (Schnecker et al., 2016). Since only minimal sample preparation is necessary and data analysis can be automated, Pyrolysis-GC/MS provides a way to quickly fingerprint SOM and detect changes to its chemical composition (Klein et al., 2020).

An example on how to use this data would be the detection of a shift towards a lower abundance of plant-derived products with a warming treatment. This could hint at

temperature-induced higher microbial activity, processing more plant-derived material than before (Schnecker et al. 2016). A lower relative abundance of an individual compound or origin class can however also be interpreted as lower input of source material (Muñoz et al., 2008; Vancampenhout et al., 2009). In the example above, lower plant productivity by drought stress induced by higher temperatures could in theory also be the cause. So, while relative abundance data gives an overview on the chemical composition and differences between samples, establishing a causal link or quantification is difficult without additional measurements.

Chemical reactions occur faster at higher temperatures as long as there is no substrate limitation (Arrhenius, 1889). From a strictly chemical point of view, the projected increase in surface temperature (1.5°C to 2°C at the end of the 21st century, IPCC et al., 2014) should also increase SOM decomposition rates. Microbially-produced extracellular enzymes are more active at higher temperatures so more OM may get depolymerized and could be respired (Conant et al., 2011). This would in turn cause a positive feedback-loop, further increasing atmospheric CO_2 concentrations and temperature (Conant et al., 2011).

As described above, the decomposition rate of a specific substrate is dependent on its molecular structure and its intrinsic temperature sensitivity (Davidson & Janssens, 2006), as well as its availability. Since the different pools represent OM in different stages of decomposition, the chemical composition and with that the temperature sensitivity varies. Evidence for different temperature sensitivities and how SOC stocks changes in soil fractions with eT is often inconclusive, which is why it is not incorporated into models (Knorr et al., 2005; Poeplau et al., 2017). A possible reason for this is that the mechanisms behind stock changes and temperature sensitivity is not fully understood. Including these mechanisms into ESM or LSM models could however be a crucial, since the passive pool (that stores the most C; Christensen, 2001; Schnecker et al., 2016) could be the most sensitive to increases in temperature (Conant et al., 2011).

The protective capabilities of aggregation and soil minerals for SOM decomposition influence the response to eT. OM inaccessible to microbes or enzymes because of occlusion within aggregates or a too high activation energy because of mineral protection

might be unaffected by temperature increases (Conant et al., 2011). Unprotected OM pools such as free POM should therefore be more susceptible to increased enzymatic activity (Conant et al., 2011) and might be depleted first. While by-products of microbial decomposition might first act as binding agents which increase aggregate stability (Jastrow, 1996; Six et al., 2000b), these molecules might themselves then be decomposed when easily-available substrate becomes depleted after the short first burst of decomposition, reducing aggregation under eT (Grunwald et al., 2016).

A lower substrate availability when labile substrates are becoming depleted might then also reduce the active microbial biomass (Allison et al., 2010). A lower number of active cells, less labile C or a lower soil connectivity due to decreased soil water content (Schimel, 2018) could induce a substrate-limitation effect, where soil respiration rates return to unwarmed levels (Walker et al., 2020).

An anthropogenic elevated atmospheric CO_2 concentration (eCO_2) does not only increase surface temperatures, it also directly influences plants and belowground carbon allocation. Plant primary production generally increases under eCO_2 (Kuzyakov et al., 2019). This also increases litter- and root-derived C input into soils (Drigo et al., 2008; Kuzyakov et al., 2019). If this additional soil C gets stabilized through mineral-association or occlusion and stays in the soil, C-losses from higher temperatures could be offset (at least partially, e.g. Schimel et al., 2000).

More microbially available C however may increase microbial biomass and with that the microbial demand for nutrients such as N and P (Kuzyakov et al., 2019). Depending on the nutrient status of the soil and plant-microbe interactions, this can lead to higher microbial activity (e.g., microbial N mining and subsequent SOM decomposition) and increased competition between plants and microbes, which can in turn hinder plant growth (Kuzyakov et al., 2019). If plants however dominate this competition, microbes can become nutrient-limited, which can in turn reduce SOM decomposition and increase soil C storage (Hu et al., 2001).

Elevated CO_2 changes the plant stoichiometry and OM quality, which also influences SOM dynamics (Drigo et al., 2008; Pendall et al., 2004). Plant tissue grown under eCO_2 for

example can have a higher C:N ratio compared to control plants under ambient conditions (Cotrufo et al., 1998), resulting in a reduced plant litter quality and a decreased microbial decomposition (Six et al., 2001). As microbial activity in part controls soil aggregation (through the production and decomposition of binding agents), the soil structure and physical protection of OM is influenced by substrate quality. For instance, lower-quality substrate (in terms of a lower C:N ratio) stemming from *L. perenne* was shown to increase macro-aggregate stability and OM stabilization through reduced microbial decomposition compared to substrate from *T. repens*, which had a higher C:N ratio (Six et al., 2001).

These examples show that the net effect of eCO_2 and eT on SOC storage is context-dependent and may differ for each ecosystem. Different plant species might react differently to eCO_2, depending on their physiology and soil nutrient and water status. Similarly, the net effect of elevated temperature on SOM pools in the end depends on both substrate availability (temperature sensitivity, plant productivity/inputs, physical and chemical protection, soil connectivity) and increased enzymatic reaction as well as microbial respiration These complex combinations of factors complicates the prediction of future SOM stocks in an overall warmer climate with higher atmospheric CO_2 concentrations.

Another layer of complexity is added when considering that most of the discussed effects of eT and eCO_2 are derived from single-factor experiments only (Dieleman et al., 2012; Song et al., 2019). As ecosystems will be subjected to elevated levels of both temperature and CO_2, possible combinatory effects have to be taken into consideration (Dieleman et al., 2012). These can differ from the effect of a single factor and can be additive, synergistic or antagonistic (Dieleman et al., 2012; Ma et al., 2020; Mantyka-Pringle et al., 2019; Pendall et al., 2004). There is a lack of data on combined effects of eT and eCO_2 on ecosystems in general (Dieleman et al., 2012; Ma et al., 2020; Song et al., 2019) and on C storage in soils especially (Yue et al., 2017). Using results from single-factor experiments to predict an ecosystem's response to climate change ignores possible interactive effects (Dieleman et al., 2012; Ma et al., 2020), so understanding them is necessary for accurate predictions.

Meta-analyses on experiments that manipulate multiple environmental factors so far yielded inconclusive results (Ma et al., 2020). Depending on the methodology used and the variables examined, they found that complex, non-linear interactions of environmental factors were either frequent (Dieleman et al., 2012; Leuzinger et al., 2011) or rare (Song et al., 2019). A recent review analysed the effect of multiple environmental factors in different combinations on terrestrial C pools (Yue et al., 2017): Soil C pools were much less sensitive to the combination of eT and eCO_2 compared to plant biomass. Warming decreased soil C, eCO_2 increased it (Yue et al., 2017). The authors suggested that the combined effect may be additive, resulting in no significant net change of soil C in the combined treatments. Whether this result is meaningful in the context of climate change is however questionable, since the authors also acknowledge the lack of data and the differences in experiments and ecosystems.

Although a lot of experiments that focus on the response of SOM to changing environmental factors were done in the past decades, there still is no consensus of the scientific community about the fate of SOM pools in a future climate, as the results were often contradicting (Song et al., 2019). A synthesis by Sulman et al. (2018) for example found that while most models predicted an increase of the CO_2-flux from soils to the atmosphere and a decline of SOC stocks with warming, experimental results often opposed these predictions. It must be noted however, that almost no long-term studies are available that allow to verify model predictions. So, either some of the key mechanisms are missing in the models, or short-term experiments fail to predict long-term responses well enough. One of the key mechanisms that is not well represented in ESMs is the individual response of different SOM fractions to climate change factors (Sulman et al., 2018). Recent studies investigated the effects of multiple environmental factors in different combinations on C dynamics in soil aggregates (Bai et al., 2020; Chen et al., 2019). The combined effects of eT and eCO_2 on soil C pools, especially regarding changes in soil aggregation and the chemical composition of organic matter and how they might influence physical fractions with different functionalities, are not yet sufficiently studied. Combining techniques to separate SOM into different pools with measurements of their chemical composition such as pyrolysis-GC/MS has the potential to give insights

into the underlying mechanisms of SOM formation and their response to changing environmental conditions (Six & Paustian, 2014).

We made use of a multifactorial climate manipulation experiment in Austria to investigate the combined effect of elevated temperatures and elevated atmospheric CO_2 concentrations on the amount and chemical composition of SOM in different grassland soil aggregate size classes and their density fractions. Specifically, we addressed the following research questions:

1) What effect does eT, eCO_2 and the combination of both factors have on soil aggregation and the distribution of SOM between mineral-associated and particulate OM?
2) Does climate change affect the chemical composition of SOM in different aggregate size classes and their physical fractions?

We broke down these research questions into the following hypotheses:

(H1) The weight proportion of macro-aggregates and total soil C will increase in eCO_2-treatments. We additionally expect that elevated temperatures will increase the decomposition of labile OM and thus lead to reduced fPOM levels as well as a lower proportion of stable macro-aggregates and overall lower bulk soil C levels.

(H2) There is no net change in aggregation and total C content in the combined warming and elevated CO_2 treatment, as the effects of eT and eCO_2 are additive, cancelling each other out in the combined treatment.

(H3) The chemical composition of SOM in maA, miA and scA is different, with maA having a higher relative abundance of pyrolysis products associated with plant-derived OM (i.e., lignins, carbohydrates), and miA have a higher relative abundance of more processed or older OM (i.e., aromatics/phenols, lipids).

(H4) Within in each aggregate size class and mineral-associated fraction, warming reduces the signal of plant material, and eCO_2 increases it. However, these effects are additive, so no change will be seen in the combined treatments.

To test these hypotheses, we applied a combination of wet-sieving and physical fractionation of the resulting aggregates. We then measured the weight, carbon and nitrogen content and the associated stable isotope ratios and analysed the chemical composition of the organic matter in all fractions by pyrolysis gas chromatography mass spectrometry.

Material and Methods

The study was conducted in a multifactorial FACE-experiment ("Free-Air Carbon Dioxide Enrichment") in Austria to test the effect of elevated temperature and elevated atmospheric CO_2 concentrations on SOM in different physical soil fractions. Wet-sieving was used to separate bulk soil samples into different aggregate sizes. The obtained aggregate size classes were then subjected to a density fractionation using a sodium polytungstate-solution (SPT) at a density of 1.6 g cm^{-3}. The weight of each fraction was determined after drying at 60°C. C and N content as well as the isotopic signature ($\delta^{13}C$) were measured using an elemental analyser (EA 1110, CE Instruments) coupled to an isotope-ratio mass-spectrometer (IRMS, DeltaPlus, Finnigan). Pyrolysis-GC/MS was used to create a chemical fingerprint of samples and to detect shifts in chemical composition of organic matter between treatments. The experimental setup and methods used are described in detail below.

Experimental Site and Setup

The sites sampled for this study are part of the ClimGrass-experiment ("Grassland Carbon and Nutrient Dynamics in a Changing Climate") at the HBLFA Raumberg-Gumpenstein (47°29'38"N, 14°06'03"E). It is classified as an alpine grassland, with mean annual temperature being 8.2°C and the mean annual precipitation 1056 mm. The soil is

described as a Cambisol with a loamy texture (Deltedesco et al., 2019; Séneca et al., 2020). The experiment was established in 2007 and was designed for response-surface regression, containing 4 by 4 m plots (n = 54) with ambient, intermediate (+1.5°C, +150 ppm) and extreme (+3°C, + 300 ppm) levels of eCO_2 and eT treatments in all possible combinations (Piepho et al., 2017). A detailed description of the experimental setup can be found in the supplementary material of Deltedesco et al. (2019). In short, temperature was increased on the eT-plots with infrared heaters and eCO_2-plots were fumigated through rings which stream CO_2-enriched air onto the vegetation. For this study, we only used the data from plots with extreme treatment combinations: A control treatment with ambient temperature and atmospheric CO_2 concentration (n = 12), eT (+3°C above ambient temperature, n = 3), eCO_2 (+300 ppm above atmospheric CO_2 concentration, n = 3) and the combined treatment or "future climate" treatment eT x eCO_2 (+3°C and +300 ppm, n = 8). The intermediate treatments were excluded to reduce complexity and gain a clearer picture of climate change effects on the measured variables in the different fractions.

Sampling

Sampling took place in October 2018. Multiple cores (4 to 5) were taken from the top 10 cm and combined to yield approximately 100 g of fresh soil per plot. Big roots and visible stones were carefully removed manually, however samples were not sieved as to not further disturb the soil structure. For transport, samples were put into sturdy aluminium containers and covered with a cardboard lid to avoid compression of the soil. In the lab, the aluminium containers were opened and loosely covered with paper towels to allow the soil to air-dry over multiple days.

Slaking and Wet Sieving

The air-dried soil was submerged in deionized water on a 250 µm sieve for 5 minutes. Then, the sieve was moved 3 cm up- and down manually at a rate of 25 strokes per minute for 2 minutes. To ensure a similar sieving rate for each sample, a metronome was used. Floating organic material was manually removed with a coarse sieve and dried in a pre-

weighed petri dish. This yielded the “coarse particulate organic matter”-fraction (cPOM). The remaining fraction on the sieve (> 250 µm, macro-aggregates, maA) was washed into a pre-weighed petri dish and dried in a drying oven at 60°C for at least 24h. The sieving process was then repeated at the same rate (25 strokes per minute for 2 minutes, 3 cm height) with the fraction < 250 µm on a 63 µm sieve, yielding the micro-aggregate (miA) fraction. The fraction < 63 µm was left to settle in a large plastic pan. Afterwards, excess water was removed with a syringe, then the remaining fraction was transferred into multiple conical falcon tubes (50 ml) per sample and centrifuged (10,000 rpm ~ 10,286 *g* for 2 minutes). Excess water was removed again with a syringe. The material contained in the multiple tubes for each sample was then combined into one pre-weighed falcon tube and centrifuged again. Then it was dried in a drying oven at 60 °C over multiple days to obtain the silt & clay sized aggregates and free particles (scA in the following). The dry weight of all size classes (maA, miA, scA) was determined, a subsample was homogenized in a ball mill (Retsch MM200, 30 rps for 3 min) and subsequently analysed via EA-IRMS and Pyrolysis-GC/MS.

Density Fractionation

To isolate different density fractions of OM in the aggregate size classes, 35 ml of SPT solution (ρ = 1.6 g cm^{-3}, TC-Tungsten Compounds) was added to 5 g of maA and miA respectively in a 50 ml conical falcon tube (Greiner). In some cases, the wet-sieving yielded less than 5 g dry material (particularly in the miA-fraction), so here 3 g of soil were used together with 21 ml of SPT to maintain a ratio of 1:7 (w/v). The samples were then carefully inverted by hand 5 times and left to settle for one hour. After a centrifugation step (4,500 rpm; 3,083 *g* for 10 min; no deceleration step), the supernatant containing the fPOM-fraction (ρ < 1.6 g * cm^{-3} was carefully decanted onto a pre-weighed glass fibre filter (Whatman Glass Microfibre filter GFC) using a vacuum filtration unit. The fPOM on the filter was then thoroughly washed with deionized water to remove excess SPT. Material sticking to the walls of the filtration unit was washed carefully onto the filter or transferred there with a spatula. The falcon tubes containing the remaining soil was filled again to 35 ml (or 21 ml) with fresh SPT. After vortexing each sample for 60s to bring it into suspension, the aggregates were dispersed using a calibrated ultrasonication probe

(58 J ml^{-1}: 2.030 kJ for 35 ml; 1.218 kJ for 21 ml). To isolate the iPOM-fraction, the samples were centrifuged again (4,500 rpm; 3,083 *g* for 20 min; no deceleration step) after another resting period of 1 hour. Like in the previous step, the supernatant containing the iPOM was collected onto a pre-weighed glass fibre filter. The filters with the POM fractions were dried at 60 °C and weighed. Subsequently, the material was carefully scraped of the filter paper using a spatula and transferred into 3 ml snap-cap reaction tubes for storage. The heavy fraction ($\rho > 1.6$ g cm^{-3}) left in the falcon tube, consisting of sand- (> 63 µm) and silt & clay sized particles (< 63 µm), was washed multiple times by repeatedly filling the tube to 40 ml with deionized water, vigorous shaking by hand, centrifuging (2 min at 4,500 rpm; 2,083 *g*) and discarding the supernatant until it had a conductivity < 200 µS cm^{-1} (measured in the supernatant with a conductivity probe, Voltcraft LWT-01). This step was necessary to remove any leftover SPT from the sample. The heavy fraction was then also dried at 60°C. To separate sand and silt & clay, this fraction was then sieved to 63 µm. It was necessary to grind the material carefully using a mortar and pestle before sieving because of the hard crust that formed during the drying process.

The soil physical fractions yielded from each aggregate size class therefore were fPOM, iPOM, silt & clay and the sand-fraction. For EA-IRMS analysis, the silt & clay sized fraction was weighed in directly into tin capsules (10 mg, in triplicates). Depending on the amount that was available, 2 mg or 0.5 mg of fPOM or iPOM, respectively, was used here. Samples were homogenized in a ball mill (Retsch MM200, 30 rps for 3 min) beforehand. If too little material was available for grinding, the samples were homogenized as good as possible with a spatula.

A subsample of the sand fraction was also milled, and 15 mg were used for EA-IRMS analysis. One sample of this fraction (from macro-aggregates) was additionally investigated microscopically using a stereoscope. For this, a small amount of dry and un-milled material was used.

Pyrolysis GC-MS

The chemical composition of density fractions and aggregate size classes was assessed using Pyrolysis GC-MS. For the fractions with a high C content (fPOM, iPOM) about 0.2 mg of finely ground sample material was weighed into pyrolysis glass tubes (DISC Pyrolysis Sample Tube, CDS Analytical). For milled bulk soil 0.6 mg and for milled bulk size classes and silt & clay sized fractions 1.5 mg of material were used. These amounts have been determined in pre-tests to yield chromatograms with the best peak separation and height. Samples were then pyrolyzed in a pyrolysator (CDS Pyroprobe 6200, CDS Analytical) by holding them at 50 °C for 5 seconds, then ramping the temperature up to 600 °C with a rate of 20 °C per second, where it was held for 20 seconds. The resulting pyrolysis products were flushed using 1 ml helium per minute into a GC-TOF-MS System (Pegasus BT, LECO) and the pyrolysis chamber was heated to 1,000°C for 15 seconds and flushed to clean it for the next sample. In the GC-System, a polar column (Supelcowax 10, Sigma-Aldrich) was used to separate the pyrolysis products. For this, the column was kept at 50 °C for 2 minutes and then gradually heated to 250 °C with a rate of 7 °C per minute, where the temperature was held for another 5 minutes. The ChromaTOF software (version 5.0, LECO) was used to identify peaks by their mass spectrum.

We developed a high-throughput semi-automatic approach for the analysis of the obtained chromatograms. For each sample type (e.g., silt & clay, POM or bulk soil) one reference sample was chosen visually that contains the most and best separated peaks. This reference chromatogram was analysed with a previously built inhouse library containing 120 substances, which can be assigned to a known origin in soil samples based on literature research (Tab. S9). We used the following classification for classes of origin: aromatics & phenols, carbohydrates, N-containing compounds, lignin-derived compounds, and lipids. These substances were previously identified by pyrolyzing soil standards and pure substances on our system and added to the library. We also included substances without a known origin if they occurred in many samples and contributed significantly to the overall peak areas; these substances are grouped in a class called “general”.

After automatically searching for all library peaks within the previously chosen reference sample, every hit was manually checked by comparing its mass spectrum to spectra from the NIST library (U.S. Department of Commerce National Institute of Standards and Technology) to confirm the identity of substances. The peaks of all other samples were then compared to those in the respective reference sample. This resulted in an aligned presence/absence list of the reference peaks for each sample with their corresponding peak area. All peaks with a signal to noise (S:N) ratio below 100 were removed from further analysis, as they, while having a low signal, contribute relatively more to the overall method error compared to peaks with higher S:N ratios (Dolan, 2009).

The obtained list of peaks for every sample were then further processed with R (version 3.6.2) using RStudio (version 1.2.5033, RStudio Inc.). A generalized full code example is provided as in the supplementary material (3). In short, peak area was normalized to the carbon content and amount of pyrolyzed sample, since higher C contents would generally lead to higher peak areas and baseline. To control for possible contamination of the pyrolysis system, a blank correction was performed by calculating the mean of the areas of substances contained in blanks (glass rods without sample; n = 6 per run) and subtracting this value from the respective substance area in each sample (for each run). The normalized and blank-corrected peak area was then treated like operational taxonomic units (OTUs) from phylogenetic analyses and the relative abundance of each peak in each sample was calculated using the “phyloseq” package (McMurdie & Holmes, 2013). Peaks were further annotated with their origin class and treatment. Peaks that were not included in the previously built library were assigned as “unidentified”.

Since manually choosing the reference sample is subjective and could introduce a bias, some data quality checks were implemented. “Unidentified” peaks that had a contribution > 1% of the total area were selected by our script and their mass spectrum was manually checked in the chromatograms. This made sure that our approach did not miss substances that were not included in our library but characteristic for the respective samples. Similarly, identified peaks that had a “match” score of 700 to 850 were manually checked to avoid wrong identification. The match score is calculated by ChromaTOF and gives information on how well the deconvoluted mass spectrum of a substance matches

the one in the library (on a scale of 0 to 1000). Previous testing revealed that hits with a match score below 700 were not necessarily reliable, so a hit was only assigned by the program when the score was above 700. Above 850 on the other hand, peak identification was deemed as reliable and only occasionally checked by hand.

This approach in the end yielded a presence-absence matrix containing the relative abundance of all reference peaks per sample type. Since we could not compare the unidentified peaks between reference samples (and therefore sample type), only the relative abundances of the substances contained in our library were used for further statistical analysis.

Calculations and Statistics

Using the EA-IRMS data as well as the dry weight of the obtained size classes, we calculated the proportion of C and N contained in each size class of the recovered amount of C and N in the bulk soil. Similarly, the C and N proportion of each density fraction of one aggregate size class was calculated based on the C and N sum of all density fractions of maA and miA respectively. Weight, as well as C and N recovery was estimated by subtracting the sum of all size classes (or density fractions) from the bulk soil (or bulk maA/mia respectively) values. We additionally calculated the C:N-ratio for each size class and density fraction by dividing the measured weight-% of C through that of N. The analysed variables based on the EA-IRMS measurements in the end were: Relative C and N content based on the sum of C and N in all size classes/fractions, C:N-ratio, δ^{13}C-value and the proportion of fumigation-derived C (see below). The relative N-content followed a similar pattern as C content and is therefore not described in detail in the following sections (for detailed data see Fig. S1 and Tables S1, S2 and S7).

All statistical calculations were done in RStudio using R. Since some of the sampled control and future climate plots were subjected to a drought treatment in 2017, a subset of the data containing only the ambient and future climate plots was tested for legacy effects of drought using type 2 ANOVAs. No significant effect of drought was detected, so these plots were included in their respective non-drought treatment in further analyses.

Linear mixed-effects models (function “lme” of package “nlme”, Pinheiro & Bates, 2013) were used to investigate the effect of the experimental factors (eT and eCO_2) on the measured variables in the different bulk aggregate size classes and density fractions. The plot identity (“Plot”) nested with what side of the experiment the plot is on (“Design”) was included as random effect. This controlled for inherent differences between plots as well as differences between the two sides (left and right) of the ClimGrass-experiment. These side differences were revealed by previous experiments and are likely because the two sides were established at different points in time (Deltedesco et al., 2020).

The complete model formula used was:

$$Variable \sim CO2 * T + (1|\frac{Plot}{Design})$$

Model residuals were checked for normality by visual inspection of the quantile-quantile plot and a Shapiro-Wilk test. If necessary, data was log-transformed, and outliers were removed to obtain normality. In data subsets (bulk size classes, density fractions) where significant model terms were present, a Tukey-HSD post-hoc test was done with the function “emmeans” of package “emmeans” (Lenth et al., 2021) to check if fractions differed significantly from each other.

In some cases, additional statistical tests were performed to validate the model results. Specifically, type 2 ANOVAs with a Tukey-HSD post-hoc test were performed when a large increase or decrease in the mean of a variable was deemed non-significant by the lme-model.

The CO_2 used for fumigating the eCO_2-plots is depleted in ^{13}C relative to atmospheric CO_2 and therefore has a $\delta^{13}C$-signature that strongly differs from the isotopic composition of the atmosphere. Thus, the $\delta^{13}C$-value of fractions on eCO_2-plots can be used to estimate the amount of “new” C incorporated into these fractions since the beginning of the experiment. The proportion of “new” C was calculated with an isotopic mixing model according to Carrillo et al., 2018:

$$Proportion\ of\ new\ C = \frac{\delta^{13}C_{Fraction} - \delta^{13}C_{Control}}{\delta^{13}C_{Root} - \delta^{13}C_{Control}} \times 100$$

With $\delta^{13}C_{Fraction}$ being the measured δ^{13}C-value of each fraction in the eCO_2-plots, $\delta^{13}C_{Root}$ the measured δ^{13}C-value of the root biomass in the eCO_2-plots and $\delta^{13}C_{Control}$ the δ^{13}C-value of the respective fraction in unfumigated control plots. Differences in the proportion of new C between the aggregate size classes and density fractions were also evaluated with LMEs, using "fraction" and "temperature" as model parameters. Since this was only possible to calculate on fumigated plots and those were almost all on the same side of the experiment (9 out of 11 plots total), we only included the plot identity as random term to keep the model as simple as possible. We were able to test for the effect of temperature because we calculated this value on all plots exposed to +300 ppm CO_2, including those that were additionally warmed (the future climate treatment). Models were calculated using all data, as well as for subsets containing either all size classes or the density fractions of maA and miA respectively. To see which fractions contained significantly more or less new C than others, a Tukey-HSD post-hoc test was again performed.

The pyrolysis-GC/MS relative abundance data of library substances was used to calculate a non-metric multidimensional scaling (NMDS) based on a Bray-Curtis dissimilarity matrix (function metaMDS of package "vegan"; Oksanen et al., 2019). A permutational analysis of variance (PERMANOVA) was used to identify significant differences in the chemical composition of the soil aggregate classes or density fractions, also in combination with treatment. This was done for similar sample types each: All bulk size classes, all POM-fractions and all silt & clay-sized fractions. Additionally, treatment differences within each fraction were investigated by calculating a NMDS containing the data from only one fraction (e.g., macro-aggregate fPOM) and running a PERMANOVA on this subset. The relative abundance of all individual compounds was also z-transformed across similar samples (bulk size classes, silt & clay-sized fractions, POM-fractions) and heatmaps were drawn based on the calculated z-score to visualize which size classes or fractions had higher abundances of certain compounds.

Results

A combination of slaking and wet-sieving was used to isolate four different size classes from sampled bulk soil (Fig. 1): Coarse POM (cPOM), macro-aggregates (maA, > 250 µm); micro-aggregates (miA, 63 µm – 250 µm); and silt and clay sized aggregates (scA, < 63 µm). For each plot, a subsample of maA and miA each was then separated into fPOM, iPOM and a heavy fraction via ultrasonication and density fractionation with sodium polytungstate (ρ = 1.6 g cm^{-3}). A sieving step was included to further separate the heavy fraction of the maA and miA into silt & clay- (< 63 µm) and sand-sized (> 63 µm) particles. C- and N-content and the isotopic signature ($\delta^{13}C$) was determined by EA-IRMS analysis in bulk soil, all size classes and density fractions. Since the sand-sized fraction contained larger amounts of C and N than expected, both parts of the heavy fraction were treated as a separate mineral-associated OM pool each (sand-associated OM and silt & clay-associated OM, SaOM and CaOM in the following).

Wet Sieving and Density Fractionation

An average of 98.58 ± 1.08 % of used bulk soil was recovered after wet sieving. The difference could be dissolved organic matter (DOM), but we did not measure this pool directly. Therefore, we cannot differentiate it from other losses, so we did not treat it as its own fraction. In the plots with ambient treatment, maA was the most prominent size class, followed by miA, scA and cPOM (Tab. 1a). Elevated CO_2 had a significant effect ($p < 0.05$) on the proportion of maA and miA, which was greater than ambient levels in eT x eCO_2 for maA, and lower for miA. A Tukey post-hoc test revealed that this difference was marginally significant ($p = 0.069$ for the maA increase and $p = 0.064$ for the miA decrease, see Tab. S5). The weight proportion of other size classes was not affected by treatment.

After density fractionation, 99.02 ± 0.67% of maA and 99.62 ± 0.06% of miA were recovered on average. Weight-wise, CaOM was the most dominant fraction in maA of ambient plots, followed by SaOM, while fPOM and iPOM were similar, but at lower levels (Tab. 1b). The weight proportion of fPOM was increased by about 36% on the eT plots and 114% on eT x eCO_2 compared to the proportion on ambient plots.

The influence of temperature on the mass of this fraction was marginally significant ($p = 0.098$), the one of CO_2 was significant ($p < 0.05$). Similarly, the weight proportion of iPOM was increased on eCO_2 and eT x eCO_2 by 55% and 46% respectively. CO_2 significantly affected the weight proportion of the iPOM in maA ($p < 0.01$). There were no other significant effects of treatment on the weight distribution of maA density fractions.

In miA, silt & clay and sand were at more similar proportions compared to those of maA (Tab. 1c). The proportion of fPOM and iPOM was lower and unaffected by treatment. Temperature influenced the proportion of silt & clay and sand significantly ($p < 0.05$). Compared to ambient, more silt & clay and less sand was found on eT and eT x eCO_2 plots (+4.04% and +4.30%, and -4.36% and -4.28% respectively).

Carbon content

Average C recovery was 103.01 ± 2.98% for size classes, 93.59 ± 4.08% for maA fractions and 97.52 ± 2.36% for miA fractions. The total C of the bulk soil was slightly increased in all treatments (Fig. 2a). We however did not detect a significant overall effect of eT or eCO_2 (Tab. 2a). This absence of a significant effect was further confirmed with a 2-way ANOVA (data not shown). The majority of C was contained in maA, followed by miA, scA and cPOM (Fig. 2d). Treatments did not significantly affect the distribution of bulk soil C between size classes. The bulk soil C:N ratio was significantly increased by eCO_2 ($p < 0.001$) on eCO_2 and eT x eCO_2 plots. The miA C:N ratio was significantly decreased by temperature on the eT plots ($p = 0.042$). The C:N ratio of all other size classes was unaffected by treatment (Tab. S1).

Bulk carbon in maA was slightly increased on eT and eCO_2 plots (Fig. 2b), however not significantly affected by treatments (Tab. 2b). Most macro-aggregate C was found in CaOM, followed by SaOM, iPOM and fPOM. In eT x eCO_2, iPOM-C was at a similar level

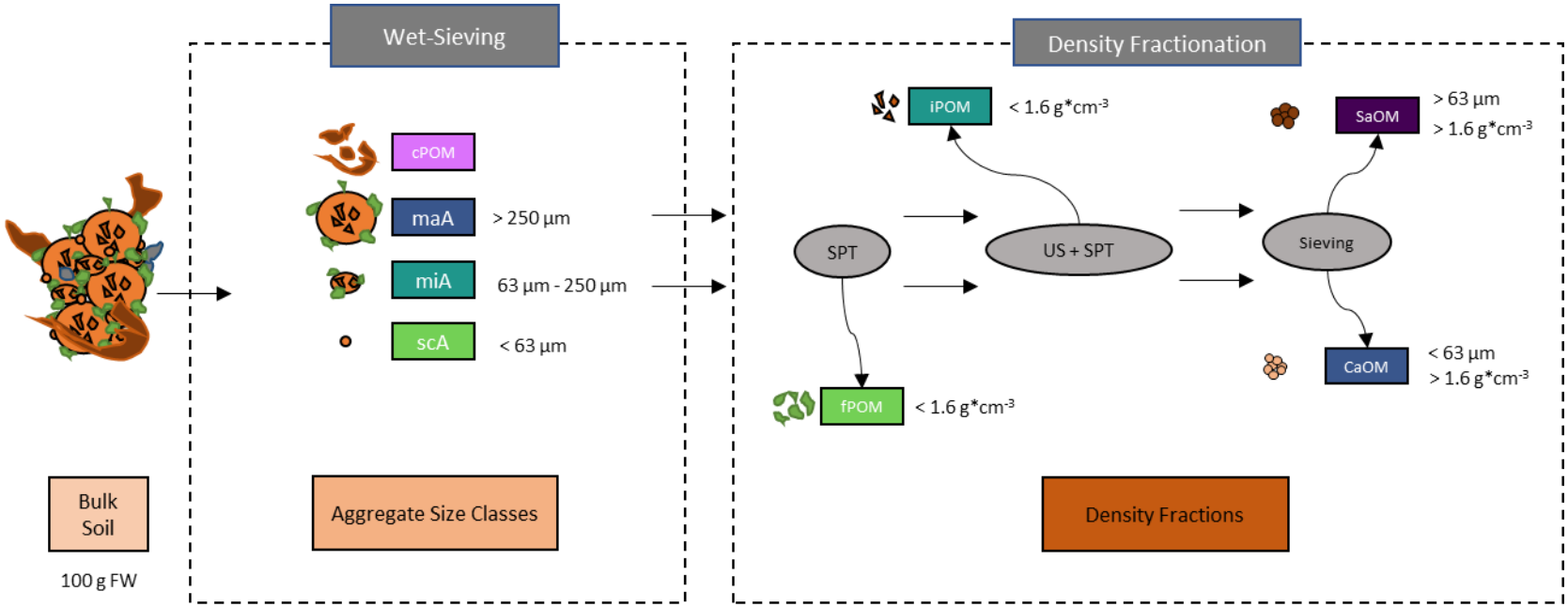

Figure 1: Schematic of the used size class separation and density fractionation approach. 100 g of fresh soil was air dried and wet-sieved to obtain aggregates of different sizes (cPOM: Course POM, maA: Macro-aggregates, miA: Micro-aggregates, scA: Silt & Clay-sized aggregates). 5 g of maA and miA were subsequently fractionated using sodium polytungstate (SPT, $Na_6[H_2W_{12}O_{40}]$) with a density of 1.6 g cm^{-3} and a ultrasonication step (US, 58 J ml^{-1}). This divided the sample into the light fraction (containing free POM (fPOM) and intra-aggregate POM (iPOM)) as well as the heavy fraction. After drying, the heavy fraction was sieved to 63 µm to differentiate between Sand-associated and Clay-associated OM (SaOM and CaOM). In addition to the dry weight, C-content, N-content as well as the isotopic signature ($\delta^{13}C$) was determined using EA-IRMS for each bulk size class and density fraction. Pyrolysis-GC/MS was further used to fingerprint the chemical composition of size classes and fractions.

Table 1: Weight distribution of size classes (a) and maA/miA density fractions (b-c) by treatment. Weight-% values are mean ± standard error (n = 26). Corresponding model results (F-value and p-value, degrees of freedom = 22) are shown on the right side of the table. Significant model factors (CO_2, temperature (T) and the interaction term (T x CO_2)) are marked in bold (α = 0.05). The column "Transf." marks cases where a data transformation was necessary to obtain a normal distribution of model residuals (log = logarithmical transformation).

a)	Weight by Treatment (in % of total weight)				eCO_2		eT		eT x eCO_2		
Size Class	Ambient	eT	eCO_2	eT x eCO_2	F	p	F	p	F	p	Transf.
maA	79.43±1.28	78.58±4.63	79.88±0.99	84.41±0.99	5.595	**0.027**	0.774	0.389	1.905	0.181	
miA	14.85±1.02	15.05±3.26	13.90±1.17	10.75±0.86	5.960	**0.023**	0.782	0.386	1.122	0.301	
scA	5.47±0.23	6.20±1.44	5.84±0.30	4.63±0.20	2.898	0.103	0.747	0.397	4.038	0.057	log
cPOM	0.26±0.06	0.17±0.06	0.38±0.15	0.21±0.03	0.224	0.641	2.636	0.119	0.147	0.705	log

b)	Weight by Treatment (in % of total maA weight)				eCO_2		eT		eT x eCO_2		
maA	Ambient	eT	eCO_2	eT x eCO_2	F	p	F	p	F	p	Transf.
fPOM	1.28±0.23	1.74±0.43	1.36±0.16	2.74±0.58	5.064	**0.035**	2.994	0.098	0.771	0.389	
iPOM	1.32±0.15	1.10±0.08	2.06±0.26	1.93±0.23	10.326	**0.004**	0.509	0.483	0.037	0.850	
CaOM	56.91±0.71	51.99±4.64	56.19±3.24	55.24±1.43	0.069	0.795	2.491	0.129	1.062	0.314	
SaOM	38.62±0.53	43.70±4.78	38.66±3.21	39.78±1.29	0.016	0.901	3.097	0.092	1.171	0.291	

c)	Weight by Treatment (in % of total miA weight)				eCO_2		eT		eT x eCO_2		
miA	Ambient	eT	eCO_2	eT x eCO_2	F	p	F	p	F	p	Transf.
fPOM	0.65±0.0.06	0.70±0.11	0.75±0.27	0.58±0.09	0.138	0.714	0.222	0.642	0.870	0.361	
iPOM	0.64±0.0.06	0.65±0.10	0.74±0.03	0.74±0.05	3.153	0.090	0.002	0.966	0.022	0.884	log
CaOM	47.86±0.65	49.80±1.16	46.30±1.99	49.92±0.65	0.592	0.450	6.849	**0.016**	0.656	0.427	
SaOM	49.49±0.67	47.33±1.26	50.83±2.04	47.37±0.61	0.672	0.421	6.779	**0.016**	0.371	0.549	

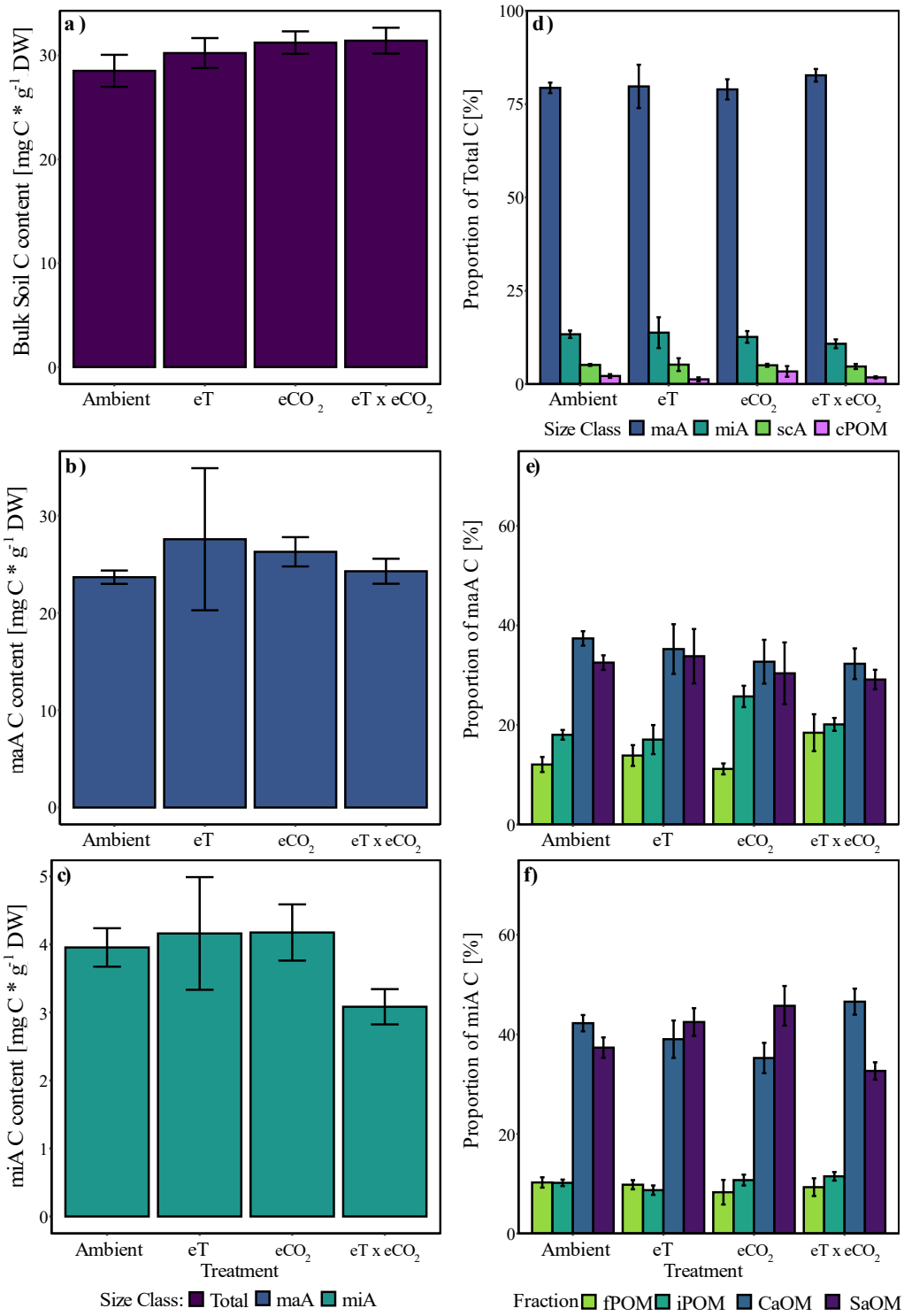

Figure 2: C content in mg C per g soil dry weight of bulk soil, bulk maA and bulk miA by treatment (a-c). LME model analysis yielded no significant effects of factors for these cases. Right side: Contribution of C in size classes to total C in bulk soil (d) and of density fraction C to total C of maA and miA respectively (e-f). Bars and error bars represent mean ± standard error. Corresponding LME model results are shown in Tab. 2.

as the ambient plots, however, the proportion of heavy fraction C (CaOM and SaOM) was lower, and fPOM-C was higher (Fig. 2e). There was no significant combined effect of eT and eCO_2 in the LME-model. eCO_2 significantly increased the proportion of C stored in maA iPOM (Tab. 2b). Temperature significantly decreased the maA fPOM and iPOM C:N ratios ($p = 0.032$ and $p = 0.018$, Tab. S2 and Fig. S2).

Bulk miA-C was reduced slightly, but non-significantly in eT x eCO_2 (Fig. 2c). The distribution between fractions differed from maA. miA contained less POM-C and more heavy fraction-C compared to maA (Fig. 2e-f). miA POM-C was not affected by treatments. While the proportion of C in CaOM was slightly decreased and C in SaOM was increased in eT and eCO_2 treatments (not significant), this pattern was flipped in the eT x eCO_2 treatment. A significant combined effect of both factors was found here in the LME model (Tab. 2c). miA CaOM C:N ratio was significantly increased on eCO_2-plots (CO_2 effect $p = 0.021$, Tab. S2). Microscopical analysis of the sand fraction revealed that it contained both clear quartz crystals as well as brownish-coloured ones and conglomerates of smaller particles (Fig. S3).

Incorporation of new C

At the sampling timepoint, roughly 4 years after the start of the treatment with elevated CO_2, the analysis of carbon isotope ratios showed that on average 18.48 ± 0.01% of bulk soil C has been derived from new carbon during these 4 years (Fig. 3a, panel 1). The factor "Size Class" had a significant effect on the proportion of new C ($p < 0.001$, Tab. 3). Bulk maA and miA were similar to bulk soil, while free silt & clay contained less new C (Fig. 3a). For all size classes, warmed plots contained less new C than ambient plots (temperature $p = 0.056$).

The factor "Fraction" significantly affected the new C content of maA and miA density fractions (Tab. 3, $p < 0.001$). In maA, the POM fractions contained a higher proportion of new C than the heavy fractions (Fig. 3b). In miA, this difference was also found, however it was overall smaller (Fig. 3c). There was no significant overall temperature effect. MiA new C was significantly affected by the interaction of "Fraction" and "Temperature"

($p < 0.01$). While the pattern observed from the bulk size classes (less new C on warmed plots) was also found in some density fractions of maA and miA, this difference was only significant for miA fPOM. Full post-hoc test results for the LME models can be seen in Tables S3 and S4.

Chemical composition

The NMDS based on the Pyrolysis-GC/MS data revealed that the aggregate size classes each formed its own separate cluster (Fig. 4a). scA had a larger variance compared to the other size classes. maA, miA and scA were differentiated mostly by the NMDS 2-axis, while cPOM was differentiated from all other size classes by NMDS 1. The PERMANOVA yielded a significant effect of "Fraction", while no treatment effects or the combined treatment and fraction effect were found (Tab. 4). The NMDS containing pyrolysis-GC/MS data from all fractions below 63 µm (scA and maA/miA CaOM, Fig 4b) showed a similar pattern. maA and miA CaOM was differentiated from each other by NMDS 2 and both from free silt & clay by NMDS 1. Only "Fraction" was significant, similar to the bulk size classes.

We did not find a significant influence of the factors eT, eCO_2 or eT x eCO_2 on the chemical composition within any investigated size class or fraction (Fig. S6-S8). The factor eCO_2 was marginally significant in the PERMANOVA for bulk micro-aggregates and macro-aggregate fPOM ($p = 0.086$ and $p = 0.062$ respectively). The same was true for the combination of eT and eCO_2 in bulk macro-aggregates ($p = 0.078$).

Table 2: LME model results (F- and p-value of included factors, df = 22) for C proportions between size classes (a) and density fractions (b for maA and c for miA). Bold values signify significant model factors (CO_2, temperature (T) and the interaction term (T x CO_2), α = 0.05). The column "Transf." marks cases where a data transformation was necessary to obtain a normal distribution of model residuals (log = logarithmical transformation).

a)	eCO_2		eT		eT x eCO_2		
Size Class	F	p	F	p	F	p	Transf.
maA	1.066	0.313	0.604	0.445	0.432	0.518	-
miA	1.952	0.176	0.130	0.722	0.396	0.535	-
scA	0.333	0.570	0.027	0.870	0.081	0.779	-
cPOM	0.543	0.469	3.789	0.065	0.020	0.889	log

b)	eCO_2		eT		eT x eCO_2		
maA	F	p	F	p	F	p	Transf.
fPOM	1.785	0.195	1.983	0.173	0.202	0.658	log
iPOM	6.847	**0.016**	3.419	0.078	1.832	0.190	-
CaOM	2.682	0.116	0.161	0.692	0.070	0.794	-
SaOM	1.695	0.207	0.001	0.980	0.178	0.677	-

c)	eCO_2		eT		eT x eCO_2		
miA	F	p	F	p	F	p	Transf.
fPOM	0.496	0.489	0.017	0.897	0.151	0.702	-
iPOM	2.466	0.131	0.154	0.699	1.130	0.299	-
CaOM	0.560	0.462	1.574	0.223	6.047	**0.022**	-
SaOM	0.738	0.400	1.457	0.240	9.640	**0.005**	-

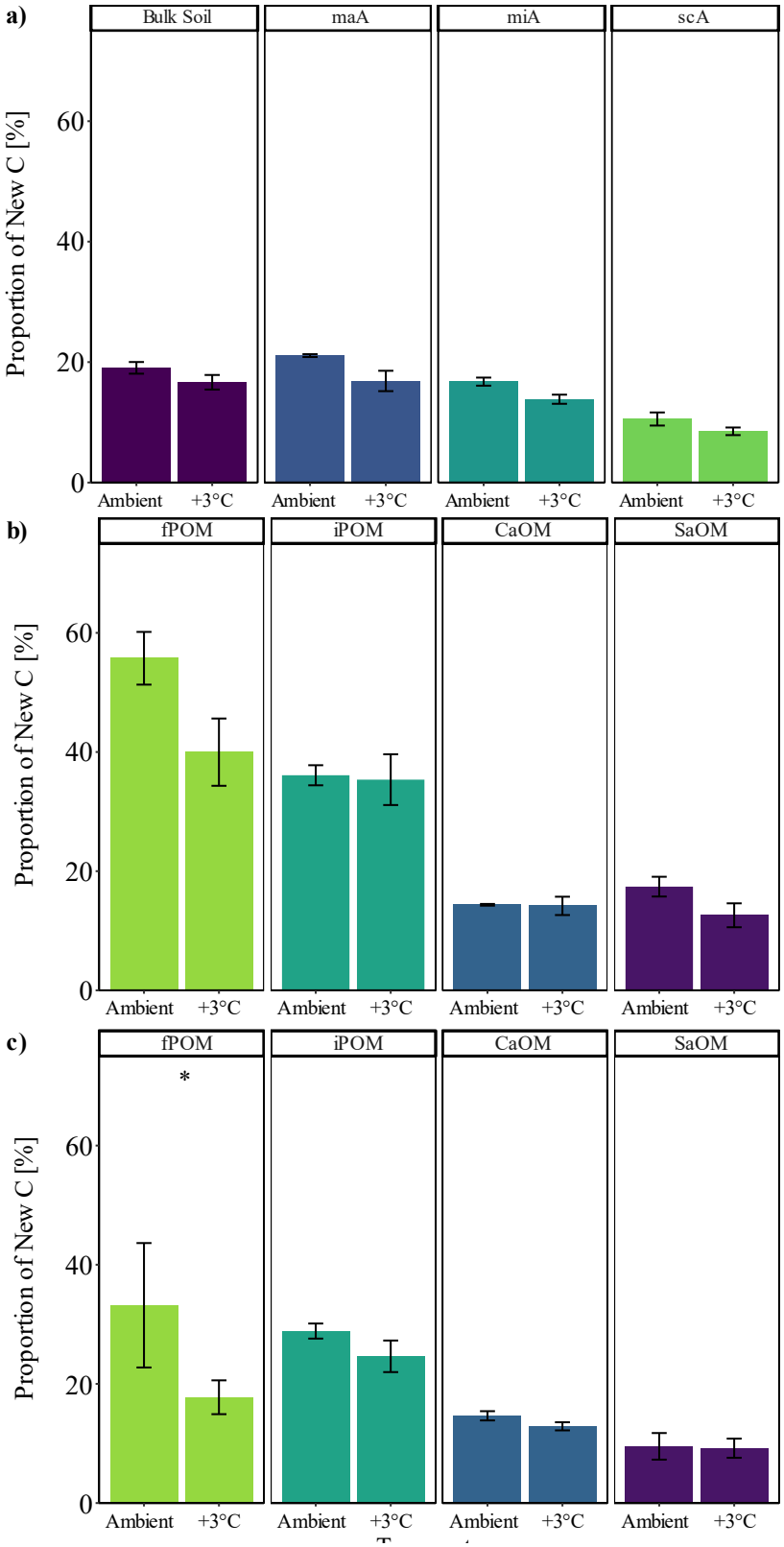

Figure 3: Proportion of new C (in % of total C) in size classes (a) and density fractions (b,c) on all fumigated plots (+300 ppm CO_2 above atmospheric CO_2 concentration) by temperature treatment (ambient temperature (n = 3) and +3 °C above ambient (n = 8)). Corresponding LME model results are shown in Tab. 3. Bars and error bars represent the mean ± standard error. Asterisks mark significant differences between ambient and warmed plots within one size class/fraction (Tukey post-hoc test, α = 0.05). Detailed post-hoc test results between all size classes/fractions can be viewed in Tables S3 and S4.

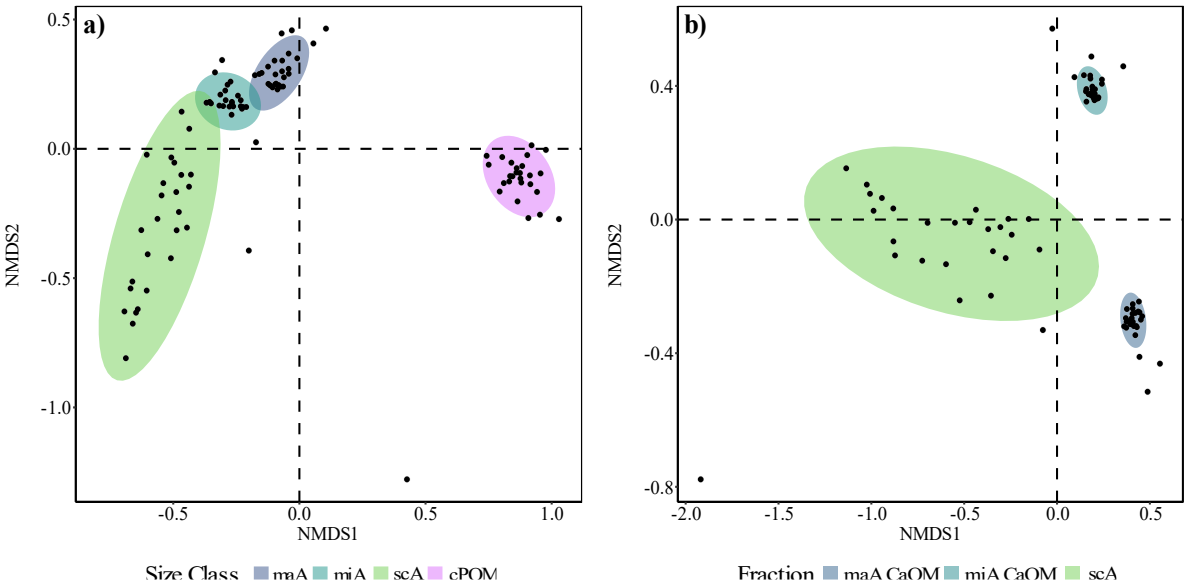

Figure 4: NMDS based on a Bray-Curtis dissimilarity matrix of relative abundance data of peaks with known origin for all bulk size classes (a) and all silt & clay sized fractions (b). The calculated stress-value was 0.077 and 0.054 respectively. PERMANOVA results corresponding to the same matrix are visible in Tab. 4.

Table 3: LME Model results (degrees of freedom (df), F- and p-value of included factors) for the proportion of new C in size classes and maA/miA density fractions. Bold values signify significant model factors (Fraction, temperature (T) and the interaction term (Fraction x T), α = 0.05).

Factor	Fraction			T			Fraction x T		
	df	F	p	df	F	p	df	F	p
Size Classes	3	27.869	**<0.001**	1	4.814	0.056	3	0.303	0.823
maA Fractions	3	43.376	**<0.001**	1	1.336	0.278	3	1.907	0.152
miA Fractions	3	12.018	**<0.001**	1	3.252	0.105	3	4.655	**<0.01**

Table 4: PERMANOVA results (degrees of freedom (df), F- and p-values) for the effect of fraction and treatment on pyrolysis-GC/MS relative abundance data of all found peaks with assignable origin from literature (based on a Bray-Curtis dissimilarity matrix). Bold values signify significant model terms (α = 0.05).

Factor	Fraction			Treatment			Fraction x Treatment		
	df	F	p	df	F	p	df	F	p
Size Classes	3	158.373	**<0.001**	3	0.979	0.436	9	0.624	0.932
Silt & Clay	2	113.761	**<0.001**	3	0.852	0.546	6	0.499	0.950

To see which substances or origin class drives the separation of size classes and fractions, the relative abundance data was z-transformed and compared in a heatmap. Comparing the aggregate size classes, N-containing substances had an overall lower relative abundance in cPOM compared to than the other size classes (Fig. 5). In turn, it had a higher relative abundance of lignin- and carbohydrate-derived compounds. miA had the highest relative abundance of lipid- and aromatics/phenol-derived compounds. scA was more similar to miA regarding the relative abundance of substances related to lipids and aromatics/phenols than maA.

When comparing all silt & clay-sized fractions, the heatmap shows a higher relative abundance of compounds related to N-containing substances, lignin and carbohydrates in maA-CaOM compared to the other fractions (Fig. 6). miA-CaOM in turn had a higher relative abundance of lipid-derived compounds and scA could be characterized by the relative abundance of some specific compounds associated with lipids and aromatics/phenols. For all POM fractions, the difference between size classes was not as pronounced as for the mineral fractions, but still significant ($p < 0.05$, see Fig. S4 and Tab. S8). Here, we also found a marginally significant effect of treatment ($p = 0.074$).

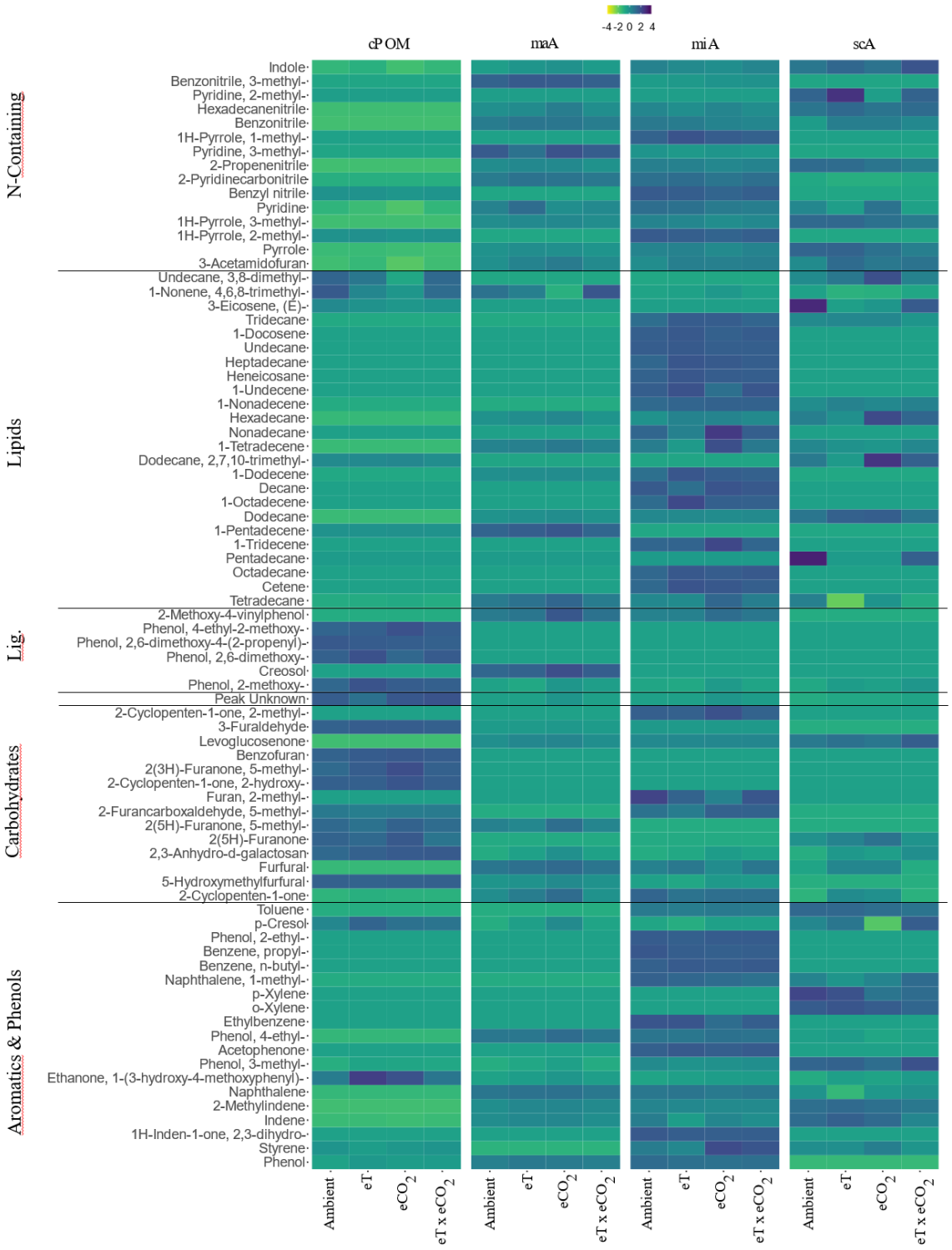

Figure 5: Heatmap showing the z-transformed relative abundance data of all found library peaks for the different bulk size classes by treatment. Substances were categorized by their probable origin molecule class. The substance "Peak Unknown" corresponds to a peak with a big relative abundance that was not identifiable via the mass spectrum. Lig. = Lignin-derived compounds.

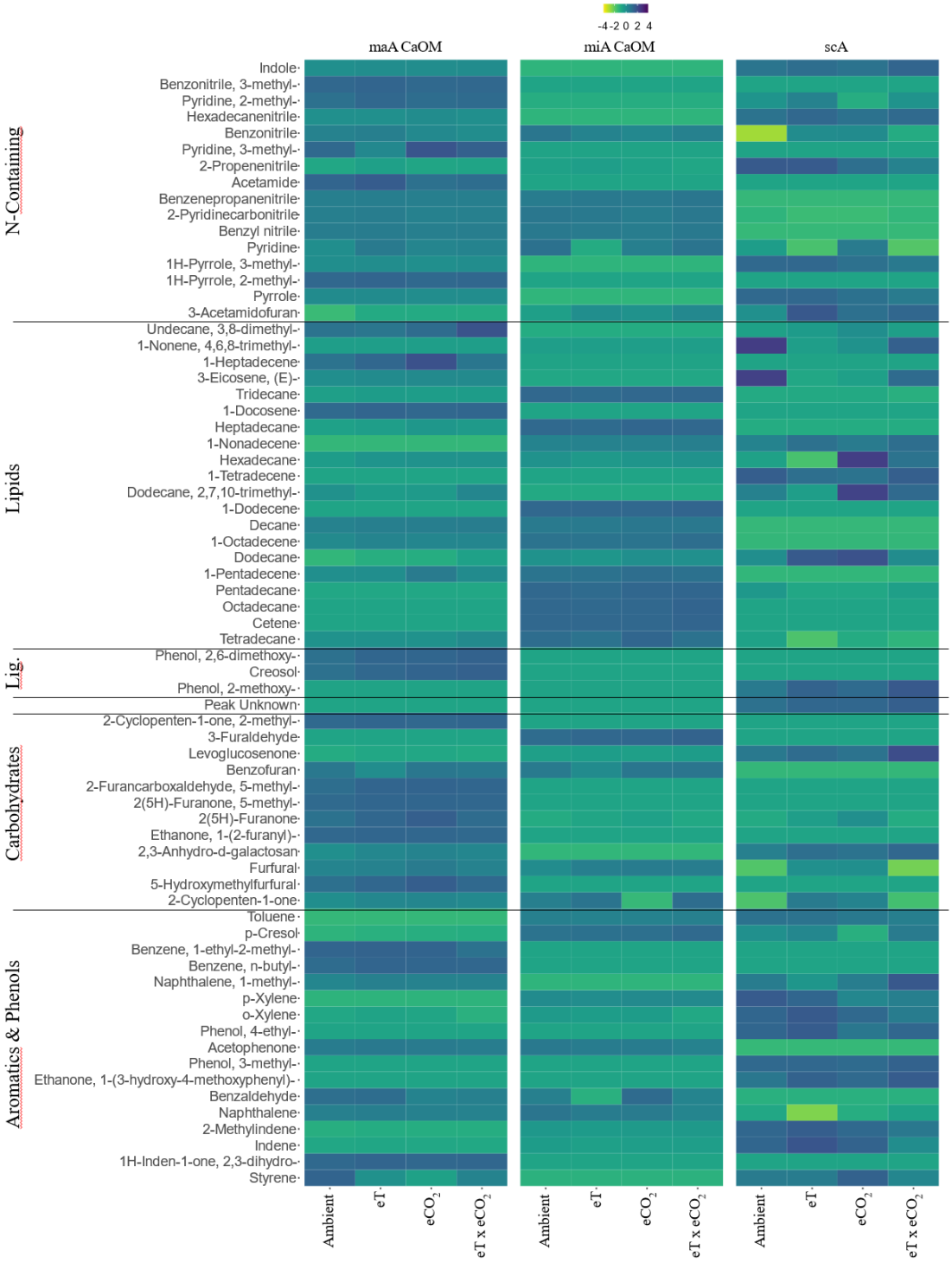

Figure 6: Heatmap showing the z-transformed relative abundance data of all found library peaks for the different silt & clay sized fractions by treatment. Substances were categorized by their probable origin molecule class. The substance "Peak Unknown" corresponds to a peak with a big relative abundance that was not identifiable via the mass spectrum. Lig. = Lignin-derived compounds.

Discussion

Analysing carbon content, isotopic composition and chemical characteristics of physical soil fractions allows to gain insight into processes and mechanisms of formation and stabilization of soil organic carbon and how they might be affected by changing environmental conditions. Here we present evidence, that elevated temperature and elevated atmospheric CO_2 concentration, or a combination of both, neither significantly influenced the total amount of C and N in bulk soil, nor the chemical composition of the size classes and fractions. There was a slight, non-significant increase in bulk soil C after 4 years of climate change treatment. While the investigated size classes differed in their chemical composition, they were unaffected by the climate change treatments. We found some evidence, however, that SOM was re-distributed between different fractions under eCO_2, and that the C turnover was slower under warming and elevated CO_2. The following section will discuss the results in more detail and in the context of the investigated research questions and hypotheses.

We investigated the distribution of SOM across the aggregate size classes and their density fractions. Overall, macro-aggregates were the most abundant size class by weight and were also responsible for storing most C and N. This is consistent with fractionation studies looking at similar ecosystems (Gioacchini et al., 2016; Six et al., 2001). Much less C and N was found in micro-aggregates, followed by silt & clay-sized aggregates. maA and miA differed in the distribution of OM between the density fractions, with maA having a higher relative proportion of fPOM and iPOM while miA in turn had a higher proportion of SaOM and CaOM. This is generally in line with the aggregate hierarchy concept and the idea that OM associated to maA is more labile than that associated to miA (Elliott, 1986; Six et al., 2000b).

About 20% of SOC was newly formed in the four years since start of the fumigation in 2014 and sampling in 2018. Doing a back-of-the-envelope calculation and assuming a steady state with constant turnover rates, this would mean that the whole SOC pool on average is turned over approximately once every 20 years in the top 10 cm. Yan et al. (2017) modelled ecosystem and soil C turnover based on primary production, C pool sizes

and climate variables. For grassland soil, they found a mean turnover time of 34.37 years, which would mean that the ecosystem studied in this experiment turns over faster than other, similar ecosystems, at least under elevated CO_2. We found a decrease of the percentage of new C with decreasing particle size, which is in agreement with the aggregate hierarchy model of Tisdall & Oades (1982), where organic matter in smaller size classes is turned over slower than OM in bigger size classes. While the mineral-associated fractions of both maA and miA contained less new C than the POM-fractions and bulk soil, a considerable amount of C, i.e., about 14%, was also turned over in these fractions. This is in line with results that challenge the concept that mineral-associated OM is chemically recalcitrant or physio-chemically protected and therefore would only turn over very slowly (Torn et al., 2013).

One particularity of this study is that we found notable amounts of C and N in the sand-sized particles of both macro- and micro-aggregates. This led us to treat it as its own, stable OM fraction. In soil fractionation studies, the heavy fraction is usually corrected by the sand content to obtain the mineral-associated OM fraction (Elliott et al., 1991; Schweizer et al., 2019). Our finding shows that doing this might neglect a quite large part of OM in soils and could theoretically lead to wrong conclusions. A sand correction is usually done because sand particles are generally thought not to form the same chemical bonds with OM as clay minerals or iron- or aluminium-oxides. So it is assumed that the sand fraction contains neglectable amounts of OM and would therefore dilute the OM content of the aggregate size class under consideration (Elliott et al., 1991). However, OM can bind to iron oxides that are attached to sand particles and form an organic coating, stabilizing OM in the sand fraction (Elliott et al., 1991; Regelink et al., 2015). Indeed we found quartz crystals that appear to have an organic coating (indicated by a reddish-brown colour, Muchovej et al., 2005) under the stereomicroscope (Fig. S3). Another possible reason for our finding could be that the heavy fraction formed a hard crust during drying that could not be broken up completely before sieving, so clumps of cemented silt and clay particles could have been found in the sand fraction if they were bigger than 63 µm. This could also have been the case in our samples, as we found a few particles >63 µm that appeared to be conglomerates of cemented smaller particles. However, this

could also have been encrusted quartz crystals – clearly it would require more research to investigate this (e.g., scanning electron microscopy-analysis or further dispersion of the sand fraction). Lavallee et al. (2020) also proposed the concept of "heavy POM" (POM that has a higher density than the density threshold used in fractionation studies), which could be a part of the heavy fraction. We however found no evidence of the presence of POM in the sand fraction using our imaging technique. If the conglomerates we found indeed are clay particles, they should be seen as a part of the CaOM pool. At this point, we were unable to determine the ratio of OM associated to (theoretical) clay-clumps in the sand fraction versus OM associated to coated sand particles, so we cannot tell whether the latter pool is of significant size and whether it has different, unique properties. However, the C:N ratio of SaOM found in both maA and miA was higher than the one of CaOM, indicating a differing chemical composition and less decomposed state. Pyrolysis-GC/MS fingerprinting of this fraction was not done but could shed more light on the composition of OM in this fraction. The distribution of OM between SaOM and CaOM was significantly altered on eT x eCO_2 plots in micro-aggregates. While these fractions did not contribute much to total soil C and N pools, the importance of micro-aggregates for long-term C and N storage (Lehmann et al., 2007) brings some relevance to this. Our results show that the sand fraction should be investigated and not be generally neglected in soil fractionation studies, since it contains OM associated to sand particles. Further investigating the formation mechanisms, general importance of, and the impact that climate change will have on OM-encrusted sand in ecosystems might improve our general understanding of SOM dynamics.

One of the main questions of this study was whether elevated temperature and elevated CO_2 affect aggregation. Our results show that eCO_2 enhanced soil aggregation by significantly increasing the relative proportion of macro-aggregates over micro- and silt & clay-sized aggregates. In addition, total soil C was slightly but non-significantly ($p = 0.124$) increased on plots exposed to elevated CO_2. This trend as well as the observed increase in aggregation supports our hypothesis, that the weight proportion of maA and the total soil carbon increased at elevated CO_2 levels (H1). The main reason for this finding most likely be higher levels of plant input in the rhizosphere (directly or via mycorrhiza) that

might have led to the formation of more macro-aggregates and/or might have stimulated the production of binding agents. This is supported by the significantly increased proportion of intra-macroaggregate POM with eCO_2. Since the C:N ratio of this fraction was unaffected by CO_2, the increase of this pool is likely due to the significant increase in the weight proportion and not to a higher C content. While we did not measure the C:N ratio of the vegetation directly, eCO_2 did not change the C:N ratio of POM, in contrast to what others have found (Cotrufo et al., 1998). An increase in aggregation due to a lower microbial activity caused by changed litter stoichiometry (e.g., Six et al., 2001) is therefore unlikely, since POM stoichiometry would likely be altered as well in that case. Instead, higher atmospheric CO_2 concentrations might have increased plant productivity and litter inputs (Drigo et al., 2008; Kuzyakov et al., 2019), which ended up as more fPOM and consequently iPOM in the investigated size classes on eCO_2 and eT x eCO_2 plots. All in all, the effect that eCO_2 had on aggregation and the distribution of OM between size classes and fractions was consistent with what is reported in literature: For example, other studies also found a higher proportion of macro-aggregates with eCO_2 (e.g., Rillig et al., 1999 and Six et al., 2001), and no strong effect of eCO_2 on bulk soil C was also reported (e.g., Dorodnikov et al., 2011 and Six et al., 2001). While SOC pools might not be directly affected by eCO_2, the higher proportion of macro-aggregates and more intra-macroaggregate POM with future climate conditions could increase the susceptibility of SOC stocks towards microbial decomposition, especially when processes that are known to destroy aggregates, such as land-use change (Wang et al., 2014) or drying/rewetting events (Navarro-García et al., 2012), are further intensified.

We expected a depletion of the labile free POM-pool on warmed plots (H1). Our data however shows no effect of temperature on the amount of C and N stored in this pool. However, we found a significant reduction of the C:N ratio of macro-aggregate fPOM and iPOM with warming. Differences in the C:N ratio compared to control plots could either be caused by stronger microbial decomposition or by a changed plant input stoichiometry. Since we found no changes to neither the C and N pool sizes nor the $\delta^{13}C$-signal of these fractions under eT, which could accompany increased decomposition (if the input does not change and small rather than big molecules are decomposed), these findings overall

hint at a changed plant stoichiometry on plots exposed to eT. Contrary to our expectations, we also found no reduction of aggregation (estimated by the proportion of macro-aggregates) on warmed plots. Total as well as bulk macro- and micro-aggregate C and N were even slightly, but non-significantly increased on the warmed plots. The distribution of OM between pools was overall not significantly affected by the 3°C temperature increase in this study.

One effect that warming had was a lower incorporation of new C coming in eCO_2 plots. This was visible in in bulk soil and size classes as well as macro- and micro-aggregate fPOM. This indicates that C turnover in these physical fractions is slower under warmer climatic conditions. A possible explanation for this could be increased microbial respiration of newly introduced, plant-derived, labile material which results in less stabilization of fresh OM and in turn a higher proportion of "old" C compared to new C. This effect was only marginally significant ($p = 0.056$). We cannot differentiate whether the slower turnover is an effect of elevated temperature alone or if it arises from an interactive effect that eT x eCO_2 might have had. Since the previously discussed findings hint at no increased decomposition on plots treated with eT alone, we can speculate that this effect is the result of the combination of both treatments: in such a scenario eCO_2 would have stimulated plant productivity leading to more fresh OM input, which would be rapidly decomposed and respired by more active microbes, which are stimulated by warming. On eT plots alone the extra source of fresh plant input might be missing, resulting in no significantly higher decomposition. A slower turnover of stable C and a faster decomposition of plant input under future climatic conditions might have implications for SOM dynamics by influencing SOM quality in the long-run and with that the microbial community composition and processes over time.

Interactive effects between climatic factors remain hard to predict and the resulting impact that the combination of warming and elevated atmospheric CO_2 concentrations might have on SOM pools remains controversial (Ma et al., 2020). While there might be evidence in this study for an interactive effect of eT and eCO_2 regarding C turnover as just discussed, the combination of both eT and eCO_2 was almost never found to be significantly different from the effects of a single factor in this study. Whenever there was a significant

effect on the measured variables on the future climate plots (eT x eCO_2), our statistical analysis mostly indicated that it came from the increase in CO_2 and not temperature. While we therefore did not observe a cancelling-out of effects on eT x eCO_2 plots as we hypothesized (H2), the results nevertheless hint at additive effects. For example, the higher weight proportion of macro-aggregates on eT x eCO_2 plots could be attributed to a CO_2 effect and was unaffected by temperature, indicated by the non-significant interactive term in the LME model results. This was therefore an effect of eCO_2 and did not come from an interaction of these factors. So overall, our results suggest that the effect of elevated temperature and elevated CO_2 were additive, with the CO_2 effect dominating, and no apparent effect of temperature. Interestingly, we did not find this increase of maA weight on plots treated with eCO_2 alone. In theory, this could be an effect of lower statistical power in the eCO_2 treatment because of the lower number of replicates compared to the future climate treatment (n = 3 vs n = 9). The increase of the maA weight proportion on eCO_2 plots compared to the control was below 1% however, while it was about 5% in eT x eCO_2 plots. More research is therefore needed to find out why we only find the CO_2 effect on the future climate plots. The absence of a temperature effect and possible interactive effects could also be due to the larger relative increase of the CO_2-concentration compared to the relative increase in temperature, since CO_2-concentrations on eCO_2 plots was almost doubled while it was increased by 3 °C on eT plots (~25% of field temperature in October, see Simon et al. 2020). This difference in effect size could lead to the domination of CO_2 effects (Dieleman et al., 2012) and possibly overshadow any temperature or interactive effects. We have to keep in mind however, that a similar increase in CO_2 and temperature as we simulated in our experiment, are possible by 2100. In a similar experiment (Carrillo et al., 2018) a reduction of soil C in fumigated and warmed plots (and no effect of warming under ambient atmospheric CO_2-concentration) was found, while using even higher levels of CO_2-fertilization (+600 ppm in the growing season).

Our results clearly show that, aside from a possible slower turnover of stable C, future climatic conditions mostly affect SOM in physical soil fractions via the increase in plant inputs. We do not know whether this finding will hold true after more years of simulated

climate change or if unpredictable interactive effects will arise in the future. For now, this study joins the ranks of those finding no significant interactive effect of elevated temperature and elevated CO_2 on SOM, at least for the physical fractions we investigated. This suggests that ESM models will not need to implement complicated interactive effects which would simplify the modelling of future SOM stocks considerably.

We hoped to gain further insight into the mechanisms that lead to the formation of the investigated SOM pools and how they might be affected by climate change by fingerprinting the chemical composition of these pools. While pyrolysis-GC/MS was used to analyse the chemical composition of SOM before, this study was the first in which pyrolysis-GC/MS was used to fingerprint the chemical composition of SOM in soil aggregate size classes and their density fractions under both eT, eCO_2 and a combined future climate treatment. The results of our high-throughput fingerprinting approach show that, overall, the chemical composition of size classes (and density fractions) differed more in between each other than in between treatments within each fraction.

Each investigated size class was characterized by its own, unique chemical fingerprint, in line with H3. We found a clustering in the NMDS that followed particle size: macro-aggregates were more similar to micro-aggregates, which were more similar to silt & clay-sized aggregates. As we hypothesized (H3), micro-aggregates were characterized by a higher relative abundance of lipids and aromatic & phenol-derived compounds than macro-aggregates. Both short-chained lipids and aromatics are generally considered to be more recalcitrant in soils and less affected by microbial decomposition than other compounds (Kögel-Knabner, 2000; Vancampenhout et al., 2009). This is indicative for a more advanced stage of decomposition of the investigated miA, consistent with the found slightly lower turnover than maA (estimated by the proportion of “new C”).

Since macro-aggregates are thought to be made up of micro-aggregates as well as binding agents (Six et al., 2000a), we would have expected a higher relative abundance of carbohydrates that presumably stem from these binding agents in maA (H3). We did, however, not find any evidence for that. For some carbohydrates, miA even had higher relative abundances than maA (e.g., 2-Cyclopenten-1-one, 2-methyl-, Furan, 2-methyl-

and 2-Furancarboxaldehyde, 5-methyl-). As the previously discussed findings suggest an older age of miA, it would be interesting to investigate if these fragments more often stem from microbially-derived carbohydrates rather than plant-derived carbohydrates. The compound library we used is not suitable to distinguish between the origin of carbohydrates (if that is possible at all), it would be necessary to isolate specific biomarkers that correspond to binding agents and include them in the analysis. The difference in lignin-derived compounds was generally not as pronounced between maA and miA as we expected. This indicates that lignin is present in both maA and miA at similar relative abundances. In soil, lignin gets gradually decomposed in a complex process (Zabel & Morrell, 2020) and could therefore still be present albeit simply more processed in the older micro-aggregates. Again, a modification of our library (adding more specific lignin biomarkers that maybe correspond to different functional groups of the polymer) would be necessary to further investigate this.

The difference between the size classes was also visible in their silt & clay sized fractions. Macro-aggregate CaOM contained more lignin-, N-containing- and carbohydrate-derived substances, while micro-aggregate CaOM again had a higher relative abundance of lipids. Although macro-aggregates contain micro-aggregates, this result further emphasizes that there is a difference between the two size classes, with OM in micro-aggregates being generally older and more decomposed (Totsche et al., 2018). Even though macro- and micro-aggregate CaOM might have a similar turnover (as measured by the incorporation of C in eCO_2-plots), they still seem to have inherently different chemical properties.

Although we expected an effect of simulated climate change on the chemical composition of the investigated size classes and fractions, we did not detect a statistically significant influence of eT or eCO_2. Apparently, the biotic and abiotic pathways that transform OM and lead to the formation of the individual fractions, exerted more control over the chemical composition in the end than any climate-driven change to plant inputs or transformation processes. These decomposition pathways themselves seem so far unaffected by climate change in this experiment. Since the chemical composition was not changed, the temperature sensitivity of the different molecules was likely also not

changed, which is in line with our previously discussed findings that elevated temperature did not significantly influence the size of the different investigated SOM pools.

The high-throughput Pyrolysis-GC/MS-workflow we developed so far only allowed us to create and compare chemical fingerprints based on the relative abundance of the substances in our library. While they can be used to track changes and differences between samples (Klein et al., 2020), they by no means provide a complete picture of the chemical composition and also no quantification of chemical compounds. Adding the relative abundances of all unknown substances created in the pyrolysis process to the multivariate analysis could give a more complete picture of the chemical composition.

Summary and Conclusion

In summary we found that total soil C was unaltered and even slightly increased after four years of simulated climate change in this experiment. We found small changes to aggregation and the distribution of OM across different fractions with elevated CO_2, especially in macro-aggregates. Higher atmospheric CO_2-concentrations resulted in more macro-aggregates and a higher relative proportion of intra-macro-aggregate POM and lower proportions of mineral-associated OM, which could increase the susceptibility of SOM towards future disturbances. While the turnover of C was slowed down in some cases by elevated temperature, we could not detect significant changes in the chemical composition of the investigated size classes and fractions with our treatments and methods. So, while the time for OM to move from one physical pool into another might have been affected by elevated temperature, the chemical fingerprint of that pool did not change. Based on these results, we do not expect changes to occur to the chemical composition of the investigated SOM fractions with elevated temperature and elevated atmospheric CO_2 concentrations. This also makes chemistry-induced changes to those processes that govern SOM stabilization and decomposition unlikely in a future climate. Surprisingly, we found a significant amount of OM associated to sand particles in maA and miA in this study. More research is needed to determine the relative importance of this pool with regard to its stability and carbon sequestration potential under climate change. Therefore, we argue against a simple sand correction of the mineral-associated OM in

fractionation studies and urge future fractionation studies to consider and further investigate this pool.

Overall, this study indicates that separating SOM into different pools with different functionalities and turnover times, together with modelling additive effects of eT and eCO_2 might be enough to predict future SOM stocks under climate change with sufficient accuracy, while including changes to the chemical composition of these pools and complex interactive effects might not be necessary. Whether these findings hold true in the long-term remains however unresolved.

Supplementary Material

1) Supplementary Figures

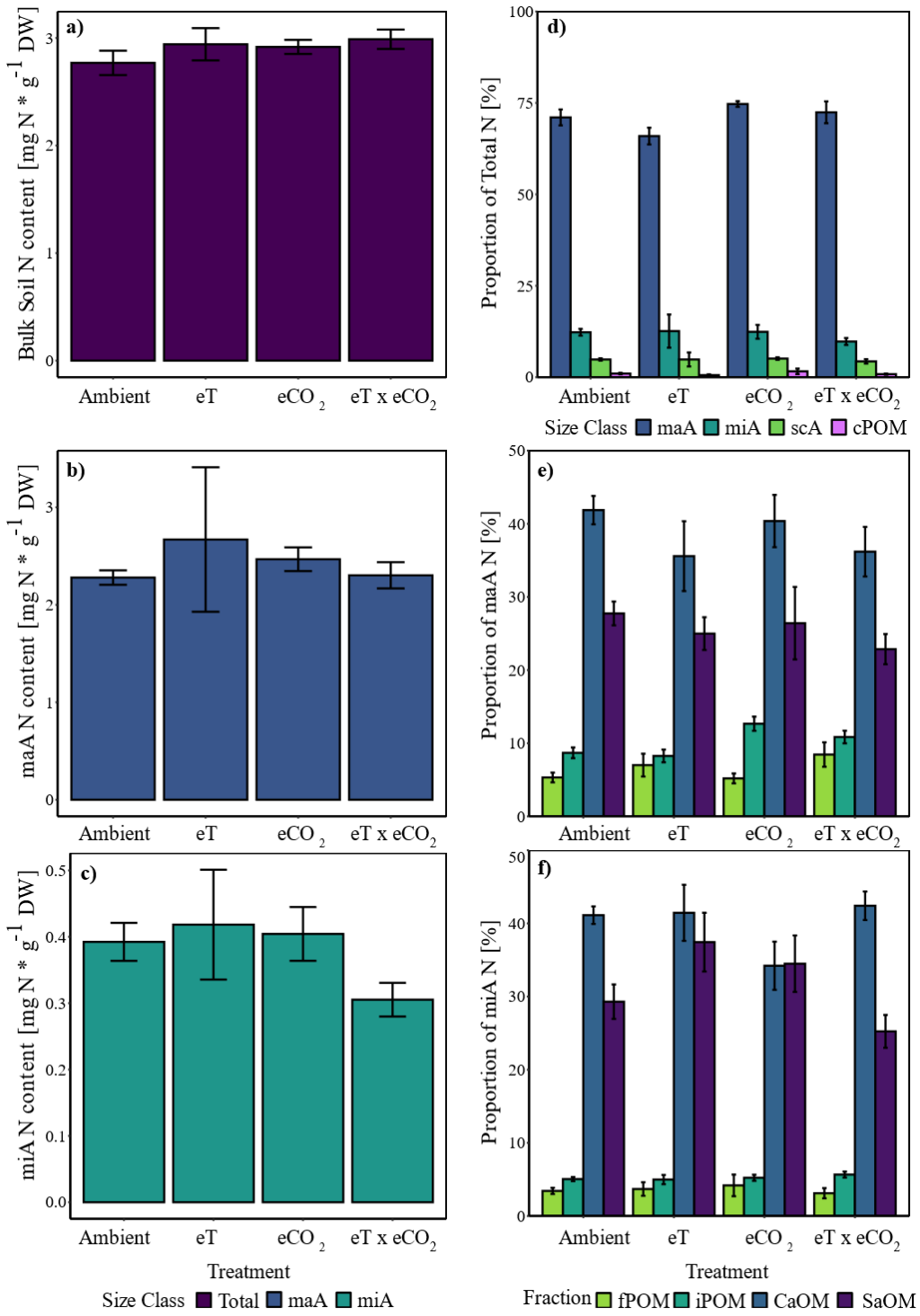

Figure S1: N content in mg N per g soil dry weight of bulk soil, bulk maA and bulk miA by treatment (a-c). Right side: Contribution of N in size classes to total N in bulk soil (d) and of density fraction N to total N of maA and miA respectively (e-f). Bars and error bars represent mean ± standard error. Corresponding LME model results are shown in Tables S1 and S2.

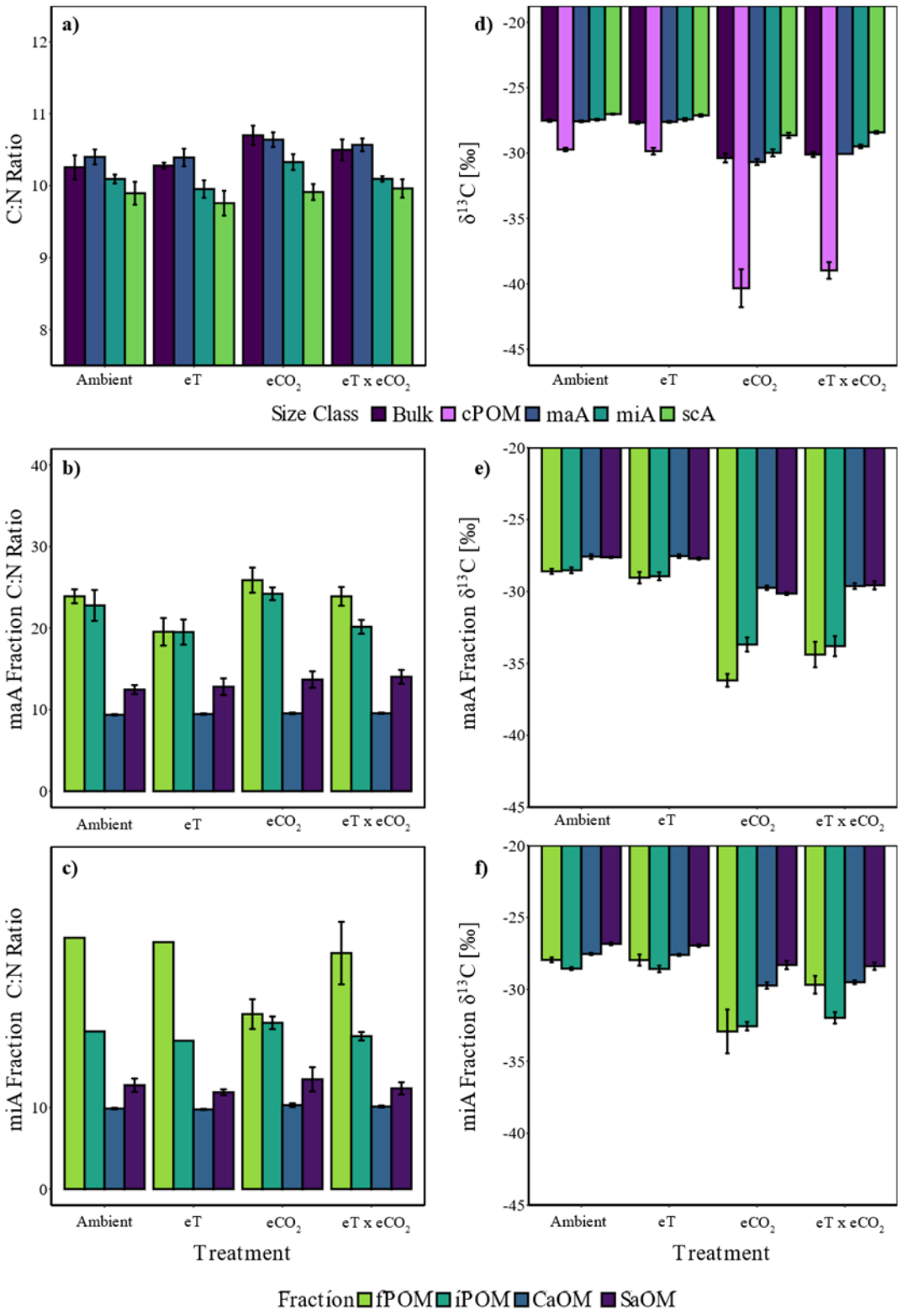

Figure S2: Left column: C:N ratios of size classes (a) and density fractions of maA (b) and miA (c) by treatment. Right column: $\delta^{13}C$-value of size classes (d) and density fractions of maA (e) and miA (f) by treatment. Bars and error bars represent mean ± standard error. Corresponding LME model results are shown in Tables S1 and S2.

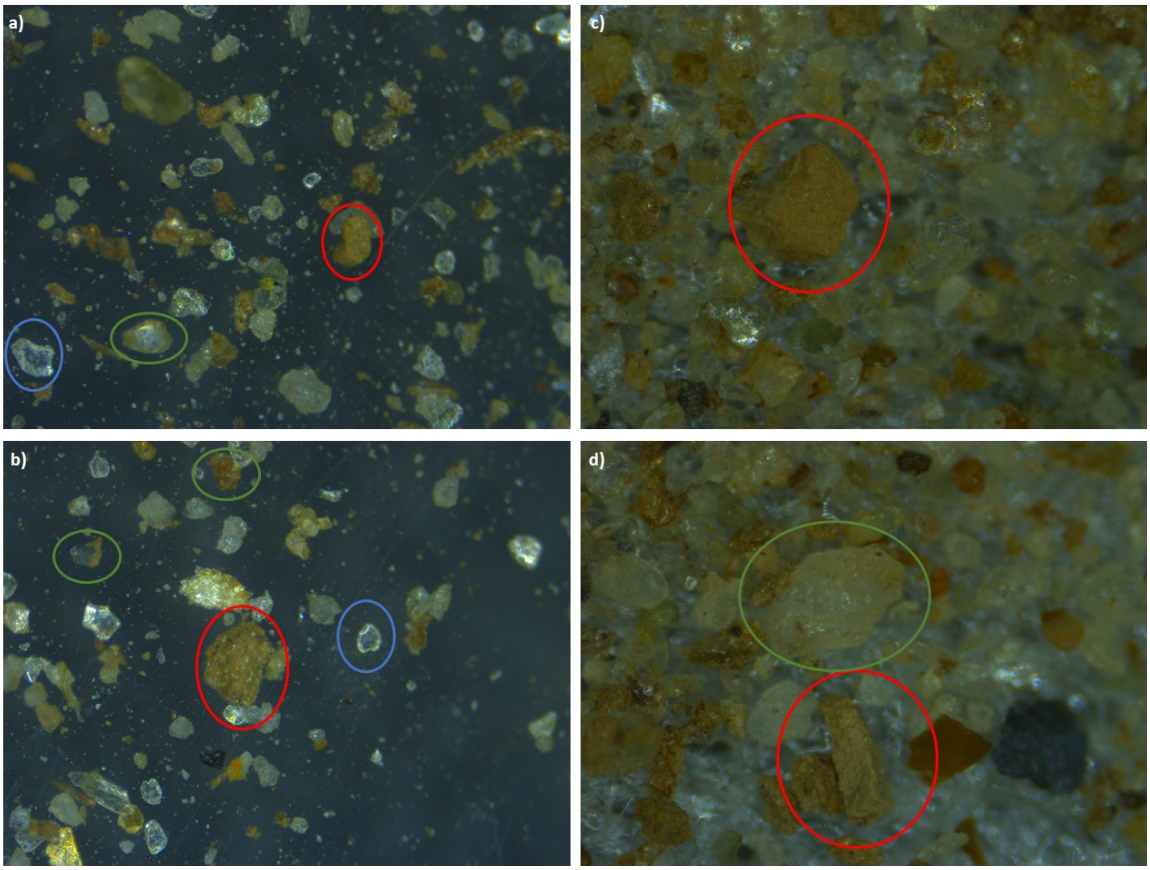

Figure S3: Pictures of the sand fraction of one macro-aggregate sample, taken with a stereoscope (once in a petri dish (a,b) and once zoomed in on sticky tape (c,d)). Blue circles: Clear, uncoated quartz crystals. Green circles: Quartz crystals possibly coated with iron oxidesa and organic matter. Red circles: Possible conglomerates of cemented smaller (silt & clay) particles.

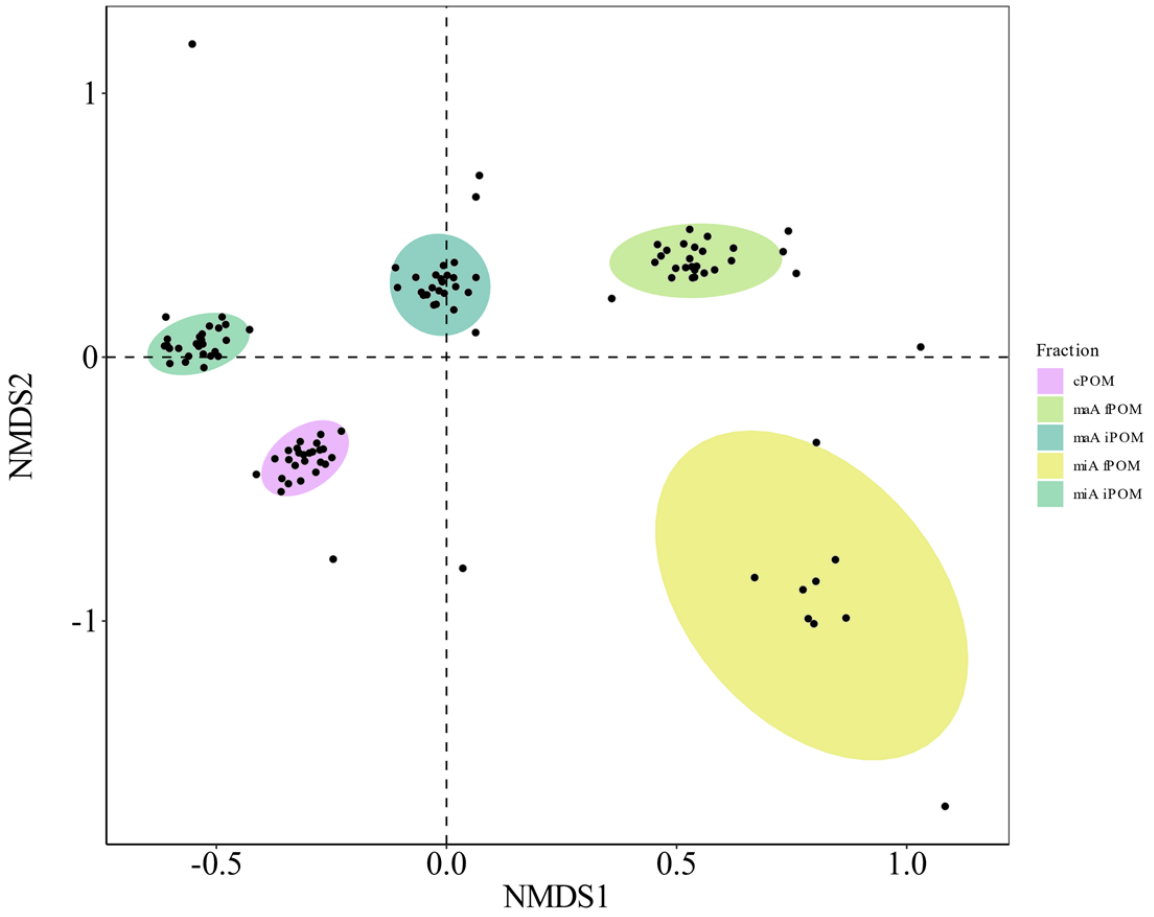

Figure S4: NMDS based on a Bray-Curtis dissimilarity matrix of relative abundance data of peaks with known origin for POM fractions. The calculated stress-value was 0.173. PERMANOVA results corresponding to the same matrix are visible in Tab. S8.

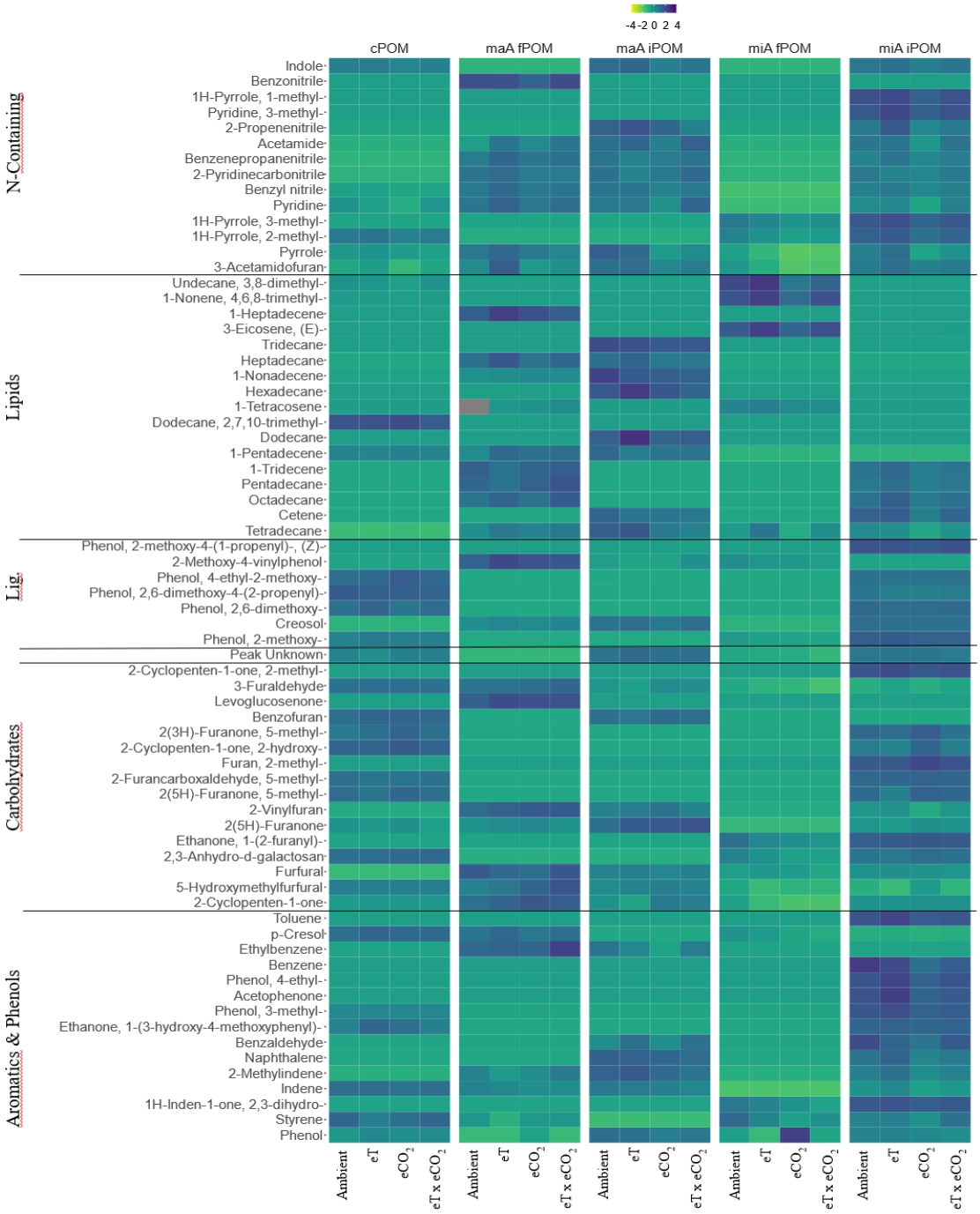

Figure S5: Heatmap showing the z-transformed relative abundance data of all found library peaks for the different POM fractions by treatment. Substances were categorized by their probable origin molecule class. The substance "Peak Unknown" corresponds to a peak with a big relative abundance that was not identifiable via the mass spectrum. Lig. = Lignin-derived compounds.

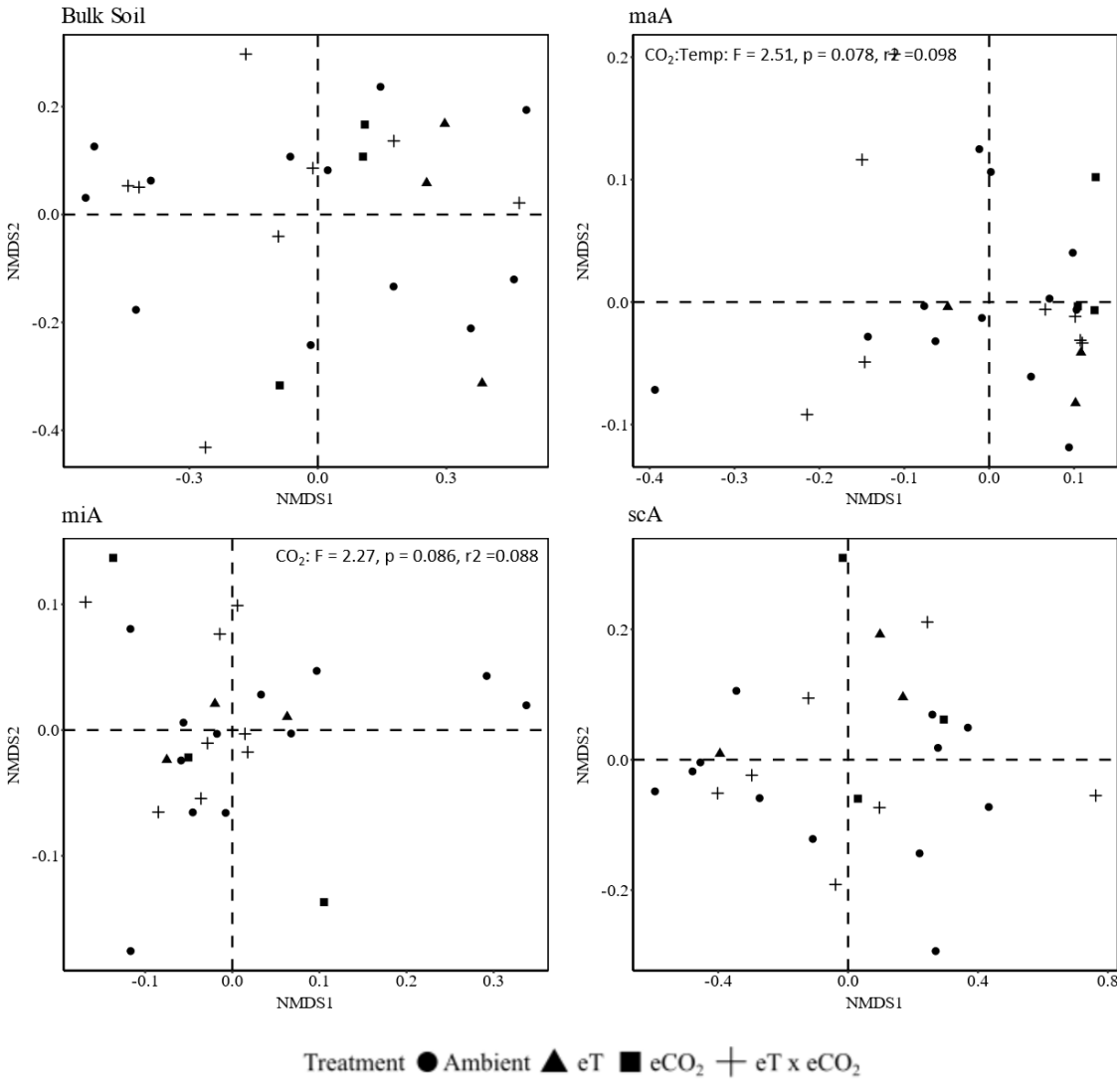

Figure S6: NMDS based on a Bray-Curtis dissimilarity matrix of relative abundance data of peaks with known origin for singular size classes. A PERMANOVA resulted in so significant treatment effects (α = 0.05). Marginally significant PERMANOVA results are indicated in the corresponding graph.

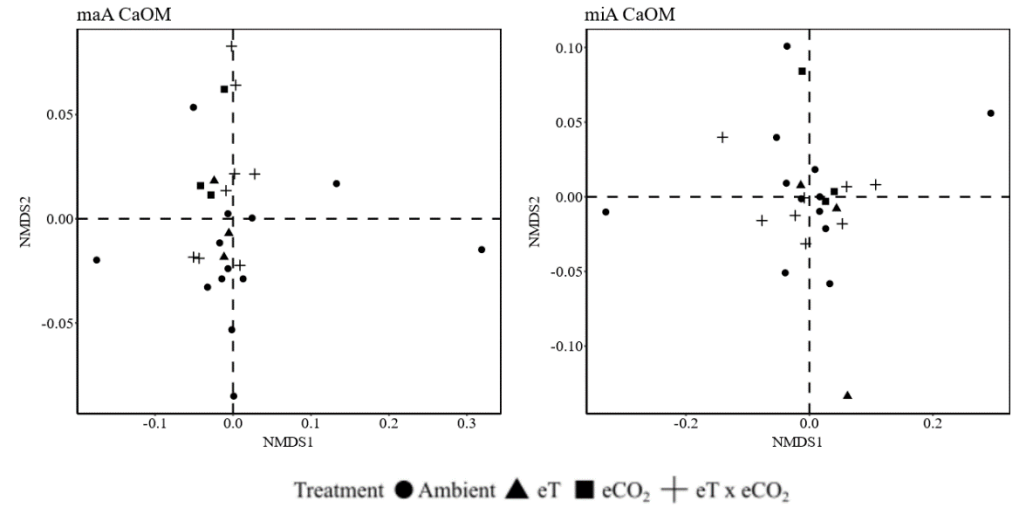

Figure S7: NMDS based on a Bray-Curtis dissimilarity matrix of relative abundance data of peaks with known origin for macro- and micro-aggregate CaOM. A PERMANOVA resulted in so significant treatment effects (α = 0.05).

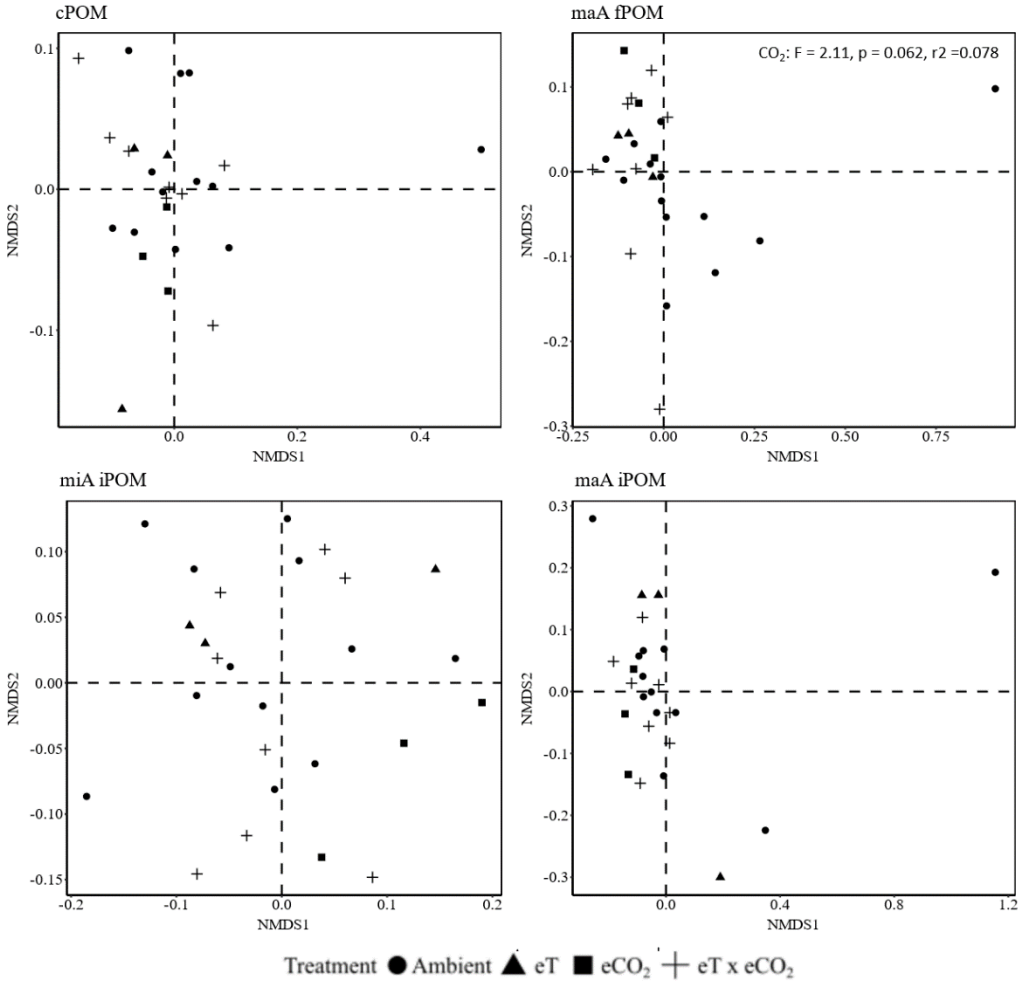

Figure S8: NMDS based on a Bray-Curtis dissimilarity matrix of relative abundance data of peaks with known origin for POM fractions A PERMANOVA resulted in so significant treatment effects (α = 0.05). Marginally significant PERMANOVA results are indicated in the corresponding graph. miA fPOM was not analysed because not enough material was available for Pyr-GC/MS analysis after density fractionation.

2) Supplementary Tables

Table S1: Linear mixed-effects model results (T and F-test) for all bulk size classes and variables. Significant model factors (CO_2, temperature (T) and the interaction term (T x CO_2)) are marked in bold (α = 0.05). "log-Lik": Log-likelihood ratio, "df": degrees of freedom. The column "Norm." contains the p-value of a Shapiro-Wilk test of model residuals, "Transf." marks cases where a data transformation or outlier removal was necessary to obtain a normal distribution of model residuals (log = logarithmical transformation). Variable abbreviations: "weight_rel": Weight contribution of size class to bulk soil (in %), "C_abs"/"N_abs": Absolute C or N content (in g) in size class per g soil DW, "C_atmperc"/"N_atmperc": Atom-% C or N of size class, "C_perc"/"N_perc": Proportion of C or N in size class of bulk soil C or N (in%), "CN": C:N ratio of size class.

				T-Test						F-Test							
				CO_2		T		CO_2 x T		CO_2		T		CO_2 x T		Norm.	Transf.
Size Class	Variable	logLik	df	t-Value	p	t-Value	p	t-Value	p	F-Value	p	F-Value	p	F-Value	p	p	
Bulk	**C_abs**	7.853	22	-0.364	0.719	-0.020	0.984	-0.509	0.616	2.559	0.124	0.317	0.579	0.259	0.616	0.127	log
	N_abs	142.160	22	-0.212	0.834	-0.324	0.749	-0.336	0.740	1.656	0.212	0.675	0.420	0.113	0.740	0.647	
	$\delta^{13}C$	-15.570	22	8.556	**< 0.001**	-0.948	0.354	1.068	0.297	248.160	**< 0.001**	0.060	0.803	1.140	0.297	0.922	
	CN	-5.870	21	-1.192	0.247	1.089	0.289	-1.505	0.147	14.600	**< 0.001**	0.000	0.995	2.260	0.147	0.893	Removed Sample 7
cPOM	**weight_rel**	-22.070	22	-0.591	0.561	1.398	0.176	-0.383	0.705	0.224	0.641	2.636	0.119	0.147	0.705	0.232	log
	C_abs	-22.390	22	-0.751	0.460	1.793	0.087	-0.559	0.582	0.523	0.477	4.047	0.057	0.313	0.582	0.055	log
	C_atmperc	-50.370	21	-1.122	0.275	2.779	**0.011**	-0.823	0.420	0.995	0.330	9.940	**0.005**	0.677	0.420	0.436	Removed Sample 49
	C_perc	-22.520	22	-1.038	0.310	1.445	0.163	-0.141	0.889	0.543	0.469	3.789	0.065	0.020	0.889	0.028	log
	N_abs	-22.740	22	-0.539	0.596	1.515	0.144	-0.479	0.637	0.211	0.650	2.865	0.105	0.230	0.637	0.111	log
	N_atmperc	9.340	22	0.164	0.872	0.837	0.412	-0.548	0.589	0.000	0.999	0.407	0.530	0.300	0.589	0.892	
	N_perc	-22.940	22	-0.872	0.392	1.213	0.238	-0.084	0.934	0.308	0.585	2.790	0.109	0.007	0.934	0.079	log
	$\delta^{13}C$	-40.580	22	10.262	**< 0.001**	-1.531	0.140	1.211	0.239	338.858	**< 0.001**	0.900	0.353	1.467	0.239	0.254	
	CN	-55.940	22	-0.922	0.366	1.133	0.270	-0.290	0.775	1.212	0.283	1.789	0.195	0.084	0.775	0.596	
maA	**weight_rel**	-66.000	22	-2.066	0.051	-1.606	0.123	1.380	0.181	5.595	**0.027**	0.774	0.389	1.905	0.181	0.450	
	C_abs	4.100	22	0.631	0.535	0.734	0.471	-1.113	0.278	0.132	0.720	0.011	0.918	1.239	0.278	0.145	log
	C_atmperc	8.840	22	1.576	0.129	1.493	0.150	-1.903	0.070	0.196	0.662	0.028	0.868	3.620	0.070	0.262	log
	C_perc	-72.110	22	-0.798	0.433	-1.012	0.322	0.658	0.518	1.066	0.313	0.604	0.445	0.432	0.518	0.975	
	N_abs	2.820	22	0.730	0.473	0.636	0.532	-1.012	0.323	0.008	0.929	0.020	0.890	1.023	0.323	0.134	log
				T-Test						F-Test							

				CO_2		T		CO_2 x T		CO_2		T		CO_2 x T		Norm.	Transf.
Size Class	**Variable**	**logLik**	**df**	**t-Value**	**p**	**t-Value**	**p**	**t-Value**	**p**	**F-Value**	**p**	**F-Value**	**p**	**F-Value**	**p**	**p**	
	N_atmperc	31.900	22	1.851	0.078	1.119	0.275	-1.815	0.083	0.550	0.466	0.080	0.781	3.294	0.083	0.077	
	N_perc	-72.100	22	-0.900	0.378	-0.814	0.424	0.632	0.534	1.154	0.294	0.267	0.611	0.400	0.534	0.839	
	$\delta^{13}C$	-15.000	21	8.423	**< 0.001**	-2.131	**0.045**	1.654	0.113	240.280	**< 0.001**	1.820	0.191	2.740	0.113	0.732	Sample 48 NA
	CN	-8.460	22	-0.853	0.403	0.349	0.730	0.349	0.730	2.445	0.132	0.073	0.789	0.050	0.825	0.728	
miA	**weight_rel**	-61.400	22	1.876	0.074	1.377	0.182	-1.059	0.301	5.960	**0.023**	0.782	0.386	1.122	0.301	0.561	
	C_abs	118.730	22	1.693	0.105	1.715	0.100	-1.475	0.154	2.719	0.113	0.881	0.358	2.177	0.154	0.329	
	C_atmperc	-1.910	22	-0.465	0.647	0.835	0.413	-1.234	0.230	5.605	**0.027**	0.007	0.934	1.522	0.230	0.274	
	C_perc	-64.270	22	1.144	0.265	0.705	0.488	-0.630	0.535	1.952	0.176	0.130	0.722	0.396	0.535	0.772	
	N_abs	169.350	22	1.774	0.090	1.554	0.134	-1.420	0.170	3.050	0.095	0.583	0.453	2.016	0.170	0.537	
	N_atmperc	48.800	22	-0.208	0.837	0.407	0.688	-1.090	0.288	4.173	0.053	0.306	0.586	1.187	0.288	0.232	
	N_perc	-65.610	22	1.112	0.278	0.659	0.517	-0.629	0.536	1.701	0.206	0.087	0.770	0.396	0.536	0.751	
	$\delta^{13}C$	-9.230	22	9.641	**< 0.001**	-2.307	**0.031**	1.619	0.120	303.450	**< 0.001**	2.710	0.114	2.620	0.120	0.797	
	CN	2.740	22	-1.140	0.267	1.885	0.073	-0.547	0.590	1.640	0.214	4.650	**0.042**	0.300	0.590	0.186	
scA	**weight_rel**	4.500	22	2.138	**0.044**	2.051	0.052	-2.010	0.057	2.898	0.103	0.747	0.397	4.038	0.057	0.073	log
	C_abs	-3.900	22	0.932	0.362	1.496	0.149	-1.108	0.280	0.714	0.407	1.012	0.326	1.229	0.280	0.058	log
	C_atmperc	8.300	22	-0.919	0.368	0.167	0.869	0.459	0.651	0.306	0.586	0.524	0.477	0.210	0.651	0.022	log
	C_perc	-44.160	22	0.484	0.633	0.320	0.752	-0.284	0.779	0.333	0.570	0.027	0.870	0.081	0.779	0.058	
	N_abs	-3.440	22	1.076	0.294	1.556	0.134	-1.209	0.239	0.910	0.350	0.970	0.335	1.460	0.239	0.145	log
	N_atmperc	8.760	22	-0.722	0.478	0.219	0.828	0.334	0.742	0.163	0.690	0.446	0.511	0.112	0.742	0.066	log
	N_perc	-44.970	22	0.478	0.638	0.431	0.670	-0.372	0.714	0.252	0.620	0.055	0.816	0.138	0.714	0.097	
	$\delta^{13}C$	-1.270	22	8.718	**< 0.001**	-1.551	0.135	1.601	0.124	272.000	**< 0.001**	0.300	0.576	2.600	0.124	0.018	
	CN	-17.150	22	-0.668	0.511	-0.162	0.873	0.443	0.662	0.202	0.658	0.053	0.820	0.197	0.662	0.135	

Table S2: Linear mixed-effects model results (T and F-test) for all maA and miA fractions and variables. Significant model factors (CO_2, temperature (T) and the interaction term (T x CO_2)) are marked in bold (α = 0.05). "log-Lik": Log-likelihood ratio, "df": degrees of freedom. The column "Norm." contains the p-value of a Shapiro-Wilk test of model residuals, "Transf." marks cases where a data transformation or outlier removal was necessary to obtain a normal distribution of model residuals (log = logarithmical transformation). Variable abbreviations: "weight_rel": Weight contribution of size class to bulk soil (in %), "weight_abs": Absolute weight of fraction (in g) per g soil DW, "C_abs"/"N_abs": Absolute C or N content (in g) in size class per g soil DW, "C_atmperc"/"N_atmperc": Atom-% C or N of size class, "C_perc"/"N_perc": Proportion of C or N in size class of bulk soil C or N (in%), "CN": C:N ratio of size class.

					T-Test						F-Test							
					CO_2		T		CO_2 x T		CO_2		T		CO_2 x T		Norm.	Transf.
Size class	Fraction	Variable	logLik	df	t-Value	p	t-Value	p	t-Value	p	F-Value	p	F-Value	p	F-Value	p	p	
maA	**fPOM**	**weight_abs**	69.290	22	-1.565	0.132	-1.965	0.062	1.042	0.309	6.108	0.022	3.078	0.093	1.085	0.309	0.194	
		weight_rel	-36.920	22	-1.325	0.199	-1.830	0.081	0.878	0.389	5.064	0.035	2.994	0.098	0.771	0.389	0.106	
		C_abs	-20.150	22	-1.300	0.207	-1.473	0.155	0.646	0.525	5.399	0.030	2.122	0.159	0.417	0.525	0.244	log
		C_atmperc	-54.700	22	-0.530	0.601	0.717	0.481	0.866	0.396	1.884	0.184	3.792	0.064	0.750	0.396	0.927	
		C_perc	-16.060	22	-0.596	0.557	-1.297	0.208	0.449	0.658	1.785	0.195	1.983	0.173	0.202	0.658	0.831	log
		N_abs	169.100	22	-1.023	0.317	-1.829	0.081	0.781	0.443	3.678	0.068	3.354	0.081	0.609	0.443	0.065	
		N_atmperc	6.140	22	1.431	0.167	-0.461	0.649	-0.153	0.880	3.016	0.096	0.688	0.416	0.024	0.880	0.164	
		N_perc	-19.150	22	-0.183	0.857	-1.315	0.202	0.079	0.938	1.808	0.192	3.322	0.082	0.006	0.938	0.274	log
		$\delta^{13}C$	-34.170	21	6.416	0.000	-3.423	0.003	2.943	0.008	179.604	<.0001	3.476	0.076	8.660	0.008	0.703	Removed 43
		CN	-58.940	22	-2.123	0.045	0.971	0.342	0.835	0.413	1.375	0.253	5.215	0.032	0.698	0.413	0.769	
	iPOM	**weight_abs**	-9.490	22	-2.862	0.009	0.239	0.813	0.405	0.689	15.219	0.001	0.595	0.449	0.164	0.689	0.387	log
		weight_rel	-21.100	22	-2.282	0.033	0.354	0.727	0.191	0.850	10.326	0.004	0.509	0.483	0.037	0.850	0.085	
		C_abs	112.650	22	-2.533	0.019	0.628	0.536	-0.204	0.841	17.129	0.000	0.486	0.493	0.042	0.841	0.449	
		C_atmperc	-56.220	20	2.508	0.021	0.985	0.336	-1.769	0.092	3.302	0.084	0.165	0.689	3.129	0.092	0.766	Removed 11, 49
		C_perc	-63.230	22	-1.228	0.233	2.256	0.034	-1.353	0.190	6.847	0.016	3.419	0.078	1.832	0.190	0.709	
		N_abs	175.520	22	-2.179	0.040	-0.620	0.542	0.382	0.706	12.623	0.002	0.248	0.624	0.146	0.706	0.333	
		N_atmperc	-1.560	22	2.385	0.026	-1.394	0.177	-1.104	0.282	0.539	0.471	10.094	0.004	1.218	0.282	0.130	
		N_perc	-58.290	22	-1.579	0.129	0.486	0.632	-0.516	0.611	10.417	0.004	0.027	0.871	0.266	0.611	0.635	
		$\delta^{13}C$	-39.560	22	5.729	0.000	0.134	0.895	0.254	0.802	107.535	<.0001	0.212	0.650	0.065	0.802	0.163	
		CN	-50.080	21	-0.427	0.674	2.669	0.014	-1.224	0.235	0.434	0.517	6.641	0.018	1.498	0.235	0.120	

					T-Test						F-Test							
					CO_2		T		CO_2 x T		CO_2		T		CO_2 x T		Norm.	Transf.
Size class	Fraction	Variable	logLik	df	t-Value	p	t-Value	p	t-Value	p	F-Value	p	F-Value	p	F-Value	p	p	
	CaOM	weight_abs	35.140	22	-2.267	0.034	-0.557	0.583	1.782	0.089	1.019	0.324	1.126	0.300	3.174	0.089	0.152	
		weight_rel	-65.720	22	-1.166	0.256	0.343	0.735	1.031	0.314	0.069	0.795	2.491	0.129	1.062	0.314	0.011	
		C_abs	108.640	22	-1.406	0.174	-1.015	0.321	1.010	0.323	1.976	0.174	0.169	0.685	1.021	0.323	0.427	
		C_atmperc	-3.140	22	-0.279	0.783	-0.928	0.364	0.128	0.899	1.143	0.297	1.465	0.239	0.016	0.899	0.874	
		C_perc	-77.370	22	0.623	0.540	0.086	0.932	0.264	0.794	2.682	0.116	0.161	0.692	0.070	0.794	0.751	
		N_abs	159.280	22	-1.375	0.183	-1.012	0.322	1.080	0.292	1.487	0.236	0.112	0.741	1.167	0.292	0.633	
		N_atmperc	47.640	22	-0.146	0.885	-0.833	0.414	0.091	0.928	0.682	0.418	1.235	0.279	0.008	0.928	0.877	
		N_perc	-79.810	22	0.163	0.872	0.380	0.708	0.186	0.854	0.943	0.342	0.556	0.464	0.035	0.854	0.101	
		$\delta^{13}C$	-19.940	22	5.995	0.000	-0.335	0.741	0.172	0.865	105.010	<.0001	0.090	0.763	0.030	0.865	0.420	
		CN	-2.380	22	-0.648	0.524	-0.092	0.927	-0.355	0.726	3.450	0.077	0.260	0.618	0.130	0.726	0.698	
	SaOM	weight_abs	40.520	22	-0.037	0.971	-1.051	0.305	-0.023	0.982	1.107	0.304	2.396	0.136	0.001	0.982	0.275	
		weight_rel	-64.330	22	1.498	0.148	-0.431	0.671	-1.082	0.291	0.016	0.901	3.097	0.092	1.171	0.291	0.022	
		C_abs	103.310	22	-0.635	0.532	-0.449	0.658	0.003	0.998	2.192	0.153	0.418	0.524	0.000	0.998	0.082	
		C_atmperc	-15.570	22	-1.036	0.312	-0.279	0.783	0.306	0.763	2.078	0.164	0.007	0.934	0.093	0.763	0.842	
		C_perc	-75.510	22	1.078	0.293	0.288	0.776	-0.422	0.677	1.695	0.207	0.001	0.980	0.178	0.677	0.514	
		N_abs	163.490	22	-0.320	0.752	-0.536	0.598	0.335	0.741	0.157	0.695	0.181	0.675	0.112	0.741	0.129	
		N_atmperc	44.230	22	-0.497	0.624	-0.229	0.821	0.651	0.522	0.030	0.864	0.122	0.730	0.423	0.522	0.944	
		N_perc	-74.140	22	1.003	0.327	0.507	0.617	-0.375	0.711	2.134	0.158	0.117	0.736	0.141	0.711	0.231	
		$\delta^{13}C$	56.170	22	-5.885	0.000	1.789	0.087	-1.525	0.142	127.700	<.0001	1.000	0.331	2.300	0.142	0.020	log*-1
		CN	7.610	22	-0.856	0.401	-0.182	0.857	-0.097	0.923	3.265	0.085	0.134	0.718	0.009	0.923	0.035	log
miA	fPOM	weight_abs	-22.920	22	1.431	0.166	1.161	0.258	-0.910	0.373	3.133	0.091	0.530	0.474	0.828	0.373	0.406	log
		weight_rel	-3.880	22	0.722	0.478	1.000	0.328	-0.933	0.361	0.138	0.714	0.222	0.642	0.870	0.361	0.925	
		C_abs	153.350	22	1.222	0.235	0.623	0.540	-0.631	0.535	2.114	0.160	0.058	0.812	0.398	0.535	0.219	
		C_atmperc	-88.850	22	0.228	0.822	-0.958	0.348	0.457	0.652	0.150	0.702	0.828	0.373	0.209	0.652	0.074	
					T-Test						F-Test							

					CO_2		T		CO_2 x T		CO_2		T		CO_2 x T		Norm.	Transf.
Size class	Fraction	Variable	logLik	df	t-Value	p	t-Value	p	t-Value	p	F-Value	p	F-Value	p	F-Value	p	p	
		C_perc	-65.360	22	0.180	0.859	-0.371	0.714	0.388	0.702	0.496	0.489	0.017	0.897	0.151	0.702	0.547	
		N_abs	-25.240	22	1.298	0.208	1.253	0.224	-1.070	0.296	1.749	0.200	0.480	0.496	1.146	0.296	0.631	log
		N_atmperc	1.100	21	1.123	0.274	1.955	0.064	-1.957	0.064	0.006	0.942	0.591	0.451	3.831	0.064	0.566	Removed 52
		N_perc	-53.820	22	0.033	0.974	0.799	0.433	-0.496	0.625	0.025	0.875	0.408	0.530	0.246	0.625	0.056	
		$\delta^{13}C$	-45.150	22	1.887	0.072	-3.555	0.002	2.582	0.017	23.897	0.000	5.974	0.023	6.666	0.017	0.253	
		CN	-11.210	22	0.210	0.836	-1.102	0.282	0.772	0.448	0.675	0.420	0.621	0.439	0.596	0.448	0.189	
	iPOM	weight_abs	148.540	22	0.540	0.595	1.425	0.168	-0.811	0.426	0.453	0.508	1.474	0.238	0.658	0.426	0.642	
		weight_rel	-1.970	22	-0.918	0.368	0.078	0.939	-0.148	0.884	3.153	0.090	0.002	0.966	0.022	0.884	0.023	log
		C_abs	168.270	22	0.594	0.559	1.622	0.119	-0.882	0.387	0.655	0.427	2.032	0.168	0.778	0.387	0.207	
		C_atmperc	-46.840	22	-0.020	0.984	0.784	0.441	0.089	0.930	0.704	0.410	1.514	0.232	0.008	0.930	0.008	
		C_perc	-52.340	22	-1.833	0.080	-0.499	0.623	1.063	0.299	2.466	0.131	0.154	0.699	1.130	0.299	0.838	
		N_abs	234.630	22	0.800	0.433	1.166	0.256	-0.772	0.448	0.915	0.349	0.774	0.389	0.596	0.448	0.500	
		N_atmperc	10.700	22	0.672	0.509	-1.586	0.127	0.569	0.575	0.627	0.437	2.899	0.103	0.323	0.575	0.352	
		N_perc	-42.600	22	-1.807	0.084	-0.807	0.428	1.138	0.268	2.767	0.110	0.001	0.981	1.294	0.268	0.303	
		$\delta^{13}C$	-26.910	22	7.123	0.000	-1.220	0.235	0.915	0.370	163.220	<.0001	0.650	0.427	0.840	0.370	0.490	
		CN	21.760	22	-0.553	0.586	1.631	0.117	-0.360	0.722	0.020	0.879	3.950	0.060	0.130	0.722	0.037	log
	CaOM	weight_abs	53.710	22	1.578	0.129	0.849	0.405	-0.684	0.501	4.689	0.042	0.263	0.613	0.468	0.501	0.265	
		weight_rel	-52.350	22	-0.085	0.933	-2.392	0.026	0.810	0.427	0.592	0.450	6.849	0.016	0.656	0.427	0.951	
		C_abs	133.470	22	1.333	0.196	0.319	0.752	-0.383	0.706	3.384	0.079	0.004	0.952	0.147	0.706	0.774	
		C_atmperc	-2.430	22	-0.713	0.484	-1.638	0.116	1.020	0.319	0.587	0.452	1.701	0.206	1.040	0.319	0.181	
		C_perc	-75.150	22	-1.762	0.092	-2.645	0.015	2.459	0.022	0.560	0.462	1.574	0.223	6.047	0.022	0.694	
		N_abs	184.390	22	1.531	0.140	0.243	0.810	-0.401	0.692	4.299	0.050	0.005	0.946	0.161	0.692	0.742	
		N_atmperc	53.710	22	1.578	0.129	0.849	0.405	-0.684	0.501	4.689	0.042	0.263	0.613	0.468	0.501	0.265	
		N_perc	-73.330	22	-2.106	0.047	-3.061	0.006	3.126	0.005	0.203	0.657	1.339	0.260	9.773	0.005	0.414	
		$\delta^{13}C$	-8.230	22	9.305	0.000	-1.132	0.270	1.041	0.309	282.690	<.0001	0.300	0.589	1.080	0.309	0.902	
		CN	-9.520	22	-1.653	0.113	0.799	0.433	-0.207	0.838	6.201	0.021	0.884	0.357	0.043	0.838	0.324	

					T-Test						F-Test							
					CO_2		T		CO_2 x T		CO_2		T		CO_2 x T		Norm.	Transf.
Size class	Fraction	Variable	logLik	df	t-Value	p	t-Value	p	t-Value	p	F-Value	p	F-Value	p	F-Value	p	p	
	SaOM	weight_abs	51.390	22	1.310	0.204	1.439	0.164	-0.756	0.458	4.428	0.047	1.673	0.209	0.571	0.458	0.266	
		weight_rel	-52.740	22	-0.026	0.980	2.237	0.036	-0.609	0.549	0.672	0.421	6.779	0.016	0.371	0.549	0.826	
		C_abs	-13.320	22	2.650	0.015	2.763	0.011	-2.660	0.014	3.957	0.059	1.475	0.237	7.076	0.014	0.951	
		C_atmperc	-23.050	22	2.119	0.046	1.961	0.063	-2.611	0.016	0.206	0.655	0.011	0.919	6.819	0.016	0.179	
		C_perc	-75.010	22	2.312	0.031	3.080	0.006	-3.105	0.005	0.738	0.400	1.457	0.240	9.640	0.005	0.683	
		N_abs	-12.510	22	2.861	0.009	2.522	0.019	-2.659	0.014	4.558	0.044	0.750	0.396	7.069	0.014	0.995	log
		N_atmperc	33.800	22	2.564	0.018	1.792	0.087	-2.914	0.008	0.243	0.627	0.210	0.651	8.489	0.008	0.261	
		N_perc	-75.190	22	2.334	0.029	2.694	0.013	-2.944	0.008	0.727	0.403	0.666	0.423	8.668	0.008	0.298	
		$\delta^{13}C$	-18.820	22	4.340	0.000	0.252	0.803	0.083	0.935	60.610	<.0001	0.210	0.655	0.010	0.935	0.789	
		CN	2.690	22	-0.225	0.824	0.687	0.499	-0.200	0.843	0.021	0.887	0.617	0.441	0.040	0.843	0.134	log

Table S3: TukeyHSD-Test results of the LME models (see Tab. 3a) for the proportion of C derived from the fumigation treatment for all size classes. Bold values mark significant differences between size class & treatment combination (α = 0.05).

	Size Classes	**Bulk Soil**		**maA**		**miA**		**Silt & Clay**	
Size Classes	**Temperature**	Ambient	+3°C	Ambient	+3°C	Ambient	+3°C	Ambient	+3°C
Bulk Soil	Ambient								
	+3°C	n.s.							
maA	Ambient	n.s.	n.s.						
	+3°C	n.s.	n.s.	n.s.					
miA	Ambient	n.s.	n.s.	n.s.	n.s.				
	+3°C	n.s.	n.s.	n.s.	n.s.	n.s.			
scA	Ambient	**0.008**	n.s.	**0.001**	n.s.	n.s.	n.s.		
	+3°C	**0.007**	**<.0001**	**0.002**	**<.0001**	**0.033**	**0.006**	n.s.	

Table S4: TukeyHSD-Test results of the LME models (see Tab. 3b + c) for the proportion of C derived from the fumigation treatment for maA/miA density fractions. Bold values mark significant differences between size class & treatment combination (α = 0.05).

maA	Fraction	fPOM		iPOM		MOM		Sand	
Fraction	**Temperature**	Ambient	+3°C	Ambient	+3°C	Ambient	+3°C	Ambient	+3°C
fPOM	Ambient								
	+3°C	n.s.							
iPOM	Ambient	**0.072**	n.s.						
	+3°C	n.s.	n.s.	n.s.					
CaOM	Ambient	**<.0001**	**0.043**	**0.034**	n.s.				
	+3°C	**0.002**	**<.0001**	**0.095**	**0.001**	n.s.			
SaOM	Ambient	**<.0001**	**0.083**	**0.099**	n.s.	n.s.	n.s.		
	+3°C	**0.002**	**<.0001**	**0.068**	**<.0001**	n.s.	n.s.	n.s.	

mIA	Fraction	fPOM		iPOM		MOM		Sand	
Fraction	**Temperature**	Ambient	+3°C	Ambient	+3°C	Ambient	+3°C	Ambient	+3°C
fPOM	Ambient								
	+3°C	**0.046**							
iPOM	Ambient	n.s.	n.s.						
	+3°C	n.s.	**0.013**	n.s.					
CaOM	Ambient	**0.041**	n.s.	n.s.	n.s.				
	+3°C	**0.063**	n.s.	n.s.	**0.031**	n.s.			
SaOM	Ambient	**0.004**	n.s.	**0.029**	n.s.	n.s.	n.s.		
	+3°C	**0.025**	n.s.	**0.074**	**0.002**	n.s.	n.s.	n.s.	

Table S5: Tukey-HSD post-hoc test results for the weight proportion of size classes or fractions with a significant treatment effect in the LME model (α = 0.05).

a) maA Bulk	Ambient	eT	eCO_2	eT x eCO_2
Ambient				
eT	n.s.			
eCO_2	n.s.	n.s.		
eT x eCO_2	0.069	n.s.	n.s.	

b) miA Bulk	Ambient	eT	eCO_2	eT x eCO_2
Ambient				
eT	n.s.			
eCO_2	n.s.	n.s.		
eT x eCO_2	0.064	n.s.	n.s.	

c) maA fPOM	Ambient	eT	eCO_2	eT x eCO_2
Ambient				
eT	n.s.			
eCO_2	n.s.	n.s.		
eT x eCO_2	0.04	n.s.	n.s.	

d) maA iPOM	Ambient	eT	eCO_2	eT x eCO_2
Ambient				
eT	n.s.			
eCO_2	n.s.	n.s.		
eT x eCO_2	0.093	n.s.	n.s.	

Table S6: Tukey-HSD post-hoc test results for the relative carbon content of size classes or fractions with a significant treatment effect in the LME model (α = 0.05).

a) maA iPOM	Ambient	eT	eCO_2	eT x eCO_2
Ambient				
eT	n.s.			
eCO_2	0.018	0.040		
eT x eCO_2	n.s.	n.s.	n.s.	

b) miA CaOM	Ambient	eT	eCO_2	eT x eCO_2
Ambient				
eT	n.s.			
eCO_2	n.s.	n.s.		
eT x eCO_2	n.s.	n.s.	0.066	

c) miA SaOM	Ambient	eT	eCO_2	eT x eCO_2
Ambient				
eT	n.s.			
eCO_2	n.s.	n.s.		
eT x eCO_2	n.s.	n.s.	0.026	

Table S7: Tukey-HSD post-hoc test results for the relative nitrogen content of size classes or fractions with a significant treatment effect in the LME model (α = 0.05).

a) maA fPOM	Ambient	eT	eCO_2	eT x eCO_2
Ambient				
eT	n.s.			
eCO_2	n.s.	n.s.		
eT x eCO_2	n.s.	n.s.	n.s.	

b) maA iPOM	Ambient	eT	eCO_2	eT x eCO_2
Ambient				
eT	n.s.			
eCO_2	n.s.	n.s.		
eT x eCO_2	0.061	n.s.	n.s.	

c) miA CaOM	Ambient	eT	eCO_2	eT x eCO_2
Ambient				
eT	n.s.			
eCO_2	n.s.	n.s.		
eT x eCO_2	n.s.	n.s.	0.027	

d) miA SaOM	Ambient	eT	eCO_2	eT x eCO_2
Ambient				
eT	n.s.			
eCO_2	n.s.	n.s.		
eT x eCO_2	n.s.	n.s.	0.059	

Table S8: PERMANOVA results (degrees of freedom (df), F- and p-values) for the effect of fraction and treatment on pyrolysis-GC/MS relative abundance data of all found peaks with assignable origin from literature (based on a Bray-Curtis dissimilarity matrix). Bold values signify significant model terms (α = 0.05).

	Fraction			**Treatment**			**Fraction x Treatment**		
	df	F	p	df	F	p	df	F	p
POM	4	1180.04	**0.020**	3	688.39	0.074	12	-170.90	0.970

Table S9: Substance library used for Pyrolysis-GC/MS analysis with assigned origin classes from literature.

Nr	*Substance*	*Origin class*	*Reference*
1	1H-Inden-1-one, 2,3-dihydro-	Aromatics & Phenols	Stewart (2012)
2	2-Methylindene	Aromatics & Phenols	Zhe et al. (2019)
3	Benzaldehyde	Aromatics & Phenols	Stewart (2012), Carr et al. (2010)
4	Benzene	Aromatics & Phenols	Vancampenhout et al. (2009), Stewart (2012), Carr et al. (2010)
5	Benzene, 1-ethyl-2-methyl	Aromatics & Phenols	Zhe et al. (2019)
6	Benzene, n-butyl-	Aromatics & Phenols	Stewart (2012)
7	Benzene, propyl-	Aromatics & Phenols	Vancampenhout et al. (2009), Stewart (2012), Carr et al. (2010)
8	Ethanone, 1-(3-hydroxy-4-methoxyphenyl)-	Aromatics & Phenols	Stewart (2012)
9	Ethylbenzene	Aromatics & Phenols	Vancampenhout et al. (2009), Stewart (2012), Carr et al. (2010)
10	Indene	Aromatics & Phenols	Vancampenhout et al. (2009), Carr et al. (2010)
11	Mesitylene	Aromatics & Phenols	Zhe et al. (2019)
12	Naphthalene	Aromatics & Phenols	Vancampenhout et al. (2009), Stewart (2012), Carr et al. (2010)
13	Naphthalene, 1-methyl-	Aromatics & Phenols	Tolu et al. (2017)
14	Naphthalene, 1,6-dimethyl-	Aromatics & Phenols	Carr et al. (2010)
15	Naphthalene, 2-methyl-	Aromatics & Phenols	Carr et al. (2010)
16	o-Xylene	Aromatics & Phenols	Carr et al. (2010)
17	p-Cresol	Aromatics & Phenols	Stewart (2012); Carr et al. (2010)
18	p-Xylene	Aromatics & Phenols	Carr et al. (2010)
19	Phenol	Aromatics & Phenols	Vancampenhout et al. (2009), Stewart (2012), Carr et al. (2010)
20	Phenol, 2-ethyl-	Aromatics & Phenols	Carr et al. (2010)
21	Phenol, 2-methyl-	Aromatics & Phenols	Carr et al. (2010)
22	Phenol, 3-ethyl-	Aromatics & Phenols	Vancampenhout et al. (2009), Carr et al. (2010)
23	Phenol, 3-methyl-	Aromatics & Phenols	Stewart (2012)
24	Phenol, 4-ethyl-	Aromatics & Phenols	Stewart (2012)
25	Styrene	Aromatics & Phenols	Vancampenhout et al. (2009), Carr et al. (2010)
26	Toluene	Aromatics & Phenols	Vancampenhout et al. (2009), Stewart (2012), Carr et al. (2010)
27	α-Methylstyrene	Aromatics & Phenols	Fabbri et al. (1998)
28	Acetophenone	Aromatics & Phenols	Stewart (2012)
29	1,4-Cyclohex-2-enedione	Carbohydrates	Stewart (2012)
30	2-Cyclopenten-1-one	Carbohydrates	Zhe et al. (2019)
31	2-Cyclopenten-1-one, 2-hydroxy-	Carbohydrates	Stewart (2012)
32	2-Cyclopenten-1-one, 2-hydroxy-3-methyl-	Carbohydrates	Stewart (2012)
33	2-Cyclopenten-1-one, 2-methyl-	Carbohydrates	Stewart (2012)
34	2-Cyclopenten-1-one, 2,3-dimethyl-	Carbohydrates	Stewart (2012)
35	2-Cyclopenten-1-one, 3-methyl-	Carbohydrates	Stewart (2012)
36	2-Furancarboxaldehyde, 5-methyl-	Carbohydrates	Vancampenhout et al. (2009), Stewart (2012)
37	2-Furanmethanol	Carbohydrates	Stewart (2012)
38	2-Propenal	Carbohydrates	Saiz-Jimenez & de Leeuw (1985)
39	2-Vinylfuran	Carbohydrates	Stewart (2012)
40	2,3-Anhydro-d-galactosan	Carbohydrates	Smith et al. 2016
41	2(3H)-Furanone, 5-methyl-	Carbohydrates	Stewart (2012)
42	2(5H)-Furanone	Carbohydrates	Stewart (2012)
Nr	**Substance**	**Origin class**	**Reference**
43	2(5H)-Furanone, 5-methyl-	Carbohydrates	Stewart (2012)

44	3-Furaldehyde	Carbohydrates	Vancampenhout et al. (2009), Stewart (2012), Carr et al. (2010)
45	5-Hydroxymethylfurfural	Carbohydrates	Stewart (2012)
46	Acetone	Carbohydrates	Saiz-Jimenez & de Leeuw (1985)
47	Benzofuran	Carbohydrates	Girona-García et al. 2019
48	Benzofuran, 2-methyl-	Carbohydrates	Stewart (2012)
49	Ethanone, 1-(2-furanyl)-	Carbohydrates	Vancampenhout et al. (2009), Stewart (2012), Carr et al. (2010)
50	Furan, 2-methyl-	Carbohydrates	Vancampenhout et al. (2009), Stewart (2012)
51	Furan, 2,3-dihydro-	Carbohydrates	Saiz-Jimenez & de Leeuw (1985)
52	Furfural	Carbohydrates	Vancampenhout et al. (2009), Stewart (2012)
53	Levoglucosenone	Carbohydrates	Vancampenhout et al. (2009), Stewart (2012)
54	Maltol	Carbohydrates	Vancampenhout et al. (2009), Stewart (2012)
55	2-Methoxy-4-vinylphenol	Lignin Derivates	Vancampenhout et al. (2009), Stewart (2012), Carr et al. (2010)
56	Creosol	Lignin Derivates	Vancampenhout et al. (2009), Stewart (2012), Carr et al. (2010)
57	Phenol, 2-methoxy-	Lignin Derivates	Stewart (2012), Carr et al. (2010)
58	Phenol, 2-methoxy-4-(1-propenyl)-, (Z)-	Lignin Derivates	Stewart (2012), Carr et al. (2010)
59	Phenol, 2,6-dimethoxy-	Lignin Derivates	Vancampenhout et al. (2009), Stewart (2012), Carr et al. (2010)
60	Phenol, 2,6-dimethoxy-4-(2-propenyl)-	Lignin Derivates	Stewart (2012), Carr et al. (2010)
61	Phenol, 4-ethyl-2-methoxy-	Lignin Derivates	Vancampenhout et al. (2009), Stewart (2012), Carr et al. (2010)
62	1-Decene	Lipids	Vancampenhout et al. (2009), Stewart (2012), Carr et al. (2010)
63	1-Docosene	Lipids	Vancampenhout et al. (2009), Stewart (2012), Carr et al. (2010)
64	1-Dodecene	Lipids	Vancampenhout et al. (2009), Stewart (2012), Carr et al. (2010)
65	1-Heptadecene	Lipids	Stewart (2012), Carr et al. (2010)
66	1-Nonadecene	Lipids	Stewart (2012), Carr et al. (2010)
67	1-Nonene	Lipids	Vancampenhout et al. (2009), Stewart (2012), Carr et al. (2010)
68	1-Nonene, 4,6,8-trimethyl-	Lipids	Vancampenhout et al. (2009), Stewart (2012), Carr et al. (2010)
69	1-Octadecene	Lipids	Vancampenhout et al. (2009), Stewart (2012), Carr et al. (2010)
70	1-Pentadecene	Lipids	Vancampenhout et al. (2009), Stewart (2012), Carr et al. (2010)
71	1-Tetracosene	Lipids	Carr et al. (2010)
72	1-Tetradecene	Lipids	Vancampenhout et al. (2009), Stewart (2012), Carr et al. (2010)
73	1-Tridecene	Lipids	Vancampenhout et al. (2009), Stewart (2012), Carr et al. (2010)
74	1-Undecene	Lipids	Vancampenhout et al. (2009), Stewart (2012), Carr et al. (2010)
75	3-Dodecene, (Z)-	Lipids	Vancampenhout et al. (2009), Stewart (2012), Carr et al. (2010)
76	3-Eicosene, (E)-	Lipids	Stewart (2012), Carr et al. (2010)
77	Cetene	Lipids	Vancampenhout et al. (2009), Stewart (2012), Carr et al. (2010)
78	Decanal	Lipids	Zang & Hatcher (2002)
79	Decane	Lipids	Vancampenhout et al. (2009), Stewart (2012), Carr et al. (2010)
80	Dodecane	Lipids	Vancampenhout et al. (2009), Stewart (2012), Carr et al. (2010)
81	Dodecane, 2,7,10-trimethyl-	Lipids	Vancampenhout et al. (2009), Stewart (2012), Carr et al. (2010)
82	Heneicosane	Lipids	Vancampenhout et al. (2009), Stewart (2012), Carr et al. (2010)
83	Heptadecane	Lipids	Vancampenhout et al. (2009), Stewart (2012), Carr et al. (2010)
84	Heptadecanoic acid,16-methyl-,methyl ester	Lipids	Stewart (2012)
85	Hexadecane	Lipids	Vancampenhout et al. (2009), Stewart (2012), Carr et al. (2010)
86	Hexadecanoic acid, methyl ester	Lipids	Stewart (2012)
87	Nonadecane	Lipids	Vancampenhout et al. (2009), Stewart (2012), Carr et al. (2010)
88	Nonanal	Lipids	Zang & Hatcher (2002)
Nr	**Substance**	**Origin class**	**Reference**

89	Nonane	Lipids	Vancampenhout et al. (2009), Stewart (2012), Carr et al. (2010)
90	Octadecane	Lipids	Vancampenhout et al. (2009), Stewart (2012), Carr et al. (2010)
91	Pentadecane	Lipids	Vancampenhout et al. (2009), Stewart (2012), Carr et al. (2010)
92	Tetradecane	Lipids	Vancampenhout et al. (2009), Stewart (2012), Carr et al. (2010)
193	Tridecane	Lipids	Vancampenhout et al. (2009), Stewart (2012), Carr et al. (2010)
94	Tridecane, 2-methyl-	Lipids	Vancampenhout et al. (2009), Stewart (2012), Carr et al. (2010)
95	Undecane	Lipids	Vancampenhout et al. (2009), Stewart (2012), Carr et al. (2010)
96	Undecane, 3,8-dimethyl-	Lipids	Vancampenhout et al. (2009), Stewart (2012), Carr et al. (2010)
97	Undecane, 4,7-dimethyl-	Lipids	Vancampenhout et al. (2009), Stewart (2012), Carr et al. (2010)
98	1H-Pyrrole, 1-methyl-	N-Containing	Stewart (2012)
99	1H-Pyrrole, 2-methyl-	N-Containing	Stewart (2012)
100	1H-Pyrrole, 3-methyl-	N-Containing	Stewart (2012), Carr et al. (2010)
101	2-Furancarbonitrile	N-Containing	Siljeström et al. 2014
102	2-Propenenitrile	N-Containing	Stewart (2012)
103	2-Pyridinecarbonitrile	N-Containing	Stewart (2012)
104	3-Acetamidofuran	N-Containing	Tolu et al. 2017
105	Acetamide	N-Containing	Tolu et al. 2017
106	Benzenepropanenitrile	N-Containing	Stewart (2012)
107	Benzonitrile	N-Containing	Vancampenhout et al. (2009), Stewart (2012), Carr et al. (2010)
108	Benzonitrile, 3-methyl-	N-Containing	Carr et al. (2010)
109	Benzyl nitrile	N-Containing	Stewart (2012)
110	Hexadecanenitrile	N-Containing	Stewart (2012)
111	Indole	N-Containing	Vancampenhout et al. (2009), Stewart (2012), Carr et al. (2010)
112	Isoamyl cyanide	N-Containing	Stewart (2012)
113	Octadecanenitrile	N-Containing	Carr et al. (2013)
114	Pyridine	N-Containing	Vancampenhout et al. (2009), Stewart (2012), Carr et al. (2010)
115	Pyridine, 2-methyl-	N-Containing	Stewart (2012), Carr et al. (2010)
116	Pyridine, 3-methyl-	N-Containing	Stewart (2012)
117	Pyrrole	N-Containing	Vancampenhout et al. (2009), Stewart (2012)
118	Peak Unknown	General & Unknown	
119	2-Propen-1-ol	General & Unknown	

3) Code Example

```
# Generic code to evaluate peak area data and calculate relative abundance

# Preparations ##############################################################

# Load Packages
library(tidyverse)
library(plyr)
library(readr)
library(ggplot2)
library(vegan)
library(dplyr)
library(tibble)
library(phyloseq)
library(metagMisc)

# Working directory where output is stored:
setwd("/Path_WD/")
output_path <- "/Path_Output/"

# Initialize Functions:
sum_treat_fun <- function(df, treatment){
  x <- sum(df$Abundance[df$Treatment == treatment])
  return(x)
}

calc_rel_fun <- function(x, sum_treatment, treatment){
  rel_x = transform_sample_counts(x, function(x) x / sum_treatment)
  df_x <- psmelt(rel_x)
  df_x <- filter(df_x, Treatment == treatment)
  return(df_x)
}

data_summary <- function(data, varname, groupnames){
  require(plyr)
  summary_func <- function(x, col){
    c(mean = mean(x[[col]], na.rm=TRUE),
      se = sd(x[[col]]/sqrt(length(x[[col]])), na.rm=TRUE))
  }
  data_sum<-ddply(data, groupnames, .fun=summary_func,
                  varname)
  data_sum <- rename(data_sum, c("mean" = varname))
  return(data_sum)
}

# Import the individual samples as .csv files:
# Exported from Chromatof in XIC and TIC and stored as .csv file

mydir = "Samples"
myfiles = list.files(path=mydir, pattern="*.csv", full.names=TRUE)
# Imported Files:
myfiles
dat csv = ldply(myfiles, read csv)
colnames(dat_csv) <- c("Sample", "Name", "RT", "Area", "RI", "Quant", "Match", "SN",
"Origin", "Type", "Group")

# Data Manipulation
##############################################################################################
#####

# Data is aligned with Reference Library and merged
# with the total Library and Treatment file to get Origin of peaks and treatment Levels
for this experiment.
# Blank correction is performed. Peaks with negative area after this step get set to 0.
NAs are put to 0 as well.

# remove TIC
dat_csv1<-subset(dat_csv,Quant!="TIC")

# Create new Column with new unique names
dat_csv1$Double<-paste(dat_csv1$Name,dat_csv1$Quant)
```

```
# remove +- character
dat_csv1$Double <- iconv(dat_csv1$Double, 'utf-8', 'ascii', sub='_')


# Import reference datafile (from reference sample)
file <- file.choose(new = FALSE)
reference <- read.csv(file,header=T,dec=".",sep=",")
reference[reference==""] <- NA
head(reference)

# remove +- character
reference$Quant <- iconv(reference$Quant, 'utf-8', 'ascii', sub='_')

# Create new Column with new unique names (same names as line 67)
reference$Double<-paste(reference$Name,reference$Quant)

# Aggregate Samples
m1 <- aggregate(Area ~ Sample + Double + Type  , data = dat_csv1, FUN = mean, na.action =
na.pass)

# Merge and align Samples and Reference
new<- merge(reference, m1, by.y = "Double")

# Select Columns we want to use
new1<-new %>%
  select(Double, Sample, Area)

# reorganize (transpose) dataframe
new1<-reshape(new1, timevar="Sample", idvar="Double", direction="wide")

# create new dataframe with Blanks
blank<-select(new1,contains("Blank"))

# Import "Double" so names are the same, put it as first column
blank<-add_column(blank, new1$Double, .before = 1)

# calculate mean of blank of every peak
blank<-data.frame(ID=blank[,1], Means=rowMeans(blank[,-1]))

# Remove blank from dataframe so only samples remain
new1<-new1[, -grep("Blank", colnames(new1))]

# put NAs to 0
new1[is.na(new1)] = 0
blank[is.na(blank)] = 0

# Substract mean of Blanks from samples
result = new1[, 2 : ncol(new1)] - blank$Means

# Create new dataframe with only important information, clean names etc, set negatives to
0
otumat <- cbind(new1$Double,result)
otumat[otumat<0] <- 0
for ( col in 1:ncol(otumat)){
  colnames(otumat)[col] <-  sub("Area.", "", colnames(otumat)[col])
}

colnames(otumat)[1]<-"Name"
a<-otumat$Name
a<-gsub(" XIC.*","",a)
otumat[, 1] <- a
otumat[is.na(otumat)] = 0

# Export file
write.csv(otumat, file.path(output_path, "AbsolutePeakAreas.csv"), row.names=FALSE)

#load samples description file (has to have same sample names as samples)
file <- file.choose(new = FALSE)
meta_table <- read.csv(file,header=T,dec=".",sep=";", row.names=1)
meta_table[meta_table==""] <- NA
meta_table$SampleID <- row.names(meta_table)
head(meta_table)

# C content of sample
meta_table$C_amount <- (meta_table$Weight * meta_table$C_perc)/100*1000  ### Unit == µg
```

```
#### Transform absolute peak area into C amount
otumat1 = setNames(data.frame(t(otumat[,-1])), otumat[,1])
otumat1 <- (otumat1*meta_table$C_amount)/rowSums(otumat1)
otumat1 = data.frame(t(otumat1))
otumat1$Name <- otumat$Name
otumat1 <- otumat1[,c(ncol(otumat1),1:ncol(otumat1)-1)]
colnames(otumat1) <- colnames(otumat)
otumat <- otumat1

# Import Library file
file <- file.choose(new = FALSE)
library <- read.csv(file,header=T,dec=".",sep=";",  stringsAsFactors = FALSE)
library[library==""] <- NA
names(library) <- c("Name", "Origin", "Identified")

# Merge library and dataframe, fill missing entries and clean data
library<- merge(otumat, library, by = "Name", all = TRUE)
library = subset(library, select = c(Name,Origin,Identified) )
library$Origin[library$Origin == "N-Containing"] <- "N Containing"
library$Origin[library$Origin == "N-Containing "] <- "N Containing"
library$Origin[is.na(library$Origin)] <- "Unidentified"
library$Identified[is.na(library$Identified)] <- "NO"

# Generate phyloseq object

# Data is treated like Sequencing data where the OTUs resemble individual peaks. origin
# and treatment are used to group them.

rownames(otumat) <- otumat[,1]
otumat <- otumat[,-1]
otumat <- data.matrix(otumat)
rownames(library) <- library[,1]
taxmat <- as.matrix(library)
meta_table$Lib.size = colSums(otumat)

OTU = otu_table(otumat, taxa_are_rows = TRUE)
TAX = tax_table(taxmat)
SAM = sample_data(meta_table)

physeq <- merge_phyloseq(phyloseq(OTU, TAX), SAM)
sample_names(SAM)

# Data Quality check

# check if any OTUs are not present in any samples
any(taxa_sums(physeq) == 0)
physeq <- prune_taxa(taxa_sums(physeq) > 0, physeq) #use this to remove the OTU that are
not found in any sample
physeq

# 3) Data normalization

# Relative area per peak per sample is calculated for the barplots with error bars.
Relative area per
# origin per treatment is calculated for the stacked barplot.

# calculate relative Abundance per Sample and transform to numeric for calculation of
indices
physeq.rel= transform_sample_counts(physeq, function(x) x / sum(x))

# Physeq Object for calculation of richness indices
physeq.rel.alpha  = transform_sample_counts(physeq.rel, function(x)
round((x*10000),digits=0))

# Convert phyloseq objects into dataframes
df_rel <- psmelt(physeq.rel)
df_norm <- psmelt(physeq)

# Export Absolute Data (normalized by C content)
write.csv(df_norm, file.path(output_path, "AbsolutePeakAreas_normalized.csv"),
row.names=FALSE)

# Export Relative Data
write.csv(df_rel, file.path(output_path, "RelativePeakAreas.csv"), row.names=FALSE)
```

```
treat_list <- levels(SAM$Treatment)

# Grouping by Treatment

# Calculate area sum for each treatment and store in vector
sum_all_treatments <-vector()

for(i in 1 : length(treat_list)){
  sum_all_treatments[i] <- sum_treat_fun(df_norm, treat_list[i])
}

# Create dataframe with relative Abundances per Treatment
data_rel <- data.frame()

for(i in 1 : length(treat_list)){
  tmp <- calc_rel_fun(physeq, sum_all_treatments[i], treat_list[i])
  data_rel <- rbind(data_rel, tmp)
}

data_rel_export <- subset(data_rel, select = c(Name,Sample,Origin,Abundance, Treatment) )

# Export Relative Data per Treatment
write.csv(data_rel_export, file.path(output_path,
"RelativePeakAreas_GroupedByTreatment.csv"), row.names=FALSE)

save.image(file="environment.RData")

# Quality Check

require("tidyverse")
require(plyr)
require(readr)
require("ggplot2")
require("vegan")
require(dplyr)
require(tibble)

# Aggregate Samples
m2 <- aggregate(Area ~ Sample + Double + Type + SN + RT + Match  , data = dat_csv1, FUN =
mean, na.action = na.pass)

# Merge and align Samples and Reference
new2<- merge(reference, m2, by.y = "Double")

# Merge library and dataframe, fill missing entries and clean data
library2<- merge(new2, library, by = "Name", all = TRUE)
library2 = subset(library2, select = c(Name,Origin, Sample, Identified, SN, RT, Match,
Area) )
library2 <- filter(library2, Identified == "YES")
library2[is.na(library2)] = 0

Peaks <- filter(library2, Match > 700)
Peaks <- filter(Peaks, Match < 850)

Peaks <- Peaks[order(Peaks$Sample, Peaks$RT),]

write.csv(Peaks, file.path(output_path, "PeaksToCheck_Similarity.csv"), row.names=FALSE)

PeakAreas <- read.csv(paste0(output_path,  "/RelativePeakAreas.csv"))

PeakAreas <- filter(PeakAreas, Identified != "YES")

PeakAreas <- filter(PeakAreas, Abundance > 0.01)

write.csv(PeakAreas, file.path(output_path, "PeaksToCheck_Area.csv"), row.names=FALSE)
```

PART 3

Summary

It is still unclear whether carbon stored in soil organic matter (SOM) will act as a source or as a sink for atmospheric carbon in future climatic conditions. The aim of the present study was to analyze how different climate change drivers (elevated CO_2 and warming) alone and in combination affect different soil aggregate classes and mineral-associated organic matter, ultimately to facilitate better model predications. Towards this goal, we used a combination of aggregate size class separation and density fractionation on soil from a multifactorial climate change experiment in Austria and analyzed the C and N content and isotopic composition, as well as the chemical composition of all obtained fractions. We found that total soil C was unaltered after four years of simulated climate change. Higher atmospheric CO_2-concentrations resulted in more macro-aggregates and more intra-macro-aggregate particulate organic matter, which could increase the susceptibility of SOM stocks to future disturbances. While elevated temperature slowed down the turnover of C in the bulk soil and aggregate size classes of plots subjected to elevated CO_2, we could not detect significant changes in the chemical composition of the investigated size classes and density fractions across our treatments. Our results further demonstrate that the combined effects of elevated CO_2 and warming on SOM fractions were additive and not interactive, at least in the short-term (4 years).

Zusammenfassung

Es ist immer noch unklar, ob der in der organischen Bodensubstanz („soil organic matter“ - SOM) gespeicherte Kohlenstoff unter zukünftigen Klimabedingungen als Quelle oder als Senke für atmosphärischen Kohlenstoff fungieren wird. Das Ziel dieser Studie war es, zu analysieren, wie bestimmte Klimawandeltreiber (erhöhte Temperatur sowie eine erhöhte atmosphärische CO_2-Konzentration) allein und in Kombination verschiedene Aggregatsklassen und mineral-assoziierte organisches Material beeinflussen, um letztlich bessere Modellvorhersagen zu ermöglichen Dafür haben wir eine Kombination aus Aggregatgrößenklassentrennung und Dichtefraktionierung an Böden aus einem multifaktoriellen Klimawandel-Experiment in Österreich durchgeführt und die erhaltenen Fraktionen auf ihren C und N-Gehalt sowie ihre isotopische und chemische Zusammensetzung hin analysiert. Unsere Ergebnisse zeigen, dass sich der Kohlenstoffgehalt des Bodens nicht durch den simulierten Klimawandel geändert hat. Höhere CO_2-Konzentrationen in der Atmosphäre haben zu mehr Makro-Aggregaten und mehr partikulärem organischem Material innerhalb dieser Aggregate geführt. Dies könnte die Anfälligkeit der SOM-Vorräte gegenüber zukünftigen Störungen des Ökosystems erhöhen. Obwohl der Umsatz von C im gesamten Boden und in den Aggregatgrößenklassen durch erhöhte Temperatur verlangsamt wurde, konnten wir keine signifikanten Veränderungen in der chemischen Zusammensetzung der untersuchten Aggregate und Dichtefraktionen mit unseren Methoden feststellen. Unsere Ergebnisse zeigen auch, dass die Effekte von erhöhter Temperatur und atmosphärischem CO_2 eher additiv als interaktiv waren, zumindest in den 4 Jahren seit Beginn des Experiments.

PART 4

References

Allison, S. D., Wallenstein, M. D., & Bradford, M. A. (2010). Soil-carbon response to warming dependent on microbial physiology. *Nature Geoscience*, *3*(5), 336–340. https://doi.org/10.1038/ngeo846

Amundson, R. (2001). The Carbon Budget in Soils. *Annual Review of Earth and Planetary Sciences*, *29*(1), 535–562. https://doi.org/10.1146/annurev.earth.29.1.535

Arrhenius, S. (1889). Über die Reaktionsgeschwindigkeit bei der Inversion von Rohrzucker durch Säuren. *Zeitschrift Für Physikalische Chemie*, *4U*(1). https://doi.org/10.1515/zpch-1889-0416

Bai, T., Wang, P., Hall, S. J., Wang, F., Ye, C., Li, Z., Li, S., Zhou, L., Qiu, Y., Guo, J., Guo, H., Wang, Y., & Hu, S. (2020). Interactive global change factors mitigate soil aggregation and carbon change in a semi-arid grassland. *Global Change Biology*, *26*(9), 5320–5332. https://doi.org/10.1111/gcb.15220

Bais, H. P., Weir, T. L., Perry, L. G., Gilroy, S., & Vivanco, J. M. (2006). the Role of Root Exudates in Rhizosphere Interactions With Plants and Other Organisms. *Annual Review of Plant Biology*, *57*(1), 233–266. https://doi.org/10.1146/annurev.arplant.57.032905.105159

Baveye, P. C., & Wander, M. (2019). The (Bio)Chemistry of Soil Humus and Humic Substances: Why Is the "New View" Still Considered Novel After More Than 80 Years? *Frontiers in Environmental Science*, *7*(March), 1–6. https://doi.org/10.3389/fenvs.2019.00027

Bronick, C. J., & Lal, R. (2005). Soil structure and management: A review. *Geoderma*, *124*(1–2), 3–22. https://doi.org/10.1016/j.geoderma.2004.03.005

Carrillo, Y., Dijkstra, F., LeCain, D., Blumenthal, D., & Pendall, E. (2018). Elevated CO_2 and warming cause interactive effects on soil carbon and shifts in carbon use by bacteria. *Ecology Letters*, *21*(11), 1639–1648. https://doi.org/10.1111/ele.13140

Chen, Z., Zhou, X., Geng, S., Miao, Y., Cao, Y., Chen, Z., Zhang, J., & Han, S. (2019). Interactive effect of nitrogen addition and throughfall reduction decreases soil aggregate stability through reducing biological binding agents. *Forest Ecology and Management*, *445*(January), 13–19. https://doi.org/10.1016/j.foreco.2019.04.057

Christensen, B. T. (2001). Physical fractionation of soil and structural and functional complexity in organic matter turnover. *European Journal of Soil Science*, *52*(3), 345–353. https://doi.org/10.1046/j.1365-2389.2001.00417.x

Chukov, S. N., Lodygin, E. D., & Abakumov, E. V. (2018). Application of 13C NMR Spectroscopy to the Study of Soil Organic Matter: A Review of Publications. *Eurasian Soil Science*, *51*(8), 889–900. https://doi.org/10.1134/S1064229318080021

Conant, R. T., Ryan, M. G., Ågren, G. I., Birge, H. E., Davidson, E. A., Eliasson, P. E., Evans, S. E., Frey, S. D., Giardina, C. P., Hopkins, F. M., Hyvönen, R., Kirschbaum, M. U. F., Lavallee, J. M., Leifeld, J., Parton, W. J., Megan Steinweg, J., Wallenstein, M. D., Martin Wetterstedt, J. Å., & Bradford, M. A. (2011). Temperature and soil organic matter decomposition rates - synthesis of current knowledge and a way forward. *Global Change Biology*, *17*(11), 3392–3404. https://doi.org/10.1111/j.1365-2486.2011.02496.x

Cotrufo, M. F., Ineson, P., & Scott, A. (1998). Elevated CO_2 reduces the nitrogen concentration of plant tissues. *Global Change Biology*, *4*(1), 43–54. https://doi.org/10.1046/j.1365-2486.1998.00101.x

Crow, S. E., Swanston, C. W., Lajtha, K., Brooks, J. R., & Keirstead, H. (2007). Density fractionation of forest soils: Methodological questions and interpretation of incubation results and turnover time in an ecosystem context. *Biogeochemistry*, *85*(1), 69–90. https://doi.org/10.1007/s10533-007-9100-8

Davidson, E. A., & Janssens, I. A. (2006). Temperature sensitivity of soil carbon decomposition and feedbacks to climate change. *Nature*, *440*(7081), 165–173. https://doi.org/10.1038/nature04514

Deltedesco, E., Keiblinger, K. M., Naynar, M., Piepho, H. P., Gorfer, M., Herndl, M., Bahn, M., Pötsch, E. M., & Zechmeister-Boltenstern, S. (2019). Trace gas fluxes from managed grassland soil subject to multifactorial climate change manipulation. *Applied Soil Ecology*, *137*(October 2018), 1–11. https://doi.org/10.1016/j.apsoil.2018.12.023

Deltedesco, E., Keiblinger, K. M., Piepho, H. P., Antonielli, L., Pötsch, E. M., Zechmeister-Boltenstern, S., & Gorfer, M. (2020). Soil microbial community structure and function mainly respond to indirect effects in a multifactorial climate manipulation experiment. *Soil Biology and Biochemistry*, *142*. https://doi.org/10.1016/j.soilbio.2020.107704

Derenne, S., & Quéné, K. (2015). Analytical pyrolysis as a tool to probe soil organic matter. *Journal of Analytical and Applied Pyrolysis*, *111*, 108–120. https://doi.org/10.1016/j.jaap.2014.12.001

Dieleman, W. I. J., Vicca, S., Dijkstra, F. A., Hagedorn, F., Hovenden, M. J., Larsen, K. S., Morgan, J. A., Volder, A., Beier, C., Dukes, J. S., King, J., Leuzinger, S., Linder, S., Luo, Y., Oren, R., De Angelis, P., Tingey, D., Hoosbeek, M. R., & Janssens, I. A. (2012). Simple additive effects are rare: A quantitative review of plant biomass and soil process responses to combined manipulations of CO_2 and temperature. *Global Change Biology*, *18*(9), 2681–2693. https://doi.org/10.1111/j.1365-2486.2012.02745.x

Dijkstra, P., Thomas, S. C., Heinrich, P. L., Koch, G. W., Schwartz, E., & Hungate, B. A. (2011). Effect of temperature on metabolic activity of intact microbial communities: Evidence for altered metabolic pathway activity but not for increased maintenance respiration and reduced carbon use efficiency. *Soil Biology and Biochemistry*, *43*(10), 2023–2031. https://doi.org/10.1016/j.soilbio.2011.05.018

Dolan, J. W. (2009). Calibration Curves, Part II: What are the limits? *LCGC North America*, *27*(4), 306–312. http://www.chromatographyonline.com/calibration-curves-part-ii-what-are-limits

Don, A., Rödenbeck, C., & Gleixner, G. (2013). Unexpected control of soil carbon turnover by soil carbon concentration. *Environmental Chemistry Letters*, *11*(4), 407–413. https://doi.org/10.1007/s10311-013-0433-3

Dorodnikov, M., Kuzyakov, Y., Fangmeier, A., & Wiesenberg, G. L. B. (2011). C and N in soil organic matter density fractions under elevated atmospheric CO_2: Turnover vs. stabilization. *Soil Biology and Biochemistry*, *43*(3), 579–589. https://doi.org/10.1016/j.soilbio.2010.11.026

Drigo, B., Kowalchuk, G. A., & Van Veen, J. A. (2008). Climate change goes underground: Effects of elevated atmospheric CO 2 on microbial community structure and activities in the rhizosphere. *Biology and Fertility of Soils*, *44*(5), 667–679. https://doi.org/10.1007/s00374-008-0277-3

Elliott, E. T. (1986). Aggregate Structure and Carbon, Nitrogen, and Phosphorus in Native and Cultivated Soils. *Soil Science of America Journal*, *50*. https://doi.org/https://doi.org/10.2136/sssaj1986.03615995005000030017x

Elliott, E. T., Palm, C. A., Reuss, D. E., & Monz, C. A. (1991). Organic matter contained in soil aggregates from a tropical chronosequence: correction for sand and light fraction. *Agriculture, Ecosystems and Environment*, *34*(1–4), 443–451. https://doi.org/10.1016/0167-8809(91)90127-J

Feng, X., & Simpson, M. J. (2008). Temperature responses of individual soil organic matter components. *Journal of Geophysical Research: Biogeosciences*, *113*(3), 1–14. https://doi.org/10.1029/2008JG000743

Fontaine, S., Mariotti, A., & Abbadie, L. (2003). The priming effect of organic matter: A question of microbial competition? *Soil Biology and Biochemistry*, *35*(6), 837–843. https://doi.org/10.1016/S0038-0717(03)00123-8

Frouz, J. (2018). Effects of soil macro- and mesofauna on litter decomposition and soil organic matter stabilization. *Geoderma*, *332*(March 2017), 161–172. https://doi.org/10.1016/j.geoderma.2017.08.039

Geng, J., Cheng, S., Fang, H., Pei, J., Xu, M., Lu, M., Yang, Y., Cao, Z., & Li, Y. (2019). Different molecular characterization of soil particulate fractions under N deposition in a subtropical forest. *Forests*, *10*(10), 1–18. https://doi.org/10.3390/f10100914

Gioacchini, P., Cattaneo, F., Barbanti, L., Montecchio, D., Ciavatta, C., & Marzadori, C. (2016). Carbon sequestration and distribution in soil aggregate fractions under Miscanthus and giant reed in the Mediterranean area. *Soil and Tillage Research*, *163*, 235–242. https://doi.org/10.1016/j.still.2016.06.009

Grunwald, D., Kaiser, M., & Ludwig, B. (2016). Effect of biochar and organic fertilizers on C mineralization and macro-aggregate dynamics under different incubation temperatures. *Soil and Tillage Research*, *164*, 11–17. https://doi.org/10.1016/j.still.2016.01.002

Hamer, U., & Marschner, B. (2005). Priming effects in soils after combined and repeated substrate additions. *Geoderma*, *128*(1–2), 38–51. https://doi.org/10.1016/j.geoderma.2004.12.014

Hu, S., Chapin, F. S., Firestone, M. K., Field, C. B., & Chiariello, N. R. (2001). Nitrogen limitation of microbial decomposition in a grassland under elevated CO_2. *Nature*, *409*(6817), 188–191.

https://doi.org/10.1038/35051576

IPCC, Pachauri, R. K., & Meyer, L. A. (2014). *Climate Change 2014 Synthesis Report*.

IPCC Working Group I. (2013). Climate Change 2013 - The Physical Science Basis. In *Researchgate.Net*. https://doi.org/10.1017/CBO9781107415324.Summary

Jastrow, J. D. (1996). Soil aggregate formation and the accrual of particulate and mineral-associated organic matter. *Soil Biology and Biochemistry*, *28*(4–5), 665–676. https://doi.org/10.1016/0038-0717(95)00159-X

Kleber, M., Sollins, P., & Sutton, R. (2007). A conceptual model of organo-mineral interactions in soils: Self-assembly of organic molecular fragments into zonal structures on mineral surfaces. *Biogeochemistry*, *85*(1), 9–24. https://doi.org/10.1007/s10533-007-9103-5

Klein, K., Gross-Schmölders, M., Alewell, C., & Leifeld, J. (2020). Heating up a cold case: Applications of analytical pyrolysis GC/MS to assess molecular biomarkers in peat. In *Advances in Agronomy* (Vol. 165, pp. 115–159). Academic Press Inc. https://doi.org/10.1016/bs.agron.2020.09.002

Knorr, W., Prentice, I. C., House, J. I., & Holland, E. A. (2005). Long-term sensitivity of soil carbon turnover to warming. *Nature*, *433*(7023), 298–301. https://doi.org/10.1038/nature03226

Kögel-Knabner, I. (1997). 13C and 15N NMR spectroscopy as a tool in soil organic matter studies. *Geoderma*, *80*(3–4), 243–270. https://doi.org/10.1016/S0016-7061(97)00055-4

Kögel-Knabner, I. (2000). Analytical approaches for characterizing soil organic matter. *Organic Geochemistry*, *31*(7–8), 609–625. https://doi.org/10.1016/S0146-6380(00)00042-5

Kögel-Knabner, I. (2017). The macromolecular organic composition of plant and microbial residues as inputs to soil organic matter: Fourteen years on. *Soil Biology and Biochemistry*, *105*, A3–A8. https://doi.org/10.1016/j.soilbio.2016.08.011

Kuzyakov, Y., Horwath, W. R., Dorodnikov, M., & Blagodatskaya, E. (2019). Review and synthesis of the effects of elevated atmospheric CO_2 on soil processes: No changes in pools, but increased fluxes and accelerated cycles. *Soil Biology and Biochemistry*, *128*(October 2018), 66–78. https://doi.org/10.1016/j.soilbio.2018.10.005

Lal, R., & Stewart, B. A. (2019). *Soil and Climate*. CRC Press.

Lavallee, J. M., Soong, J. L., & Cotrufo, M. F. (2020). Conceptualizing soil organic matter into particulate and mineral-associated forms to address global change in the 21st century. *Global Change Biology*, *26*(1), 261–273. https://doi.org/10.1111/gcb.14859

Lehmann, J., Hansel, C. M., Kaiser, C., Kleber, M., Maher, K., Manzoni, S., Nunan, N., Reichstein, M., Schimel, J. P., Torn, M. S., Wieder, W. R., & Kögel-Knabner, I. (2020). Persistence of soil organic carbon caused by functional complexity. *Nature Geoscience*, *13*(8), 529–534. https://doi.org/10.1038/s41561-020-0612-3

Lehmann, J., Kinyangi, J., & Solomon, D. (2007). Organic matter stabilization in soil microaggregates: Implications from spatial heterogeneity of organic carbon contents and carbon forms. *Biogeochemistry*, *85*(1), 45–57. https://doi.org/10.1007/s10533-007-9105-3

Lehmann, J., & Kleber, M. (2015). The contentious nature of soil organic matter. *Nature*, *528*(7580), 60–68. https://doi.org/10.1038/nature16069

Lehmann, J., Solomon, D., Kinyangi, J., Dathe, L., Wirick, S., & Jacobsen, C. (2008). Spatial complexity of soil organic matter forms at nanometre scales. *Nature Geoscience*, *1*(4), 238–242. https://doi.org/10.1038/ngeo155

Lenth, R. (2020). emmeans: Estimated Marginal Means, aka Least-Squares Means. R package Version 1.5.1. https://CRAN.R-project.org/package=emmeans

Leuzinger, S., Luo, Y., Beier, C., Dieleman, W., Vicca, S., & Körner, C. (2011). Do global change experiments overestimate impacts on terrestrial ecosystems? *Trends in Ecology and Evolution*, *26*(5), 236–241. https://doi.org/10.1016/j.tree.2011.02.011

Liang, C., Amelung, W., Lehmann, J., & Kästner, M. (2019). Quantitative assessment of microbial necromass contribution to soil organic matter. *Global Change Biology*, *25*(11), 3578–3590. https://doi.org/10.1111/gcb.14781

Lützow, M. V., Kögel-Knabner, I., Ekschmitt, K., Matzner, E., Guggenberger, G., Marschner, B., & Flessa, H. (2006). Stabilization of organic matter in temperate soils: Mechanisms and their relevance under different soil conditions - A review. *European Journal of Soil Science*, *57*(4), 426–445. https://doi.org/10.1111/j.1365-2389.2006.00809.x

Ma, Z., Chen, H. Y. H., Li, Y., & Chang, S. X. (2020). Interactive effects of global change factors on terrestrial net primary productivity are treatment length and intensity dependent. *Journal of Ecology*, *108*(5), 2083–2094. https://doi.org/10.1111/1365-2745.13379

Mantyka-Pringle, C., Leston, L., Messmer, D., Asong, E., Bayne, E. M., Bortolotti, L. E., Sekulic, G., Wheater, H., Howerter, D. W., & Clark, R. G. (2019). Antagonistic, synergistic and direct effects of land use and climate on Prairie wetland ecosystems: Ghosts of the past or present? *Diversity and Distributions*, *25*(12), 1924–1940. https://doi.org/10.1111/ddi.12990

Marschner, B., Brodowski, S., Dreves, A., Gleixner, G., Gude, A., Grootes, P. M., Hamer, U., Heim, A., Jandl, G., Ji, R., Kaiser, K., Kalbitz, K., Kramer, C., Leinweber, P., Rethemeyer, J., Schäffer, A., Schmidt, M. W. I., Schwark, L., & Wiesenberg, G. L. B. (2008). How relevant is recalcitrance for the stabilization of organic matter in soils? *Journal of Plant Nutrition and Soil Science*, *171*(1), 91–110. https://doi.org/10.1002/jpln.200700049

McMurdie, P.J., Holmes, S. (2013). phyloseq: An R package for reproducible interactive analysis and graphics of microbiome census data. PLoS ONE 8(4):e61217.

Mooshammer, M., Wanek, W., Zechmeister-Boltenstern, S., & Richter, A. (2014). Stoichiometric imbalances between terrestrial decomposer communities and their resources: Mechanisms and implications of microbial adaptations to their resources. *Frontiers in Microbiology*, *5*(FEB), 1–10. https://doi.org/10.3389/fmicb.2014.00022

Muchovej, R. M., Hanlon, E. A., Ozores-Hampton, M., Shakla, S., & Yamaki, H. (2005). Sugarcane production in Southwest Florida: Mineral soils and amendments. *Electronic Data*

Information Source (EDIS), Soil and Water Science Department, University of Florida, *SL230*, 1–6. http://scholar.google.com/scholar?hl=en&btnG=Search&q=intitle:Sugarcane+Production+in+Southwest+Florida+:+Mineral+Soils+and+Amendments#0%5Cnhttp://edis.ifas.ufl.edu/sc073

Muñoz, C., Monreal, C. M., Schnitzer, M., & Zagal, E. (2008). Influence of Acacia caven (Mol) coverage on carbon distribution and its chemical composition in soil organic carbon fractions in a Mediterranean-type climate region. *Geoderma*, *144*(1–2), 352–360. https://doi.org/10.1016/j.geoderma.2007.12.002

Navarro-García, F., Casermeiro, M. Á., & Schimel, J. P. (2012). When structure means conservation: Effect of aggregate structure in controlling microbial responses to rewetting events. *Soil Biology and Biochemistry*, *44*(1), 1–8. https://doi.org/10.1016/j.soilbio.2011.09.019

Norman, J. M., & Anderson, M. C. (2005). Soil-Plant-Atmosphere Continuum. In *Encyclopedia of Soils in the Environment* (pp. 513–521). Elsevier. https://doi.org/10.1016/B0-12-348530-4/00416-1

Oades, J. M. (1989). An Introduction to Organic Matter in Mineral Soils. In *Minerals in Soil Environments, Chapter 3* (2nd ed.). Soil Science Society of America.

Oksanen, J., Blanchet, F.G., Friendly, M., Kindt, R., Legendre, P., McGlinn, D., Minchin, P.R., O'Hara, R. B. Simpson, G.L. Solymos, P., Stevens, M.H.H., Szoecs, E., and Wagner, H. (2019). vegan: Community Ecology Package. R package version 2.5-6. https://CRAN.R-project.org/package=vegan

Pendall, E. (2018). Fast microbes regulate slow soil feedbacks. *Nature Climate Change*, *8* (October), 859–860. https://doi.org/10.1038/s41558-018-0291-x

Pendall, E., Bridgham, S., Hanson, P. J., Hungate, B., Kicklighter, D. W., Johnson, D. W., Law, B. E., Luo, Y., Megonigal, J. P., Olsrud, M., Ryan, M. G., & Wan, S. (2004). Below-ground process responses to elevated CO_2 and temperature: A discussion of observations, measurement methods, and models. *New Phytologist*, *162*(2), 311–322. https://doi.org/10.1111/j.1469-8137.2004.01053.x

Piepho, H. P., Herndl, M., Pötsch, E. M., & Bahn, M. (2017). Designing an experiment with quantitative treatment factors to study the effects of climate change. *Journal of Agronomy and Crop Science*, *203*(6), 584–592. https://doi.org/10.1111/jac.12225

Pinheiro J, Bates D, DebRoy S, Sarkar D, R Core Team (2020). nlme: Linear and Nonlinear Mixed Effects Models. R packageversion 3.1-149, <URL:https://CRAN.R-project.org/package=nlme>.

Poeplau, C., Don, A., Dondini, M., Leifeld, J., Nemo, R., Schumacher, J., Senapati, N., & Wiesmeier, M. (2013). Reproducibility of a soil organic carbon fractionation method to derive RothC carbon pools. *European Journal of Soil Science*, *64*(6), 735–746. https://doi.org/10.1111/ejss.12088

Poeplau, Christopher, Don, A., Six, J., Kaiser, M., Benbi, D., Chenu, C., Cotrufo, M. F., Derrien, D., Gioacchini, P., Grand, S., Gregorich, E., Griepentrog, M., Gunina, A., Haddix, M., Kuzyakov, Y., Kühnel, A., Macdonald, L. M., Soong, J., Trigalet, S., … Nieder, R. (2018). Isolating organic carbon fractions with varying turnover rates in temperate agricultural soils – A comprehensive method comparison. *Soil Biology and Biochemistry*, *125*(July), 10–26. https://doi.org/10.1016/j.soilbio.2018.06.025

Poeplau, Christopher, Kätterer, T., Leblans, N. I. W., & Sigurdsson, B. D. (2017). Sensitivity of soil carbon fractions and their specific stabilization mechanisms to extreme soil warming in a subarctic grassland. *Global Change Biology*, *23*(3), 1316–1327. https://doi.org/10.1111/gcb.13491

Poirier, N., Sohi, S. P., Gaunt, J. L., Mahieu, N., Randall, E. W., Powlson, D. S., & Evershed, R. P. (2005). The chemical composition of measurable soil organic matter pools. *Organic Geochemistry*, *36*(8), 1174–1189. https://doi.org/10.1016/j.orggeochem.2005.03.005

Radujković, D., Verbruggen, E., Sigurdsson, B. D., Leblans, N. I. W., Janssens, I. A., Vicca, S., & Weedon, J. T. (2018). Prolonged exposure does not increase soil microbial community compositional response to warming along geothermal gradients. *FEMS Microbiology Ecology*, *94*(2), 1–10. https://doi.org/10.1093/femsec/fix174

Rasmussen, C., Heckman, K., Wieder, W. R., Keiluweit, M., Lawrence, C. R., Berhe, A. A., Blankinship, J. C., Crow, S. E., Druhan, J. L., Hicks Pries, C. E., Marin-Spiotta, E., Plante, A. F., Schädel, C., Schimel, J. P., Sierra, C. A., Thompson, A., & Wagai, R. (2018). Beyond clay: towards an improved set of variables for predicting soil organic matter content. *Biogeochemistry*, *137*(3), 297–306. https://doi.org/10.1007/s10533-018-0424-3

Regelink, I. C., Stoof, C. R., Rousseva, S., Weng, L., Lair, G. J., Kram, P., Nikolaidis, N. P., Kercheva, M., Banwart, S., & Comans, R. N. J. (2015). Linkages between aggregate formation, porosity and soil chemical properties. *Geoderma*, *247–248*, 24–37. https://doi.org/10.1016/j.geoderma.2015.01.022

Rillig, M. C., Wright, S. F., Allen, M. F., & Field, C. B. (1999). Rise in carbon dioxide changes soil structure. *Nature*, *400*(6745), 628. https://doi.org/10.1038/23168

Rustad, L. E., Huntington, T. G., & Boone, R. D. (2000). Controls on soil respiration: Implications for climate change. *Biogeochemistry*, *48*(1), 1–6. https://doi.org/10.1023/A:1006255431298

Schimel, D., Melillo, J., Tian, H., McGuire, A. D., Kicklighter, D., Kittel, T., Rosenbloom, N., Running, S., Thornton, P., Ojima, D., Parton, W., Kelly, R., Sykes, M., Neilson, R., & Rizzo, B. (2000). Contribution of increasing CO2 and climate to carbon storage by ecosystems in the United States. *Science*, *287*(5460), 2004–2006. https://doi.org/10.1126/science.287.5460.2004

Schimel, J. P. (2018). Life in Dry Soils: Effects of Drought on Soil Microbial Communities and Processes. *Annual Review of Ecology, Evolution, and Systematics*, *49*(1), 409–432. https://doi.org/10.1146/annurev-ecolsys-110617-062614

Schlesinger, W., & Bernhardt, E. (2013). *Biogeochemistry: An Analysis of Global Change* (3rd ed.). Academic Press. https://doi.org/https://doi.org/10.1016/C2010-0-66291-2

Schlüter, S., Eickhorst, T., & Mueller, C. W. (2019). Correlative Imaging Reveals Holistic View of Soil Microenvironments. *Environmental Science and Technology*, *53*(2), 829–837. https://doi.org/10.1021/acs.est.8b05245

Schnecker, J., Borken, W., Schindlbacher, A., & Wanek, W. (2016). Little effects on soil organic matter chemistry of density fractions after seven years of forest soil warming. *Soil Biology and Biochemistry*, *103*, 300–307. https://doi.org/10.1016/j.soilbio.2016.09.003

Schweizer, S. A., Bucka, F. B., Graf-Rosenfellner, M., & Kögel-Knabner, I. (2019). Soil microaggregate size composition and organic matter distribution as affected by clay content. *Geoderma*, *355*(August). https://doi.org/10.1016/j.geoderma.2019.113901

Séneca, J., Pjevac, P., Canarini, A., Herbold, C. W., Zioutis, C., Dietrich, M., Simon, E., Prommer, J., Bahn, M., Pötsch, E. M., Wagner, M., Wanek, W., & Richter, A. (2020). Composition and activity of nitrifier communities in soil are unresponsive to elevated temperature and CO_2, but strongly affected by drought. *ISME Journal*, 3038–3053. https://doi.org/10.1038/s41396-020-00735-7

Sigurdsson, B. D., Leblans, N. I. W., Dauwe, S., Gudmundsdóttir, E., Gundersen, P., Gunnarsdóttir, G. E., Holmstrup, M., Ilieva-Makulec, K., Kätterer, T., Marteinsdóttir, B., Maljanen, M., Oddsdóttir, E. S., Ostonen, I., Peñuelas, J., Poeplau, C., Richter, A., Sigurdsson, P., Van Bodegom, P., Wallander, H., … Janssens, I. (2016). Geothermal ecosystems as natural climate change experiments: The ForHot research site in Iceland as a case study. *Icelandic Agricultural Sciences*, *29*(1), 53–71. https://doi.org/10.16886/IAS.2016.05

Six, J., Bossuyt, H., Degryze, S., & Denef, K. (2004). A history of research on the link between (micro)aggregates, soil biota, and soil organic matter dynamics. *Soil and Tillage Research*, *79*(1), 7–31. https://doi.org/10.1016/j.still.2004.03.008

Six, J., Elliott, E. T., & Paustian, K. (2000a). Soil macroaggregate turnover and microaggregate formation: A mechanism for C sequestration under no-tillage agriculture. *Soil Biology and Biochemistry*, *32*(14), 2099–2103. https://doi.org/10.1016/S0038-0717(00)00179-6

Six, J., Elliott, E. T., & Paustian, K. (2000b). Soil Structure and Soil Organic Matter. *Soil Science Society of America Journal*, *64*(3), 1042. https://doi.org/10.2136/sssaj2000.6431042x

Six, J., Carpentier, A., Van Kessel, C., Merckx, R., Harris, D., Horwath, W. R., & Lüscher, A. (2001). Impact of elevated CO_2 on soil organic matter dynamics as related to changes in aggregate turnover and residue quality. *Plant and Soil*, *234*(1), 27–36. https://doi.org/10.1023/A:1010504611456

Six, J., Feller, C., Denef, K., Ogle, S., De Moares Sa, J. C., & Albrecht, A. (2002). Soil organic matter, biota and aggregation in temperate and tropical soils - Effects of no-tillage. *Agronomie, EDP Sciences*, *22*(7–8), 755–775. https://doi.org/0.1051/agro:2002043.hal-00885974

Six, J., & Paustian, K. (2014). Aggregate-associated soil organic matter as an ecosystem property and a measurement tool. *Soil Biology and Biochemistry*, *68*, A4–A9. https://doi.org/10.1016/j.soilbio.2013.06.014

Song, J., Wan, S., Piao, S., Knapp, A. K., Classen, A. T., Vicca, S., Ciais, P., Hovenden, M. J., Leuzinger, S., Beier, C., Kardol, P., Xia, J., Liu, Q., Ru, J., Zhou, Z., Luo, Y., Guo, D., Adam Langley, J., Zscheischler, J., … Zheng, M. (2019). A meta-analysis of 1,119 manipulative experiments on terrestrial carbon-cycling responses to global change. *Nature Ecology and Evolution*, *3*(9), 1309–1320. https://doi.org/10.1038/s41559-019-0958-3

Spohn, M., Klaus, K., Wanek, W., & Richter, A. (2016). Microbial carbon use efficiency and biomass turnover times depending on soil depth - Implications for carbon cycling. *Soil Biology and Biochemistry*, *96*, 74–81. https://doi.org/10.1016/j.soilbio.2016.01.016

Sulman, B. N., Moore, J. A. M., Abramoff, R., Averill, C., Kivlin, S., Georgiou, K., Sridhar, B., Hartman, M. D., Wang, G., Wieder, W. R., Bradford, M. A., Luo, Y., Mayes, M. A., Morrison, E., Riley, W. J., Salazar, A., Schimel, J. P., Tang, J., & Classen, A. T. (2018). Multiple models and experiments underscore large uncertainty in soil carbon dynamics. *Biogeochemistry*, *141*(2), 109–123. https://doi.org/10.1007/s10533-018-0509-z

Swanston, C. W., & Trumbore, S. E. (2009). *Storage and Turnover of Organic Matter in Soil*. https://escholarship.org/uc/item/4k87b5v4

Tisdall, J. M., & Oades, J. M. (1982). Organic matter and water-stable aggregates in soils. *Journal of Soil Science*, *33*(2), 141–163. https://doi.org/10.1111/j.1365-2389.1982.tb01755.x

Torn, M. S., Kleber, M., Zavaleta, E. S., Zhu, B., Field, C. B., & Trumbore, S. E. (2013). A dual isotope approach to isolate soil carbon pools of different turnover times. *Biogeosciences*, *10*(12), 8067–8081. https://doi.org/10.5194/bg-10-8067-2013

Totsche, K. U., Amelung, W., Gerzabek, M. H., Guggenberger, G., Klumpp, E., Knief, C., Lehndorff, E., Mikutta, R., Peth, S., Prechtel, A., Ray, N., & Kögel-Knabner, I. (2018). Microaggregates in soils. *Journal of Plant Nutrition and Soil Science*, *181*(1), 104–136. https://doi.org/10.1002/jpln.201600451

Vancampenhout, K., Wouters, K., De Vos, B., Buurman, P., Swennen, R., & Deckers, J. (2009). Differences in chemical composition of soil organic matter in natural ecosystems from different climatic regions - A pyrolysis-GC/MS study. *Soil Biology and Biochemistry*, *41*(3), 568–579. https://doi.org/10.1016/j.soilbio.2008.12.023

von Lützow, Margit, Kögel-Knabner, I., Ekschmitt, K., Flessa, H., Guggenberger, G., Matzner, E., & Marschner, B. (2007). SOM fractionation methods: Relevance to functional pools and to stabilization mechanisms. *Soil Biology and Biochemistry*, *39*(9), 2183–2207. https://doi.org/10.1016/j.soilbio.2007.03.007

Walker, T. W. N., Janssens, I. A., Weedon, J. T., Sigurdsson, B. D., Richter, A., Peñuelas, J., Leblans, N. I. W., Bahn, M., Bartrons, M., De Jonge, C., Fuchslueger, L., Gargallo-Garriga, A., Gunnarsdóttir, G. E., Marañón-Jiménez, S., Oddsdóttir, E. S., Ostonen, I., Poeplau, C., Prommer, J., Radujković, D., … Verbruggen, E. (2020). A systemic overreaction to years versus decades of warming in a subarctic grassland ecosystem. *Nature Ecology & Evolution*, *4*(1), 101–108. https://doi.org/10.1038/s41559-019-1055-3

Walker, T. W. N., Kaiser, C., Strasser, F., Herbold, C. W., Leblans, N. I. W., Woebken, D., Janssens, I. A., Sigurdsson, B. D., & Richter, A. (2018). Microbial temperature sensitivity and biomass change explain soil carbon loss with warming. *Nature Climate Change*, *8*(October). https://doi.org/10.1038/s41558-018-0259-x

Wang, H., Guan, D., Zhang, R., Chen, Y., Hu, Y., & Xiao, L. (2014). Soil aggregates and organic carbon affected by the land use change from rice paddy to vegetable field. *Ecological Engineering*, *70*, 206. https://doi.org/10.1016/j.ecoleng.2014.05.027

Wilpiszeski, R. L., Aufrecht, J. A., Retterer, S. T., Sullivan, M. B., Graham, D. E., Pierce, E. M., Zablocki, O. D., Palumbo, A. V., & Elias, D. A. (2019). Soil Aggregate Microbial Communities: Towards Understanding Microbiome Interactions at Biologically Relevant Scales. *Applied and Environmental Microbiology*, *85*(14), 1–18. https://doi.org/10.1128/AEM.00324-19

Yan, Y., Zhou, X., Jiang, L., & Luo, Y. (2017). Effects of carbon turnover time on terrestrial ecosystem carbon storage. *Biogeosciences*, *14*(23), 5441–5454. https://doi.org/10.5194/bg-14-5441-2017

Yue, K., Fornara, D. A., Yang, W., Peng, Y., Peng, C., Liu, Z., & Wu, F. (2017). Influence of multiple global change drivers on terrestrial carbon storage: additive effects are common. *Ecology Letters*, *20*(5), 663–672. https://doi.org/10.1111/ele.12767

Zabel, R. A., & Morrell, J. J. (2020). Chemical changes in wood caused by decay fungi. In *Wood Microbiology* (pp. 215–244). Elsevier. https://doi.org/10.1016/b978-0-12-819465-2.00008-5

Zechmeister-Boltenstern, S., Keiblinger, K. M., Mooshammer, M., Penuelas, J., Richter, A., Sardans, J., & Wanek, W. (2015). The application of ecological stoichiometry to plant–microbial–soil organic matter transformations. *Ecological Monographs*, *85*(2), 133–155.

Zhou, X., Weng, E., & Luo, Y. (2008). Modeling patterns of nonlinearity in ecosystem responses to temperature, CO_2, and precipitation changes. *Ecological Applications*, *18*(2), 453–466. https://doi.org/10.1890/07-0626.1

Zimmermann, M., Leifeld, J., Schmidt, M. W. I., Smith, P., & Fuhrer, J. (2007). Measured soil organic matter fractions can be related to pools in the RothC model. *European Journal of Soil Science*, *58*(3), 658–667. https://doi.org/10.1111/j.1365-2389.2006.00855.x